

PHOTOSENSITIZATION OF ZnS NANOPARTICLES WITH METAL-FREE
DYE SENSITIZER BASED ON THIAZOLE AND ISATIN DERIVATIVES FOR
SOLID STATE DYE SENSITIZED SOLAR CELL

A THESIS SUBMITTED IN FULLFILMENT
OF THE REQUIREMENTS FOR THE DEGREE OF
MASTER OF SCIENCE IN CHEMISTRY

OF

THE UNIVERSITY OF NAMIBIA

BY

NDAPEWA LINDA ENKALI

200610333

October 2025

MAIN SUPERVISOR: PROF. VEIKKO UAHENGO (Department of Chemistry and
Biochemistry, University of Namibia)

CO-SUPERVISOR: PROF. LIKIUS DANIEL (Department of Chemistry and
Biochemistry, University of Namibia)

ABSTRACT

Zinc Sulphide (ZnS) is one of the wide band gap (Wurtzile; 3.91eV and Spalerite; 3.54eV) semiconductors suitable for application in dye-sensitized solar cell (DSSCs). However, ZnS absorb UV light which only contribute about 5% total energy of solar radiation. By sensitizing ZnS photo anode with dye sensitizer in DSSC, light absorption is extended to visible regions (which contribute 43% total energy) of solar radiation spectrum. Despite this, discovering the best photo anode materials (sensitizer and semiconductor) remains a challenge in DSSCs. In this work, an experimental study on the photosensitization of ZnS nanoparticles with five different metal-free dyes was carried out. The ZnS nanoparticles and five different Thiazole and Isatin based metal-free dyes were synthesized and characterized. Grafted ZnS-dye samples were fabricated and characterized and the effect of solvatochromism on dyes on ZnS were investigated. All data were collected from X-ray diffractometer (XRD), Proton Nuclear Magnetic Resonance ($^1\text{HNMR}$), Fourier Transform Infrared (FTIR) spectroscopy and analyzed Ultraviolet and Visible light (UV-vis) spectroscopy. XRD confirms that the crystal structure of the ZnS nanoparticles and the chemical structures of dyes and their vibration frequencies were confirmed by $^1\text{HNMR}$ and FTIR, respectively. Among the five dyes, Dye1, Dye2 and Dye5 showed best photo response before and after grafted on ZnS nanoparticles. Broad peaks and high absorption intensities were observed on these dyes. Little or no absorption were observed for Dye3 and Dye4 before and after grafted on ZnS nanoparticles.

Keywords: Photosensitization, nanoparticles, solvatochromism, grafting, characterization, metal-free dyes

TABLE CONTENTS

ABSTRACT.....	i
LIST OF SCHEMES	iv
LIST OF FIGURES	v
LIST OF TABLES	vi
ABBREVIATIONS AND ACRONYMS.....	vii
ACKNOLEWLEDGEMENTS	ix
DEDICATION	x
DECLARATIONS	xii
CHAPTER 1: INTRODUCTION.....	1
1.1 Background of the study	1
1.2 Statement of the problem.....	5
1.3 Objectives of the study	5
1.4 Significance of the study	6
1.5 Limitation of the study	6
1.6 Delimitation of study	6
CHAPTER 2: LITERATURE REVIEW.....	7
2.1 Overview of the DSSC.....	7
2.2 Photo-generation mechanism of a DSSC.....	8
2.3 Zinc Sulphide nanoparticles	10
2.3.1 Zinc Sulphide as Photoanode.....	11
2.4 Dye photosensitizers	12

2.4.1 Metal-free (organic) sensitizers.....	14
2.4.1.1 Synthetic sensitizer.....	15
2.5 Solvatochromism	18
2.6 Isatin and Thiazole based dyes.....	20
2.7 Theoretical background of experimental instrumentations	21
2.7.1 ¹ H NMR Spectrophotometry	21
2.7.2 XRD spectrophotometry.....	23
2.7.2 FTIR spectrophotometry	25
2.7.3 UV-Vis spectrophotometry	28
3.1 Research design.....	31
3.1.1 Chemicals required for synthesis.....	31
3.2 Research instruments	32
3.3 Procedures.....	32
3.3.1 Synthesis of ZnS	32
3.3.2 Synthesis of metal-free dyes	33
3.3.2.1 Synthesis of Dye1.....	33
3.3.2.2 Synthesis of Dye2.....	34
3.3.2.3 Synthesis of Dye3.....	35
3.3.2.4 Synthesis of Dye4.....	36
3.3.2.5 Synthesis of Dye5.....	37
3.3.4 Preparation of solvatochromism dye samples	38

3.3.5 Characterization.....	38
3.3.5.1 ZnS nanoparticles characterization	38
3.3.5.2 Metal-free dyes characterization	39
3.3.6 Fabrication and characterization of grafted ZnS-dye samples.....	39
4.1 Grafted ZnS-dye Samples	40
4.2 ¹ H NMR spectral interpretation of dyes.....	41
4.3 XRD analysis of ZnS	42
4.4 Analysis of vibrational Frequencies	43
4.4.1 FTIR transmittance spectrum: ZnS	43
4.4.2 FTIR Transmittance spectrum of Dyes and grafted ZnS-dyes.....	43
4.4.2.1 FTIR spectra of Dye1 and ZnS-Dye1	44
4.4.2.2 FTIR spectra of Dye2 and ZnS-Dye2	46
4.4.2.3 FTIR spectra of Dye3 and ZnS-Dye3	48
4.4.2.5 FTIR spectra of Dye5 and ZnS-Dye5	52
4.5 Solvatochromic effect and UV-vis analysis of metal-free dyes.....	54
4.5.1 Solvent effect on UV-vis absorption spectra of dyes	54
4.5.2 Optimized dye concentration for UV-vis analysis of dyes.....	59
4.6 UV-vis analysis of ZnS and grafted ZnS-Dyes nanoparticles.....	61
4.7 Naked eye analysis and comparisons of the synthesized dye structures in relation to UV-vis spectra data	67
4.8 Evaluation of dyes based on UV-vis analysis and naked eyes analysis of dye structures	68

CHAPTER 5: CONCLUSION AND RECOMMENDATIONS	70
5.1 Conclusion	70
REFERENCES.....	73
APPEDICES.....	86
APPENDIX A: Research permission letter and Ethical clearance.....	86
APPENDIX B: Pictures of the synthesized ZnS nanoparticles and metal free dyes.....	88
APPENDIX C: ¹H NMR Spectra of Dyes	91
APPENDIX D: Dye graphs at different concentrations	92
APPENDIX E: Identified moieties on dye structures	94

LIST OF SCHEMES

Scheme 1: Scheme diagram of a DSSC	1
Scheme 2: Energy distribution of the solar spectrum on Earth surface [17].....	3
Scheme 3: Illustration of the types of solvatochromic shifts	4
Scheme 4: Donor - π -linker Acceptor design of metal free dye [19].....	15
Scheme 5: Energy levels of $I = 1/2$ spin states by external magnetic field B_0	22
Scheme 6: Working illustration of XRD.....	24
Scheme 7: X-ray diffraction by crystal planes	25
Scheme 8: Working principle of FTIR spectrophotometer	26
Scheme 9: UV - Vis working principle	29
Scheme 10: Flow chart of Research design	31
Scheme 11: Reaction mechanism of Dye1	34
Scheme 12: Reaction mechanism of Dye2.....	35
Scheme 13: Reaction mechanism of Dye3.....	36
Scheme 14: Reaction mechanism of Dye4.....	37
Scheme 15: Reaction mechanism of Dye5.....	38

LIST OF FIGURES

Figure 1: Crystal structures of Zinc Sulphide [39]	10
Figure 2: Grafted ZnS-dye1 to ZnS-dye5 samples (from left to right).....	40
Figure 3: XRD pattern of ZnS	42
Figure 4: FTIR spectrum of ZnS.....	43
Figure 5: FTIR spectrum of Dye1	45
Figure 6: FTIR spectrum of ZnS, Dye1 and ZnS-Dye1	46
Figure 7: FTIR spectrum of Dye2.....	47
Figure 8: FTIR spectra of ZnS, Dye2 and ZnS-Dye2.....	48
Figure 9: FTIR spectrum of Dye3.....	49
Figure 10: FTIR spectra pf ZnS, Dye3 and ZnS-Dye3	50
Figure 11: FTIR spectrum of Dye4.....	51
Figure 12: FTIR spectra of ZnS, Dye4 and ZnS-dye4.....	52
Figure 13: FTIR spectrum of Dye5.....	53
Figure 14: FTIR spectra of ZnS, Dye5 and ZnS-dye5.....	54
Figure 15: Solvatochromic effect of solvents on Dye1 and Dye2	56
Figure 16: Solvatochromic effect on Dye3, Dye4 and Dye5.....	58
Figure 17: UV-Vis absorption spectra of dyes in 0.1 mM of Solutions	60
Figure 18: UV-vis spectrum of ZnS nanoparticles	62
Figure 19: UV-vis absorption spectra of (a) ZnS-Dye1, (b) ZnS-Dye2, (c) ZnS-Dye3, (d) ZnS-Dye4 and (e) ZnS-Dye5	64
Figure 20: Absorption spectra of grafted samples	65

LIST OF TABLES

Table 1: XRD peaks, particle size and absorption peaks of ZnS nanoparticles from different synthesis methods	11
Table 2: Dielectric constants of common solvents [73].....	18
Table 3: IR vibrational frequencies of some chemical bonds	28
Table 4: H NMR Chemical shifts, (ppm) of Dyes	41
Table 5: The λ_{\max} and absorption intensities (a.u) of the dyes in different solvents	59
Table 6: Band width, λ_{\max} and absorption intensity (a.u) of pure dyes and grafted ZnS-dyes	66
Table 7: Dyes moieties and their deduced structural configuration.....	68

ABBREVIATIONS AND ACRONYMS

DSSCs	Dye Sensitized Solar Cells
TFSC	Thin Film Solar Cells
TiO₂	Titanium dioxide
ZnO	Zinc oxide
ZnS	Zinc Sulphide
UV/VIS	Ultraviolet and visible
HOMO	Highest occupied molecular orbitals
LUMO	Lowest unoccupied molecular orbitals
UV	Ultraviolet
XRD	X-ray diffraction
D- π- A	Donor - pi linker - Acceptor
DMSO	Dimethylsulfoxide
DMF	Dimethylformamide
THF	Tetrahydrofuran
ppm	parts per million
FTIR	Fourier transform infrared radiation
¹H NMR	Proton nuclear magnetic resonance
δ	Chemical shift
MW	Molecular weight
C, N, H, O, S	Carbon, Nitrogen, Hydrogen, Oxygen, Sulfur
EtOH	Ethanol
MeOH	Methanol
CHCl₃	Chloroform

CH₃CN	Acetonitrile
C₃H₆O	Acetone
CH₃OOC₂H₅	Ethyl Acetate
λ_{max}	Maximum absorption wavelength
θ	Theta

ACKNOWLEDGEMENTS

Firstly, I wholeheartedly thank the God for keeping me alive till today, blessing me with strength, health, wisdom, knowledge and understanding, and everything.

With utmost gratitude I would like to acknowledge the following people, who have contributed to this study:

Prof. V UAHENGO: For your immense knowledge, and excellent mentorship. The success of this master's project would not be possible if it was not for your hard work, dedication, motivation and passion for research. You made sure that distance was not a barrier for success. With your enthusiasm, inspiration, and great efforts to explain things clearly.

Prof. L DANIEL: For your support, guidance and your valuable contributions in this project, I am tremendously grateful.

Dr P HISHIMONE: For your motivation and mentoring regardless of your extremely busy schedule.

I would like to thank the University of Namibia at large especially the Department of Chemistry and Biochemistry for allowing us to carry out our laboratory experiments. The list is endless, but I cherish each contribution to my development as a scholar, without them I could not have gone this far.

DEDICATION

This work is dedicated, firstly to the Almighty God, the source of strength. I also dedicate this thesis to my best friend Josef Shimhanda, my mother Selma Shalongo, my colleagues: Prof. H. Miranda, Dr. S. Naukushu and Mr. S. Ashili for moral and spiritual support. Remain blessed always.

DECLARATIONS

I, Ndapewa Linda Enkali, hereby declare that this study, Photosensitization of ZnS nanoparticles with metal-free dye sensitizer based on Thiazole and Isatin derivatives for solid state dye sensitized solar cells, is my own work and is a true reflection of my research, and that this work, or any part thereof has not been submitted for a degree at any other institution.

No part of this thesis may be reproduced, stored in any retrieval system, or transmitted in any form, or by means (e.g. electronic, mechanical, photocopying, recording or otherwise) without the prior permission of the author, or The University of Namibia in that behalf.

I, Ndapewa Enkali, grant The University of Namibia the right to reproduce this thesis in whole or in part, in any manner or format, which The University of Namibia may deem fit.

NDAPEWA LINDA ENKALI



02/10/ 2025

Name of student

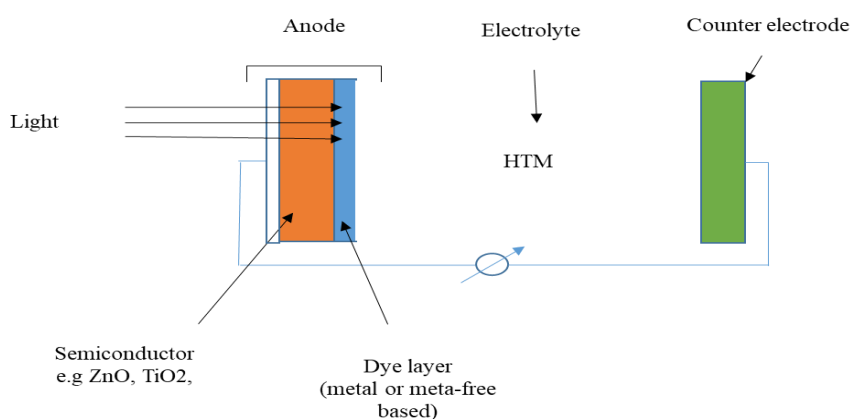
Signature

Date

CHAPTER 1: INTRODUCTION

1.1 Background of the study

The world's energy consumption is increasing and the dramatic depletion of non-renewable energy sources is considered to be a threat to human life, from now to the next generation [1]. Solar energy represents an alternative source of clean and renewable energy, and is one of the research fields leading globally. Photovoltaic technologies have been discovered to convert light from the sun into electricity. A dye-sensitized solar cell (DSSC) is a third type of photovoltaic technologies, that emerged after a second type; a thin-film solar cell (TFSC), aimed to improve the efficiency while maintaining its low production cost [2]. It is made up of photo anode, counter electrode and an electrolyte [3–5]. On the photo anode, a layer of a metal or metal-free dye is adsorbed on the semiconductor nanoparticles surface where photosensitization is taking place. Dyes are natural, organic (metal-free) or inorganic (metal) sensitizers that play an important role in absorbing sunlight for energy conversion, as shown with a schematic representation of a DSSC (Scheme 1). In a solid state DSSC (ssDSSC), the electrolyte is a solid Hole Transporting Material (HTM) responsible for charge transportation between the two electrodes [3].



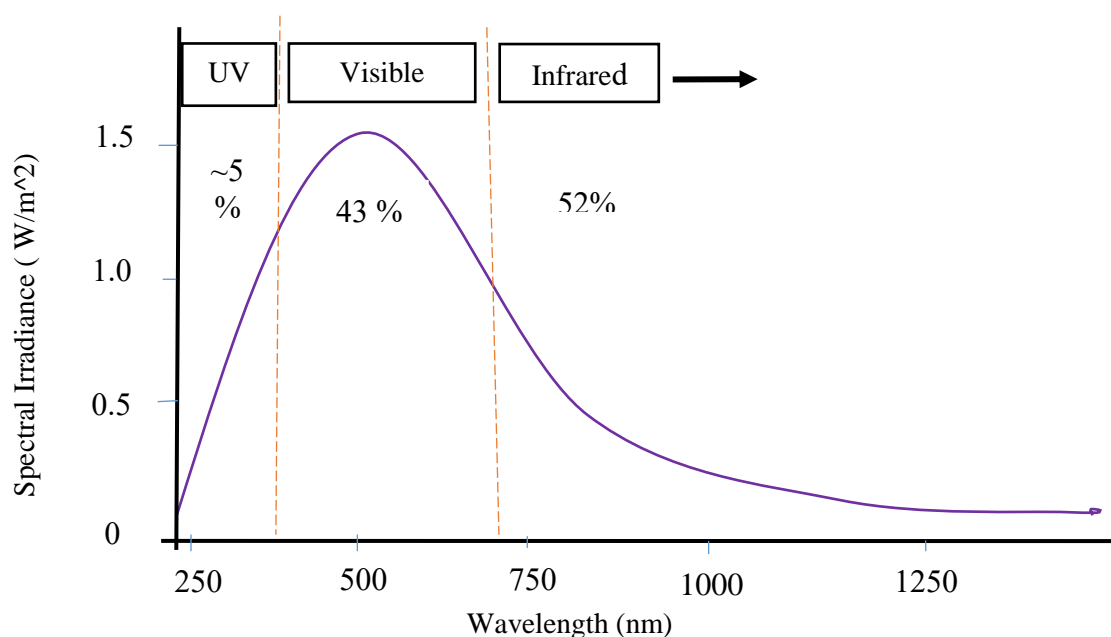
Scheme 1: Scheme diagram of a DSSC

More research has been done on metal oxides like TiO₂ and ZnO as semiconductors for electron transportation in DSSC technology. In recent years, the use of ZnS semiconductor emerged as an alternative, due to its stability and greatly efficient electrochemical properties [6, 7]. ZnS is a photoactive material which occurs in two different forms; the alpha (Wurtzite) and beta (Spalorit) with a wide band gap of 3.91eV and 3.54eV, respectively [6]. Compared to TiO₂ and ZnO nanoparticles, ZnS have a wider band gap [8], hence it is most suitable for electron transportation in DSSC. Nosheen E et al [7] and Reda S M et al [9] have reported an increased performance of a DSSC based on ZnS nanoparticles due to effective adsorption of a metal dye renowned ruthenium N719 dyes. and metal-free dyes like Crystal violet and Methyl blue dye, respectively.

For an effective DSSCs, a sensitizer should play its key role successfully among other components of a DSSC. A sensitizer is considered to be effective if it is stable, having a strong and wide absorption range from visible to near infrared region of the spectrum for light harvesting [2]. In the past few years, Ruthenium and other metal based dyes were reported as the most successful sensitizers that achieved high efficiency in DSSC [10, 11]. Despite this, metal-free based dye sensitizers emerged as an alternative and has become one of the main focus in research today. This is because they are available, cheap, environmental friendly, they have flexible molecular structure and large absorption coefficient [10–13].

Metal-free dyes are colored compounds with a general structure consisting of a donor (d), a conjugation linkage (π) and acceptor (a) [10, 11, 14, 15]. While ZnS absorb UV light, metal-free dyes absorb light in the UV-vis to near infrared region of the spectrum [16]. As shown in Scheme 2 below, the peak of energy distribution on earth surface is in the visible region of a spectrum. Thus, metal-free dyes are the promising sensitizers

in DSSC to extend the light absorption range to visible region of the spectrum, hence absorb more light.



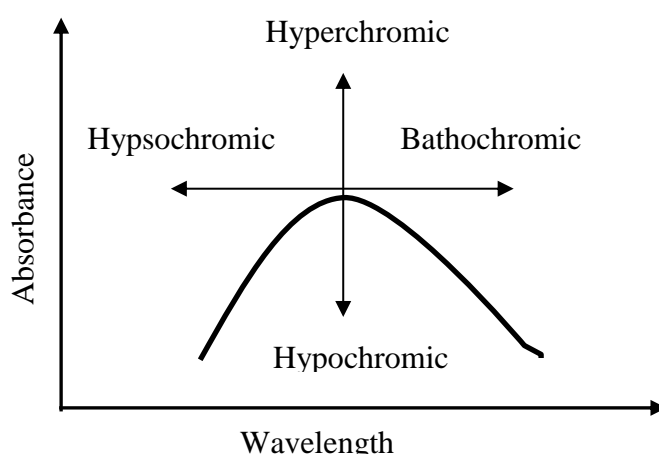
Scheme 2: Energy distribution of the solar spectrum on Earth surface [17]

The electricity produced from the DSSC device depends on the amount of sunlight absorbed and converted successfully to electrical energy. Until now, the commercial applications of DSSC technology is limited due to poor conversion efficiency of light to electrical energy [5]. Even though the efficiency of a DSSC based on metal-free dye has been reported as lower than that of metal based DSSC [18, 19], researchers have been striving to design and synthesize new metal-free dyes that are effective in light absorption, improving the performance of the DSSC.

As a sensitizer in DSSC, the molecular design structure of a dye plays a role in contributing to effective light absorption [11, 20]. The geometry and the moieties of a dye molecule affect the dye absorption of light from the sun. It is reported that introducing a bulky planarity moiety and many anchoring groups leads to increasing light absorption [21]. Different structures of metal-free dyes based on Triphenylamine,

Indole, Carbazole and Thiazole have been synthesized [20, 22] and characterized, but the challenge of obtaining a dye with strong and large absorption range, and hence a good performing DSSC is still standing.

The absorption of light by sensitizers is determined by UV-vis absorption spectroscopy technique and is influenced by the surrounding medium. Many researchers have used this technique to determine the ability of UV-vis light absorbing sensitizers for DSSCs. Solvatochromism occur when dye molecules interact with solvent molecules, affecting the absorption bands of the spectra and this is caused by difference in solvation energies between the ground and excited states of light absorbing molecules [23, 24]. The polarity of the solvent aid the stabilization or destabilization of the excited states of the sensitizer which cause a shift in λ_{\max} of absorption spectra [25, 26]. Solvent-solute molecules interaction changes the position, the shape and the intensity of the absorption band of the spectrum [25]. The position of the band shifts either positively (bathochromic) or negatively (Hypsochromic), while its absorption intensity increases (hyperchromic) or decreases (hypochromic). Scheme 3 below illustrate the four types of absorption band shifts that occurs due to solvent effect.



Scheme 3: Illustration of the types of solvatochromic shifts

In this research, five metal-free dyes were synthesized and characterized by FTIR, ¹HNMR and UV-vis spectroscopy. ZnS nanoparticles were also synthesized and grafted with metal-free dyes based on Thiazole and Isatin derivatives, and characterized. The effect of solvatochromism on dyes was also investigated.

1.2 Statement of the problem

An increase in energy demand have brought challenges such as the depletion of non-renewable energy sources and climate change. These challenges have created rooms for discovering new alternatives for acquiring energy for the survival of human kind. As the most promising photovoltaic technology, more research needs to be executed in DSSC in order to improve its power conversion efficiency. Currently, the power conversion efficiency in DSSC was improved up to about 14.3% [4, 27]. This efficiency is still low and hence hinders the commercialization of DSSC [28, 29]. Researchers have indicated that one of the hindrances that prevent DSSC power conversion efficiency from increasing is with respect to photocurrent [3]. The issue of determining the best photo anode materials (sensitizer and semiconductor) of DSSC remain the challenge. Therefore, there is a need to improve light absorption efficiency in DSSC, hence leading to higher photocurrent and better performance of the cell.

1.3 Objectives of the study

The objectives of the study are to:

- Synthesize and characterize ZnS nanoparticles
- Design, synthesize and characterize Thiazole and Isatin based metal-free (organic) dyes
- Fabricate and characterize the grafted ZnS-dye samples
- Investigate the effect of solvatochromism on dye samples

1.4 Significance of the study

Isatin and Thiazole derived organic dyes are reported as promising candidates of DSSCs sensitizers. Thus, more research is needed to investigate the solvatochromic behavior of the new designed Isatin and Thiazole derived dyes. A grafted ZnS-dye with good sensitization properties enhance light absorption efficiency, hence improving the performance of the DSSCs. So, the findings of the study have societal benefits by enhancing the harvesting of clean solar energy in order to meet the overgrowing energy demand. The problem of climate change due to pollution caused by the use of fossil fuels as non-renewable energy sources may be alleviated. It is also adding value to Zinc mined in Namibia, as it is used to manufacture ZnS nanocrystalline. The anticipated results filled up more gaps and open up more research fronts in this area.

1.5 Limitation of the study

Lack of instruments in the research working area may cause delays in obtaining results, due to time required to send some samples for analysis to University of Johannesburg.

1.6 Delimitation of study

The study was only focusing on the comparison of the photosensitization of ZnS nanoparticles with five different organic dyes, the performance of the dyes in solar cells is not evaluated.

CHAPTER 2: LITERATURE REVIEW

2.1 Overview of the DSSC

A DSSCs, also known as Gratzel cell is one of the encouraging third generation photovoltaic technique for future energy supply, developed by Gratzel and O'Regan in 1991 [30]. It emerged after the crystalline silicon solar cell (first generation) and thin film solar cell (second generation) photovoltaic techniques which are restricted due to toxic, scarcity and expensive materials used in their manufacturing processes [2, 31]. The discovery of a DSSC technique aim to enhance the efficiency of light to electrical energy conversion using nontoxic, cheap and available materials.

Currently, the crystalline silicon photovoltaic technology dominates and achieved high efficiency of about 25%, followed by thin film solar cell with the efficiency in the range of 10 - 20 % [29]. These have all reached the point of commercialization and are in the market places. Even though the production cost of thin film solar cell is reduced compared to crystalline silicon solar cell due to less material used, the toxic and rare materials used in their manufacturing process restrict their extensive applications in future. DSSC remain a competitive alternative photovoltaic technology due to its cheap and clean fabrication process which also promote climate change alleviation. In addition, a DSSC offer a major benefit of operating even under diffuse light.

Despite its advantages, the efficiency of DSSC is so low compared to crystalline silicon and thin film solar cell. In the first attempt, the efficiency of DSSC showed less than 2%, obtained from a TiO₂ based dye sensitized solar cell, with chlorophyll dye as a sensitizer [32]. Major research on optimization of each of the component of DSSC to enhance their efficiencies while maintaining the low cost and reducing the

environmental impact has been done. This leads to emerging alternatives to component materials such as replacing chlorophyll with effective but low-cost dyes, using electrolyte with good thermal stability and other cheap, clean, available and effective component materials. Today, the efficiency of DSSC has improved up to about 14.3 % and it is on the edge of commercialization.

However, there are still challenging issues preventing the commercialization of DSSC and hence requires much more determination. These are limited efficiency and shorter lifespan of DSSCs [28, 33]. Mariotti et al.[28] and Mozaffari et al. [29], reported that the lifespan of a DSSC is affected by leakage and evaporation of electrolyte, decay of cathode electrode by redox couple, electrolyte bleaching and elimination of adsorbed dye from the semiconductor surface. Hence, effort has been made to find solutions to these problems, such as replacing the liquid electrolyte with quasi solid stated electrolyte to overcome the issue of leakage and evaporation [3]. This leads to emerged solid state dye sensitized solar cell (ssDSSC).

2.2 Photo-generation mechanism of a DSSC

As a photovoltaic technique, a DSSCs resemble the mechanism of photosynthesis used by plants to produce fruits. While plants use chlorophyll in their leaves to absorb light energy from the sun, the sensitizer on the photo anode of the DSSCs absorb light energy from the sun. According to Carella A. et al [4] and Mehmood U. et al [34], the mechanism process is outlined as follow:

- ❖ When light strike on the dye, the electron in the HOMO level gains more kinetic energy and exited to the LUMO level.

- ❖ The excited electron is then injected into the conduction band of a semiconductor, leaving a hole charge in dye molecule. Thus, the dye becomes oxidized.
- ❖ With the help of the semiconductor as charge transporter, the injected electron diffuses through the semiconductor to the photo electrode and flows to the external circuit, hence producing current.
- ❖ An electrolyte situated between the two electrodes helps with the regeneration of an oxidized sensitizer by reduction, while the cathode electrode acts as a reducing agent supplying electrons to an electrolyte from external circuit, to gain its normal state. At this point, the circuit is complete and the cycle continues while producing electricity.

For this mechanism to function effectively, the energy levels of conduction band of a semiconductor, dye molecule and the redox couple in electrolyte should be in good orientation. For an electron to be transferred to the conduction band of semiconductor, the LUMO energy level of a dye must be higher than the energy level of a semiconductor conduction band [19]. In addition, the HOMO energy level of redox couple in electrolyte must be higher than the HOMO energy level of a dye molecule. This allows an oxidized dye to receive an electron from the electrolyte. Appropriate molecular energy levels ensure successful electron injection, dye regeneration and electron recovering at cathode from external load, hence the completion of electronic circuit.

However, loss of photoelectrons may occur when some of the injected electrons in the conduction band of the semiconductor recombine with the oxidized sensitizer or redox species of the electrolyte, or by electron decay [35, 36]. To produce current, the electron injected in the conduction band of a semiconductor should not recombine

with the oxidized dye or electrolyte. Therefore, the rate of electron injection in the conduction band and electron diffusion through the semiconductor, and the rate at which the oxidized sensitizer is regenerated by the redox species determine the performance of DSSC. Fast rate of electron injection and diffusion through the semiconductor, and sensitizer regeneration by redox species prevent electron decay and recombination process, hence promoting better performance of DSSCs [34].

2.3 Zinc Sulphide nanoparticles

The two forms of ZnS; the Sphalerite and Wurtzite are shown in figure 1. Sphalerite is a cubic form structure that is stable at room temperature, while Wurtzite is grown at high temperature [6]. ZnS is one of the first semiconductors discovered and has a variety of applications such as in electroluminescent device, solar cells and other optoelectronic devices, due to its photochemical and electrochemical properties like good electron mobility, tunable band gap, good charge transport properties and photo stability [37, 38].

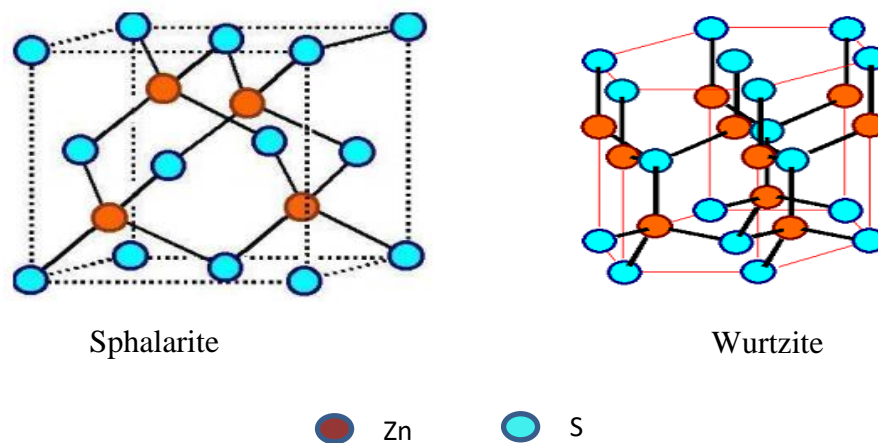


Figure 1: Crystal structures of Zinc Sulphide [39]

Different methods have been used to synthesis ZnS nanoparticles such as by co-precipitation [7], green method [9], hydrothermal method [40], Chemical reduction

technique [41] and Sol-gel method [42]. The average spherical particle size of ZnS nanoparticle diameter from all synthesis methods are in the range of 10 – 30 nm, with diffraction peaks that shows cubic phase of ZnS except for ZnS nanoparticles prepared from sol-gel method that showed hexagonal phase. The absorption spectrum peaks were all found in the range of 250 – 345 nm, as shown in the Table 1 below.

Table 1: XRD peaks, particle size and absorption peaks of ZnS nanoparticles from different synthesis methods

Synthesis method	XRD peaks	Particle diameter size at 2Θ (nm)	Absorption spectrum peak (nm)	Source
Co-precipitation	28.7, 48.2, 57.0	15 ± 2	270	[7]
Sol-gel	32.9, 35.5, 37.4	20 – 30	Around 345	[9]
Hydrothermal	28.6, 47.6, 56.4	13 – 28	Around 250	[40]
Green synthesis	37.0, 53.4, 66.7	10	317	[41]
Chemical route	~27, ~48, ~56	20	330	[42]

2.3.1 Zinc Sulphide as Photoanode

With its wide band gap and high absorption coefficient in the UV region of the optical spectrum, ZnS attracts more attention in photovoltaic research field. Its versatile properties give ZnS nanoparticles the potential to be used as alternative to ZnO, TiO₂, SnO₂, CdS and other semiconductors, in photoanode of DSSCs. Although TiO₂ is considered to be the promising semiconductor for DSSC fabrication, ZnS is reported to have similar advantages as TiO₂, such as low cost, availability, nontoxic, electron mobility and thermal stability [43]. Both TiO₂ and ZnS are associated with the

challenges of low electron transfer and high charge recombination rate [37, 44]. However, they all have fast electron injection and reduced charge recombination possibilities.

Many studies have been focusing on enhancing the performance of photovoltaic materials with ZnS. For example, in the year 2015, Rouhi J. et al. reported on the improved performance of DSSC based on ZnO/ZnS heterostructure photoanode. They highlighted that the efficiency improvement could be attributed by reduced charge recombination process by ZnS coating on ZnO nanocones [45]. The fabrication of composite ZnS nanoparticles, graphene and polypyrrole photoanode of a DSSCs also lead to an increase in photovoltaic efficiency [38]. It is also reported that the presence of ZnS in a constructed photoanode made of TiO₂ and a combination of ZnS, CdS and CdSe nanoparticles in a Quantum dot sensitized solar cells facilitates charge transfer to the surrounding species and prevent electron leakage from TiO₂ to electrolyte [46]. However, ZnS has not received much attention as an active photoanode component.

ZnS nanoparticles can be photosensitized with dyes for applications in DSSCs. Although the efficiency of ZnS nanoparticles-based solar cell is reported to be low [47], this issue can be tackled by modifying its surface. Dye sensitization of semiconductor is one of the methods that have been employed to enhance the photovoltaic performance of DSSC. An increased efficiency of ZnS based DSSCs is reported by sensitization with different metal dyes [7] and metal-free dyes [9].

2.4 Dye photosensitizers

A dye is a good light harvesting material and is one of the crucial components of DSSCs. Its main function is to capture sunlight photons and supply the electrons to the semiconductor. Excellent light absorption efficiency of the dye is displayed by a

red-shifted absorption spectra of the dye [15]. For an efficient DSSC performance, a dye (sensitizer) should possess the following several requirements, according to Amin N. et al. [2] and Mariotti N. et al [28]:

- ❖ Excellent molar absorption coefficient to enable the use of thinner semiconductor films and still maintain high rate of light absorption.
- ❖ Broad absorption spectrum that cover the whole visible to near-IR region, to cover as many photons as possible.
- ❖ Suitable LUMO and HOMO energy levels for effective electron injection and dye regeneration.
- ❖ Effective anchoring group, for strong binding to the semiconductor and long-term stability
- ❖ Good photostability, to sustain many years of use
- ❖ Should be able to hamper dye aggregation, to avoid the decay of the excited electron to the ground state
- ❖ Lower tendency of charge recombination, i.e. the positive charge resulting after electron injection should be localized on the donor part of the dye, which is far from the semiconductor surface.

Both inorganic and organic dyes have been used as sensitizers for DSSC applications. Inorganic (metal) dyes are complex structures made up of a central metal atom surrounded by ligands, while organic (metal-free) dyes contain no metal atom. Among the metal dyes, ruthenium and zinc based dyes are the common dyes that achieved high DSSC efficiency of 14.3 % [48] and 12.3% [49], respectively. Although Ruthenium based dyes are considered to be the most successful sensitizers in terms of efficiency, its rarity, toxicity and high purification cost have restricted it from applications in DSSCs [2], while Zn based dye is obtained in lower yield [18].

Therefore, great attention has been given to metal-free dyes to be used as alternative to ruthenium-based dyes in DSSCs.

2.4.1 Metal-free (organic) sensitizers

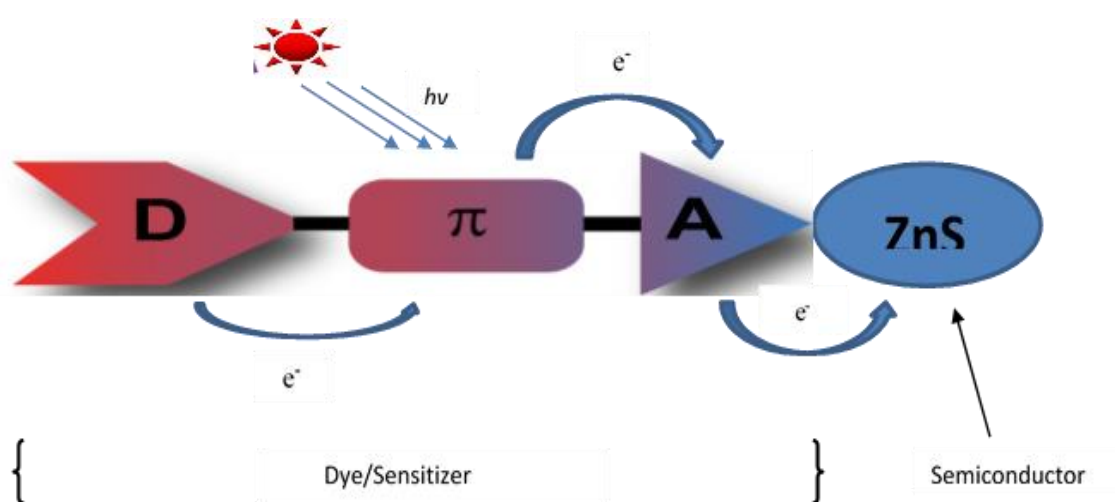
In the last 10 – 15 years, more effort has been dedicated to the preparations and investigations of metal-free dyes for DSSCs, due to its tremendous advantages compared to costly, toxic and limited metal dyes. However, metal-free dyes are also associated with shortcomings such as, strong π -stacked aggregates between the dye molecules and semiconductor surface, low light absorption ability and low stability [50] . Luckily, these issues can be tackled by modifying the structure of the dye molecule.

Metal-free dyes are classified into two different types, the natural and synthetic dyes. Natural dyes are extracted from different parts of the plants and are classified as carotenoids, flavonoid, anthocyanin, chlorophyll etc.[28, 30, 51], while synthetic dyes are manmade dyes prepared from chemical reactions. The application of natural dyes has been considered as promising sensitizer for DSSCs due to their availability, nontoxicity, low cost and energy saving production, and easily extractable [30, 51]. Research on DSSCs based on natural dyes have been studied extensively to enhance its efficiency. From the reviewed articles written by Shelke R.S et al [52], and by Pallikkara A. and Ramakrishna K. [30], the maximum efficiencies of DSSCs based on natural dyes from different plants found is about 3%. Investigation on the co-sensitization of different natural dyes carried out showed better performance of the DSSC, compared to single dye based DSSC [53, 54]. Taya S.A. et al [55] , investigated on fresh and dried natural dyes as sensitizers and the results showed that some fresh sensitizers perform well than dried sensitizers. However, the overall efficiency of natural dyes is reported to be lower than for synthetic dyes due to degradation tendency

by sunlight, and their absorption range in the spectrum is limited (400nm – 700nm) [28]. Thus, the synthetic dyes are considered as favorable over natural dyes sensitizers for DSSCs.

2.4.1.1 Synthetic sensitizer

With its general design of D- π -A configuration, the effectiveness of a metal-free sensitizer depends on the ability of its electron donating and electron withdrawing moieties, as well as the characteristics of a π -bridge. As the light strike the dye molecule on the photoanode of DSSC, the excited electrons from the electron donor to the electron acceptor through the conjugated system of a dye molecule are injected into the conduction band of semiconductor (Scheme 4). While the conjugated system in a dye molecule facilitates intramolecular charge transfer, the electron acceptor ensures an effective electron injection from the dye into conduction band of the semiconductor [14]. The energy gap between the LUMO of the dye and conduction band of semiconductor ensure the electron injection from the dye to the semiconductor [20]. Thus, the dye molecular geometry and alignment with other components of the DSSC have impacts on electron injection.



Scheme 4: Donor - π -linker Acceptor design of metal free dye [19]

Due to limited light absorption ability and low stability of metal-free dyes observed in many researches works on metal-free based DSSCs, researchers are still striving to discover new effective organic dyes for the efficiency enhancement of the DSSCs. The D- π -A configuration of a dye molecular structure has been investigated and found to be limited to narrow absorption of sunlight [11]. Thus, different ways of tailoring the absorption of metal-free dyes have been discovered. These includes, addition of supporting electron donors, electron acceptors and extension of efficient conjugation length [4, 20]. In addition, a sensitizer with suitable conjugated donor and acceptor across the linker is observed to possess a broad absorption band in the visible and near-infrared region [56]. For example, Liu Z. et al. [11] reported on the enhancement of three dyes based on Triarylamine donor and Benzoic acid acceptor, after the addition of auxiliary Benzothiadizole or Diketopyrrolopyrrole acceptor. The addition of these auxiliary acceptors increases the molar extinction coefficient, light absorption ability and photovoltaic performance. In another research work, a comparison between single and double acceptors of Thiophene based dyes was made, and improved light absorption was observed with double acceptor based dye [57]. Wen Y. et al [58] and Kim M.J. Et al. [59] investigated the effect of increasing the conjugation length of dyes in their articles, their results showed higher performance of dyes with extended conjugation linker. Through the tuning of dye molecular structure, different design configuration structures such as, D-A- π -A [60], D-D- π -A [61], A-D- π -D-A [62], A-D- π -A, D- π -A- π -A [15], D- π - π -A etc, have been developed and drawn more attention. From these structural configurations, most of the researchers have reported an increase in the efficiency of these metal-free based DSSCs compared to the general configuration. Although the expansion of π -conjugation may cause dye aggregation through π - π interaction between molecules, incorporation of more anchoring group

was reported to suppress dye aggregation [63]. In addition, the insertion of aromatic ring into the conjugation link facilitates fast electron injection and reduce charge recombination.

Furthermore, the linkage positioning, substitution or addition of electron withdrawing or electron donating group have impacts on the absorption spectrum of a dye. Zang and his co-workers investigated the effect of linkage positioning in D – A organic dye on its efficiency. Linkages were inserted at the ortho, meta and para positions, and it was observed that para position linkage displayed the highest efficiency compared to the ortho and meta positions [64]. The substitution of halogens on oxindole bridged acceptor units showed impacts on the dye efficiency. In this research work, a DSSC based on Bromine substituted oxindole bridged acceptor showed high efficiency than Fluorine and Iodine incorporated dyes. Furthermore, He L.J. et al [65] modified the linkage by incorporating different electron withdrawing groups, and the results showed red-shifted absorption spectra and extended absorption range.

As electron donating groups in metal-free dyes, Diphenylamine, Triphenylamine, Fluorenamine, Phenothiazine, Carbazole, Acetaldehyde, Hydroquinoline, Indoline, Diethylaniline [66–68] and so on, have been used in designing different dye molecules. Among these, Triphenylamine donor has been commonly used and showed promising because of its good donating ability, effective stability and its bulk aryl group help prevents charge recombination by suppressing dye aggregation [63, 68].

The electron acceptor of dye molecules is responsible for efficient electron injection through its anchoring group. Among the acceptors used such as, Acrylic acid, Cyanoacetic acid, Cyanoacrylic acid, Carboxylic acid, Benzimidazole, Acetylene etc., the stable and easily synthesized Cyanoacrylic acid has been one of the widely used as

acceptor moiety, with carboxyl group as the common anchoring group [4, 20]. However, with all the promising metal-free dye moieties discovered so far, the narrow absorption spectrum of metal free dyes, where their peaks often appear in the shorter wavelength region still remain the challenge [69] . Despite this, researchers are still striving to develop new dyes with wide absorption spectra.

2.5 Solvatochromism

In DSSCs, the choice of the best dye solvent is crucial for an effective light absorption. Solvatochromism refer to changes in absorption spectra of dyes with different solvents, due to varied interactions between the dyes and different solvents [70, 71]. Homcaianu M. et al [25] and Weilgus M. et al [72] reported that the position, intensity and the shape of the absorption spectra bands changes for a dye dissolved in different solvents due to difference in polarity. The polarity of a solvent is measured by its dielectric constant, which is a measure of the solvent ability to partly cancel the field strength of the electric field of particles added to it. The higher the dielectric constant, the more polar the solvent is [73]. Table 2 below shows the dielectric constants of some common solvents used in this research, from more polar to low polar solvent.

Table 2: Dielectric constants of common solvents [73]

Name of the solvent	Formula	Dielectric Constant (ϵ)
Dimethylsulfoxide (DMSO)	C ₂ H ₆ OS	46.68
Acetonitrile	CH ₃ CN	37.50
Dimethylformamide (DMF)	C ₃ H ₇ NO	36.71
Methanol	CH ₃ OH	32.70
Ethanol	C ₂ H ₅ OH	24.55

Acetone	C ₃ H ₆ O	20.70
Tetrahydrofuran (THF)	C ₄ H ₈ O	7.58
Ethyl acetate	CH ₃ COOC ₂ H ₅	6.02
Chloroform	CHCl ₃	4.81

The solvatochromism effect of dye samples are analyzed with UV-vis measurement, and classified as bathochromic (Positive or red) or hypsochromic (Negative or blue) shift. A dye solution that undergoes a bathochromic shift, its shortest wavelength absorption band shift to longer wavelength while for a dye solution that shows a hypsochromic shift, its absorption band shift to shorter wavelength [72]. Twafik A. et al [23] investigated the solvatochromic effect of three dyes in nine different solvents. The absorption maxima of the three dyes shifted positively or negatively in different solvents, with increasing polarity. Furthermore, Mamdouh S. et al [74] analyzed the solvatochromic behavior of some azo based dyes and found that the chemistry of the solvents has impacts on solvatochromic behavior.

The effect of solvent on the absorption spectra depends on the light-absorbing molecules, charge transfer between the donor and acceptor of the molecule and the nature of electronic transition [75]. The UV-vis spectra of dye compounds arise from π - π^* and/or n - π^* transitions, due to π - electrons and the presence of heteroatoms with lone pair electrons. Generally, the n - π^* and π - π^* electronic transitions is associated with weak band (low intensity) and strong band (high intensity) in the UV-vis region, respectively [76]. It is observed that the λ_{\max} of the absorption spectra of dyes shift differently with increasing solvent polarity. When polar solvents aid stabilization of a ground state than of an excited state, the transition energy becomes larger, causing

hypsochromic shift and in bathochromic shift, the excited state is better stabilized than the ground state in polar solvent, lowering the transition energy [24, 76]. This is because the dipole moment of the excited state is larger than the dipole moment of ground state in bathochromic shift and the dipole moment of the excited state is smaller than that of the ground state in the case of hypsochromic shift [77, 78].

Solvatochromism depends on solvent molecules, the ability to interact with dye molecules. There are general solute-solvent and specific chemical interactions that may occur between dye and solvent molecules [77]. The general solute-solvent interactions involve the dipole moment of the molecules. When the dipole moment of the molecules increases upon excitation, polar solvent will stabilize the excited state, leading to red shift. Equally, when the dipole moment of the molecules decreases upon excitation, it stabilizes the ground state and thus, blue shift occur.

Specific chemical interactions between the chromophore (dye) and solvent molecule are such as hydrogen bonding and charge transfer interactions. In hydrogen bonding, the energy levels are lowered by the interaction of a positively polarized hydrogen atom of the solvent with a lone pair of electrons on a chromophore atom in the ground or the excited state. During electronic transition, charges may move away or toward the chromophore atom leading to blue shift or red shift, respectively [77].

2.6 Isatin and Thiazole based dyes

Isatin (Indoline-2,3-dione) is an Indole-based compound, used in synthesis of different heterocyclic and carbocyclic compounds. The study of this compound reactivity is more focusing on its electron withdrawing carbonyl group, a good electrophile due to amide moiety present [79]. Hydrazines, Indoles, Oxindoles, Quinolones etc., are some of Isatin derivatives that have been studied mostly for biological activities such as,

anti-inflammatory, analgesic, antimicrobial, antimalarial, anticancer and antioxidant [80]. However, the synthesis of Isatin derived organic dyes as sensitizers in DSSCs has not received much attention. Tangire YS et al. [81] reported on different halogen substituted Oxidole based organic sensitizers (Isatin derived) that were synthesized for DSSCs applications, and a cell based on bromine incorporated dye showed higher efficiency. Different Thieno[2,3-*b*]indole based dyes were synthesized and showed an effective absorption in the visible spectral range (440 -740nm) and high efficiency of 14.2% DSSCs was also reported by co-sensitizing Thieno[3,2-*b*]indole based organic dyes with a porphyrin sensitizer [82]. The results from these reports indicate that Isatin derived organic dyes are promising candidates of good DSSC sensitizers, hence more research is needed on designing new Isatin derived organic dyes for DSSCs applications.

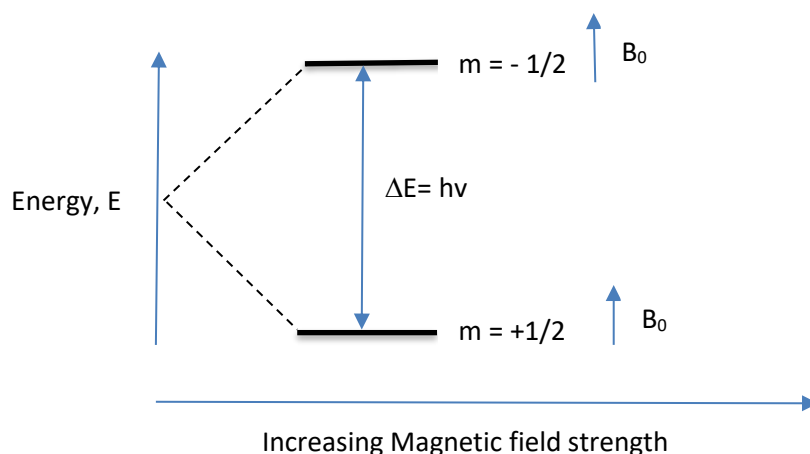
On the other hand, Thiazoles are five membered heterocyclic compound and its derivatives displayed many chemical and biological activities. It act as electron acceptor due to its electron withdrawing nitrogen of the imine group and the synthesis of dyes containing Thiazole moiety emerged due to their effectiveness as photosensitizers in DSSCs [83]. Rody S.R et al. [84] reported of a dye with three units of Thiazole as the best photosensitizer among the eight coumarin dyes studied by varying the π -bridge with different Thiophene and Thiazole units.

2.7 Theoretical background of experimental instrumentations

2.7.1 ^1H NMR Spectrophotometry

^1H NMR stands for proton nuclear magnetic resonance spectroscopy. It is a technique based on the magnetic properties of proton nuclei and employed to determine the structures of organic molecules. Nuclei of some atoms have a magnetic property

characterized by nuclear spin quantum number I , which may have integers such as $I = \frac{1}{2}, 1, \frac{3}{2}, 2$, etc [85, 86]. However, nuclei with $I = \frac{1}{2}$ is reported to have favorable properties and attracts more attention [86]. ^1H NMR spectrometer measure the energy required to change the direction of magnetic nuclei of sample protons in an applied magnetic field and cause transition of magnetic nuclei between possible energy levels. These possible energy levels are restricted to two angular quantum numbers, $m = \pm \frac{1}{2}$. Thus, when a sample is exposed to radio waves radiation, the energy relate to the spin state transition of specific nuclei cause excitation of nuclei from lower $+\frac{1}{2}$ (α) spin state to higher state $-\frac{1}{2}$ (β) spin state [85–87]. The transition energy ΔE (energy difference between spin energy states), at which any signal in the ^1H NMR spectrum appear corresponds to the frequency of the absorbed radio waves of electromagnetic radiation and depends on the strength of the applied magnetic field B_0 [87, 88].



Scheme 5: Energy levels of $I = 1/2$ spin states by external magnetic field B_0

For a proton nucleus to flip from α spin state to β spin state, a corresponding RF (radio frequency) energy is absorbed, and when the nucleus falls back from β spin state to stable α spin state, RF energy is emitted. Thus, the constant flipping of nucleus back and forth between the spin energy state creates resonance.

In ^1H NMR, the frequency at which protons within a sample molecule absorb is different according to the surrounding chemical environment of adjacent atoms and chemical bonds within the molecule [85, 88]. This variation is called chemical shift (δ). Experimentally, chemical shift is the difference in observed shift between a sample and the reference, divided by spectrometer frequency.

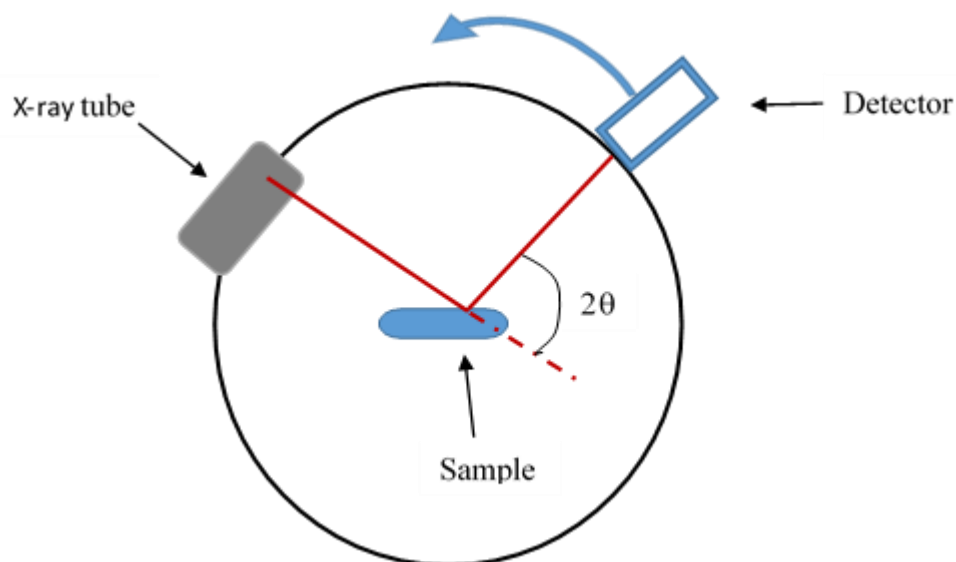
$$\text{Chemical shift, } \delta = \frac{V_{\text{sample}} - V_{\text{ref}}}{V_{\text{nmr}}}$$

Where V_{sample} is the frequency of the sample nucleus, V_{ref} is the frequency of reference nucleus and V_{nmr} is the spectrometer frequency.

In the spectrum, the proton signals indicate the frequency at which specific nucleus absorb radio waves. These signals are distributed along the frequency axis, characterized by their chemical shifts and the intensity of the signal peak corresponds to the number of protons giving rise to the signal [85]. The position of each proton signal on the frequency axis is determined by the shielding effect of the adjacent nucleus by the orbiting electron. Protons shielded to external magnetic field appear up field (right side) and protons de-shielded appear downfield [88]. The shielding effects depends on the electronegativity of atoms next to the protons in a molecule.

2.7.2 XRD spectrophotometry

X-ray diffraction is an analytical technique used to measure the structural properties such as lattice parameters, crystalline size and the orientation phase composition of the material [89]. A sample placed at the center of an instrument is irradiated with a collimated beam of x-ray as incident. The x-ray tube and the detector move in a circular motion around the sample, and the signal coming from the sample is recorded and graphed [85]. This is illustrated in scheme 6.

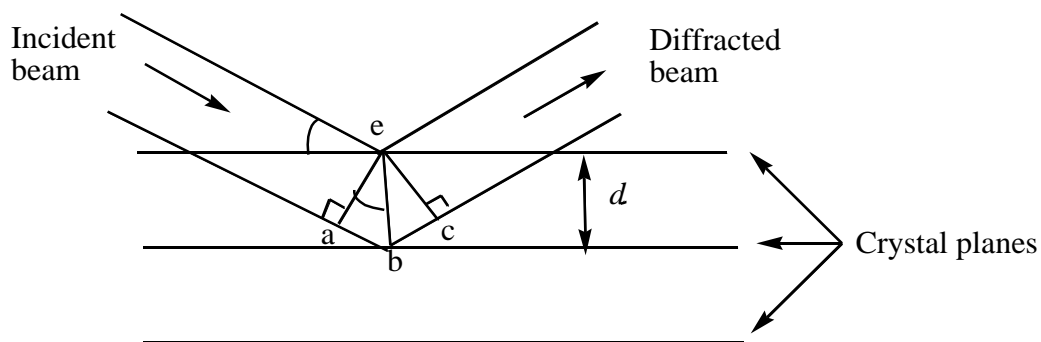


Scheme 6: Working illustration of XRD

At a particular angle, the x-rays reflected from a set of crystal planes gives a diffraction pattern. The angle at which the x-ray encounters the sample and are diffracted are designated by theta θ . In a crystal, the repeating arrangement of atoms form different planes separated by well-defined distances. If the distance between atoms is similar to the wavelength of the x-ray, the x-ray is scattered in random directions. When the parallel beam of both incident and diffracted rays each causes a path difference of ab or bc (Scheme 8), then the total path difference is $ab + bc$. The crystal diffraction is explained by Bragg's law which is expressed as

$$2d\sin\theta = n\lambda \quad [85]$$

In this equation, d is the atomic spacing, θ is the angle of diffraction and n is the integer (i.e order of diffraction). This implies that for diffraction to occur, the total path difference should be a whole number of wavelengths. That is, $ab + bc = n\lambda = 2d\sin\theta$

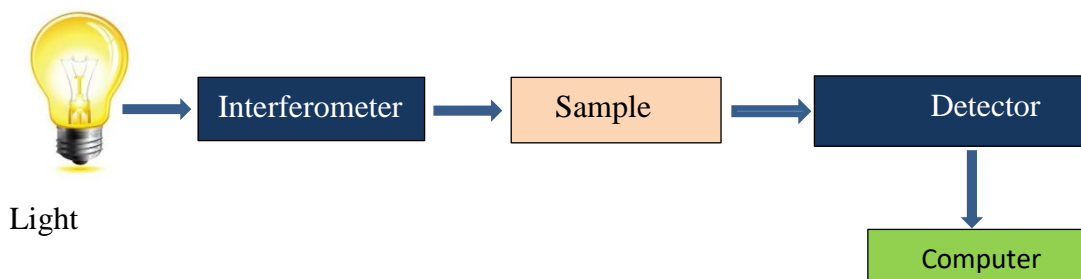


Scheme 7: X-ray diffraction by crystal planes

Each material has its own diffraction pattern and each peak in the spectrum corresponds to a particular atomic plane. As the distance between atoms (d) decreases, the $\sin\theta$ increase or vice versa, leading to peaks at different positions in the spectrum. The peak intensity is determined by the position of atoms within the lattice, while the peak width depends on the crystalline size [90]. It is reported that broad peaks correspond to smaller crystalline size [90].

2.7.2 FTIR spectrophotometry

FTIR is an advanced infrared spectroscopy utilized by analysts to identify organic compounds, by providing quality infrared spectra. The instrument used to obtain the spectra of compounds is called FTIR spectrophotometer, which have the light source, collimator (beam splitter), interferometer, a sample and the detector and readout as key components [86, 91] . Scheme 8 presents the flowchart of FTIR spectrophotometer working principles.



Scheme 8: Working principle of FTIR spectrophotometer

When the incident IR beam from the source enters the interferometer, it produces a unique beam signal that has all IR frequencies. The beam of light is transmitted when the sample is exposed to it from the interferometer and specific frequencies of energy are absorbed and measured by the detector [91]. Finally, the measured signal is sent to the computer and presented as an infrared spectrum. The transmitted IR radiation frequencies measured provide information on the values of absorbed frequencies. From the relationship $A = -\log T$ where A is absorbance and T is transmittance, the absorbance can be calculated from percentage transmittance using the formula:

$$A = \log(100/\%T) \quad [85]$$

The incident radiation absorbed by the sample is associated with energy that causes the atoms in the molecules to vibrate [92]. This is the energy at which the bands appear in the IR absorption spectrum and correspond to the vibrational frequency of the sample molecular fragment. That is,

$E = h\nu = h\frac{c}{\lambda}$, where h is Planck's constant, ν is the frequency of photon, c is the speed of light and the wavelength λ of photon.

IR bands can be classified as narrow for thin and pointed bands, or broad for wide and smooth bands. They can also be classified as strong (s), medium (m) or weak (w),

depending on the intensity of the bands [93]. However, the intensity of the bands is determined by magnitude of the dipole moment associated with the bond of specific molecular fragment [85, 93]. Since the dipole moment of molecular bond is necessary for IR absorption, not all bonds are IR active and hence only polar bonds display bands in IR spectrum. Strong polar bonds display strong IR bands, weak and symmetric bonds display weak or invisible bands.

In addition, the spectra obtained from FTIR spectrophotometer gives information about the presence or absence of specific functional groups of a particular chemical compound. The infrared radiation is found in the range of $4000 - 400 \text{ cm}^{-1}$ of electromagnetic radiation [86]. In IR spectrum, there are two regions; the fingerprint region and functional group region. The fingerprint region ranges from $1600 - 400 \text{ cm}^{-1}$ and it produce molecular fingerprint which is used to compare samples, and the region from $4000 - 1600 \text{ cm}^{-1}$ display information on functional groups of sample molecule [86]. Two different compounds cannot display same IR spectra. However, the IR spectra may be affected by the environment, such as change in the level of carbon dioxide and water vapor, while taking measurements [85]. This may result in observed absorption peaks of CO_2 and water vapor in the samples IR spectra. The reported IR absorption peaks of CO_2 and water vapor in different IR samples were observed in the range of $2380 - 2280 \text{ cm}^{-1}$ and $3900 - 3500 \text{ cm}^{-1}$, respectively [92]. The table 3 presents general IR spectrum vibrational frequencies of some chemical bonds found in the synthesized dye structures of the present research work [85, 92].

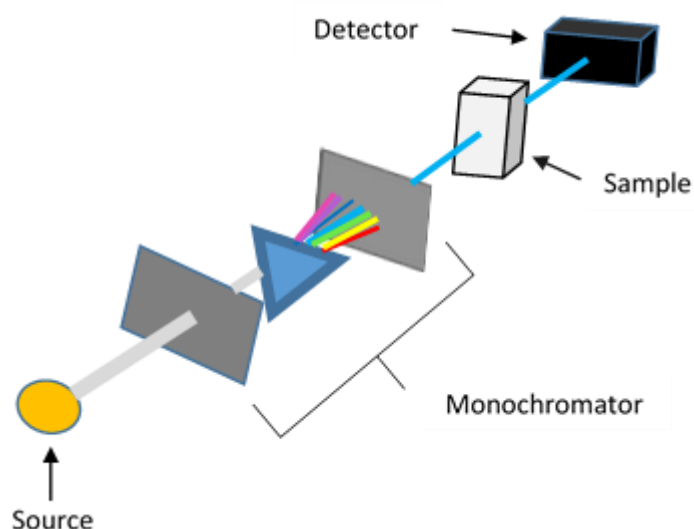
Table 3: IR vibrational frequencies of some chemical bonds

Name of chemical bond	Vibrational Frequencies (cm ⁻¹)
N–C stretching	1360 – 1250,
N–H (Heterocyclic)	3200 – 3500
O–H (Phenol)	3500 – 3000
C=O (ketone)	1850 – 1650
O–C	1300 – 1000
C=C (aromatic) and C=N	1600 – 1400
C–H (bend Aromatic)	1275 – 690
C-H (Aromatic stretching)	3100 – 3000
S–C stretching	700 – 600

2.7.3 UV-Vis spectrophotometry

UV-vis spectroscopy is a method of investigating how light interact with matter in the range of near ultraviolet to near infrared region of electromagnetic spectrum. This technique has been applied in different areas such as in pharmaceutical, environment and food analysis to determine the organic compounds [94]. The UV-vis region range from about 190 – 200nm and is divided into two regions, the ultraviolet region ranging 190 - 400nm and the visible region from 400 - 800nm of the electromagnetic spectrum [94]. Processes such as absorption, emission and transmission occur when electromagnetic light interact with matters. However, the absorbance spectrum of a

sample (matter) is determined by measuring its absorbance. The key components of the spectrophotometer, for measuring UV-vis light absorbance of a sample are; the source (UV and visible lamp), a monochromator (beam splitter), sample container, a detector and the recorder [94, 95]. Simply, a sample is placed between the light source and the detector, and the intensity of light absorbed by a sample when a beam of light pass through it is measured. The light absorbed is associated with energy given by $E = hv$, where E is the energy, h is plank's constant and v is the frequency of radiation (Scheme 9).



Scheme 9: UV - Vis working principle

A group of atoms in a molecule that absorb light of a particular wavelength are known as chromophores. For a molecule to absorb light in the range of 190 – 800nm, it should contain either π bond or lone pair atoms. The energy absorbed by the chromophore in the uv or vis region is used to excite the electrons from the HOMO (π bonding orbitals or non-bonding orbital) to the LUMO (π anti-bonding orbital) [86]. The energy difference between the HOMO and the LUMO is called energy gap. That is, the energy difference between the ground state and the excited state.

$$\Delta E = E_1 - E_2 = h\nu$$

The two electronic transitions; $\pi - \pi^*$ and $n - \pi^*$ require less energy to excite an electron to its excited state, [85, 86, 96]. Sample molecules that undergo these two electronic transitions absorb light in the near UV to near IR region of the spectrum. According to James W. R., Eileen M.S. and George M. F. [85], the organic compounds that contain Nitrogen, Oxygen and Sulphur generally contain nonbonding electrons (lone pairs) and hence absorb UV/Vis radiations.

Beer Lambert's law explained the principle of determining the absorbance. This law states that the absorbance of a sample at a given wavelength is proportional to its molar absorptivity, the thickness and the concentration of a sample [86, 97]. Mathematically, the equation that explains Beer Lambert law is:

$$A = \log\left(\frac{I_0}{I}\right) = \epsilon cl$$

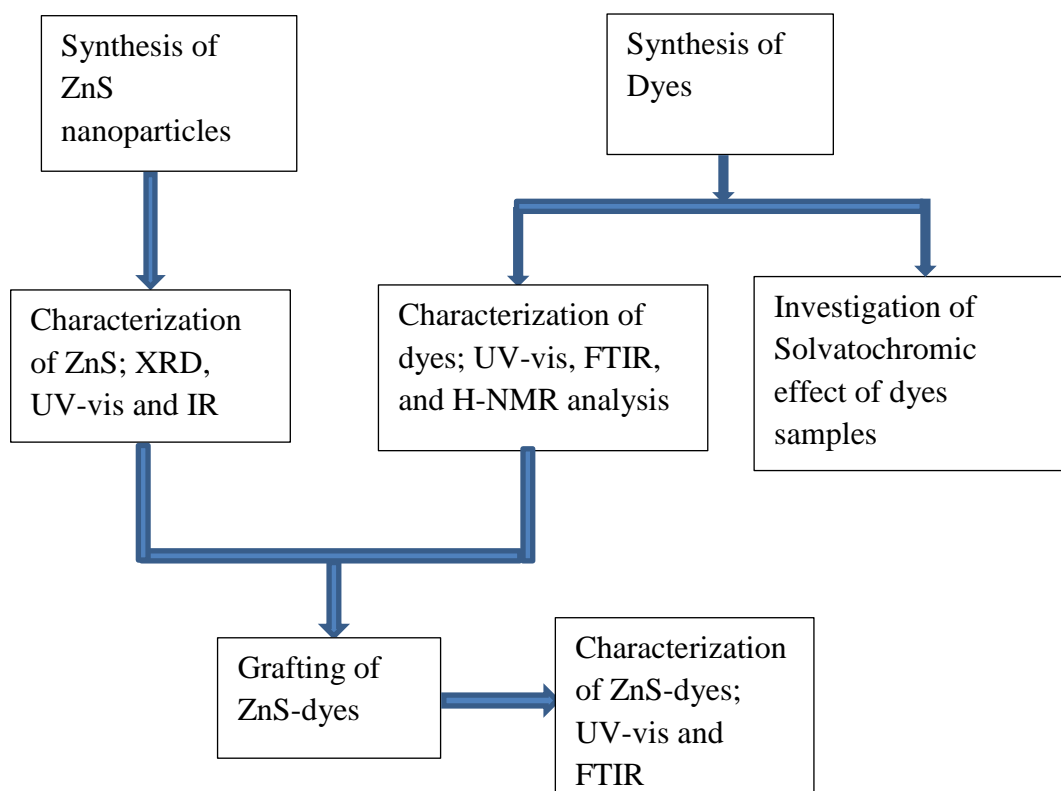
Where A is the absorbance, I_0 is intensity of incident light (light entering the sample and reference cell), I is transmitted light intensity through the sample, ϵ is absorptivity coefficient of a sample, c is the concentration of the sample, and the thickness or path length of the sample where light is transmitted through to the detector. Higher peak in the absorption spectrum results from high concentration of the sample, and low peak results from low concentration of the sample. In addition, the transmittance T is the ratio of transmitted light intensity over the intensity of incident light, i.e. $T = \frac{I}{I_0}$.

Thus, absorbance has a logarithmic relationship to transmittance.

CHAPTER 3: RESEARCH METHOD

3.1 Research design

Zinc Sulphide nanoparticles and five designed metal-free dyes were synthesized. The ZnS nanoparticles were characterized using XRD, UV-vis UV-vis and FTIR spectroscopy, while the five metal-free dyes and grafted ZnS-dye samples were characterized using UV and FTIR spectroscopy. Solvatochromic effect of dyes were investigated and their optical properties were studied. The flow chart below shows how the research was designed.



Scheme 10: Flow chart of Research design

3.1.1 Chemicals required for synthesis

The chemicals used in this research work were procured from Sigma Aldrich and are as follow:

Sodium Sulphide, Zinc (II) acetate, 2-hydroxy-naphthaldehyde, p-Phenylenediamine, Isatin, 2-Aminothiazol, 2-Thiophenecarboxaldehyde, 2,6-diaminopyridine, 1,5-Diaminonaphthalene, Acetic acid, Ethanol, Methanol, Acetone, N, N-Dimethyl formamide (DMF), Dimethyl sulfoxide (DMSO), Tetrahydrofuran (THF), Acetonitrile, Chloroform, Ethyl acetate. Their percentage purity is in the range of 95 -100 %.

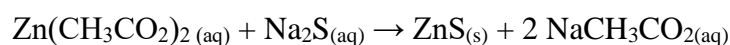
3.2 Research instruments

The following instruments have been used in this work for analysis of the synthesized materials. The XRD to check the purity and crystallinity of the ZnS sample. UV-vis spectrophotometry has been used to study the photo response properties of dyes, and the FTIR and ¹H-NMR spectroscopy were used to confirm the identity of dye structures. In addition, the FTIR was also used to provide proof of dye grafting on the ZnS nanoparticles.

3.3 Procedures

3.3.1 Synthesis of ZnS

ZnS nanoparticles were synthesized using Zinc Acetate and Sodium Sulphide, by precipitation method and characterized, according to the procedures reported by Nosheen E. et al. [7]. To this solution, a 50 mL aqueous solution of Sodium Sulphide was added dropwise under continues stirring. The mixture was then stirred for overnight and centrifuged at 400 rpm, at the temperature of 25°C, for 5 minutes. After decantation, the white precipitate was washed with 35 mL of methanol and kept in the desiccator for drying. The chemical reaction equation for the synthesis of ZnS is:

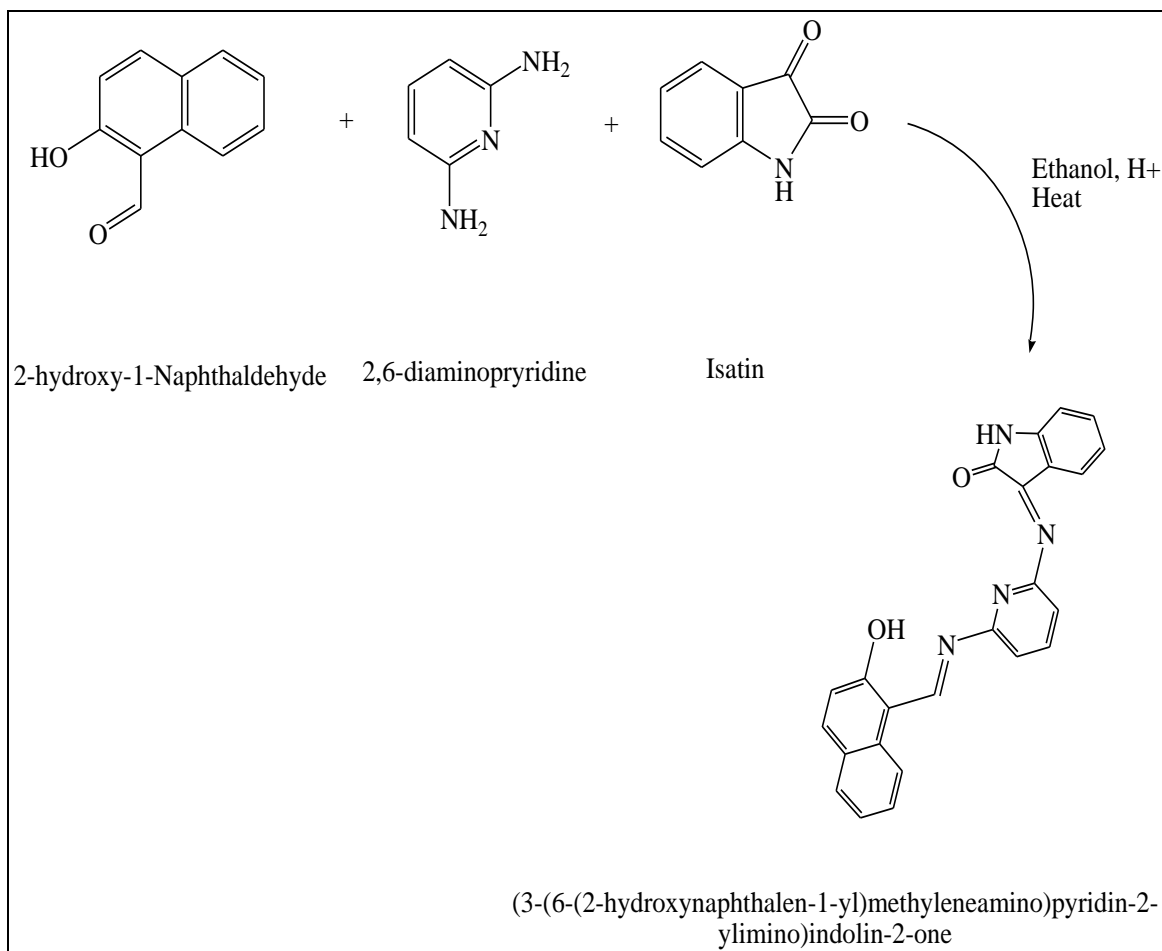


3.3.2 Synthesis of metal-free dyes

The metal-free dyes were prepared by Schiff base condensation and characterized by evaluating the results obtained from the instruments used.

3.3.2.1 Synthesis of Dye1

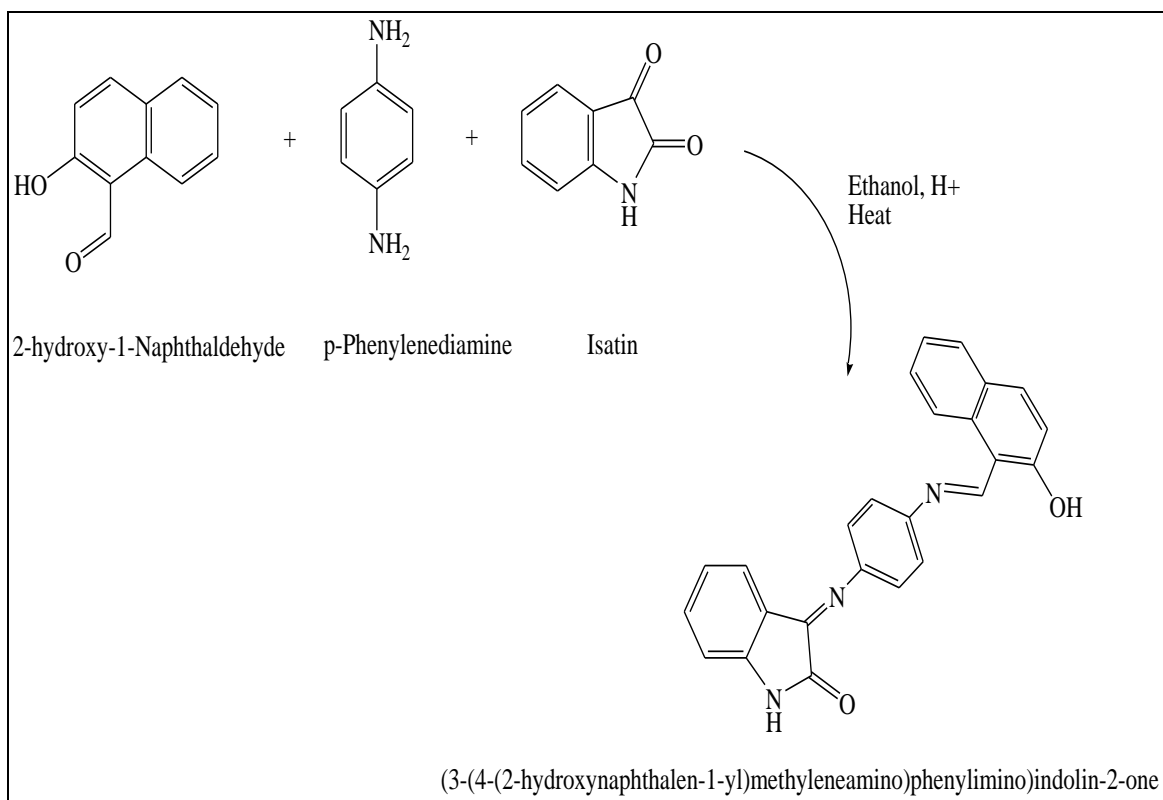
Three solutions of 2-hydroxy-1-Naphthaldehyde (1.0004g, 0.0058 mol), 2,6-diaminopyridine (0.6340g, 0,0058 mol) and Isatin (0.8548g, 0.0058 mol) in 15 mL Ethanol each were prepared. To a solution of 2-hydroxy-1-Naphthaldehyde, a solution of 2,6-diaminopyridine was added followed by a solution of Isatin, in a round-bottom flask. Four drops of acetic acid were added and the solution was refluxed while stirred at the temperature of 50 – 60 °C range, for about 4 hours. A brown precipitate formed was collected by suction filtration and kept in the desiccator for drying. The Scheme 11 shows the schematic reaction equation.



Scheme 11: Reaction mechanism of Dye1

3.3.2.2 Synthesis of Dye2

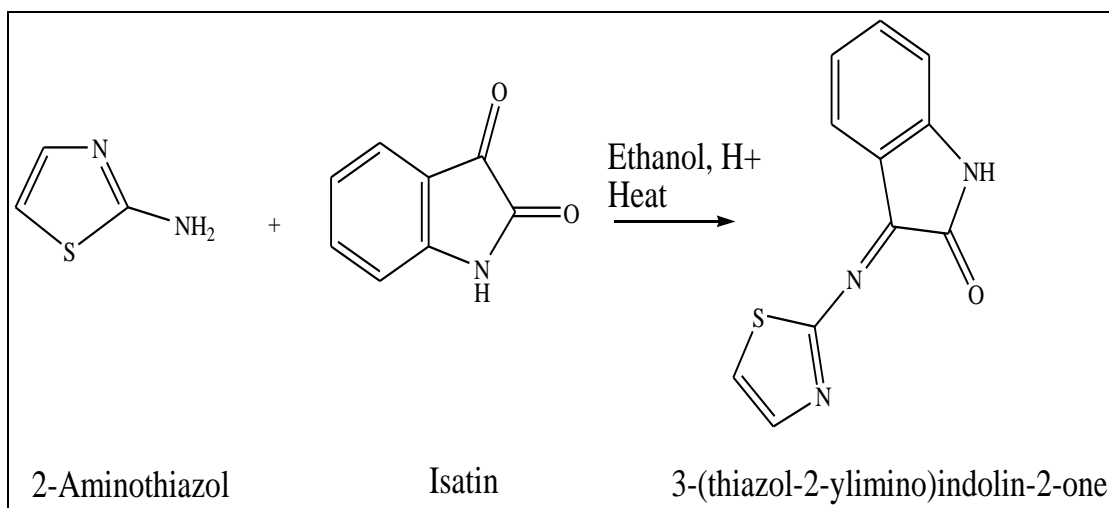
Three solutions of 2-hydroxy-1-Naphthaldehyde (1.0004g, 0.0058 mol), p-phenolyenediamine (0.6281g, 0.0058 mol) and Isatin (0.8548g, 0.0058 mol) in 15 mL Ethanol each were prepared. To a solution of 2-hydroxy-1-Naphthaldehyde, a solution of p-Phenolyenediamine was added followed by a solution of Isatin, in a round-bottom flask. Four drops of Acetic acid were added and the solution was refluxed while stirred at the temperature of 50 – 60 °C range, for about 4 hours. An orange precipitate formed was collected by suction filtration, washed with warm and cold Ethanol, and kept in the desiccator for drying. Scheme 9 presents the synthesis of Dye2.



Scheme 12: Reaction mechanism of Dye2

3.3.2.3 Synthesis of Dye3

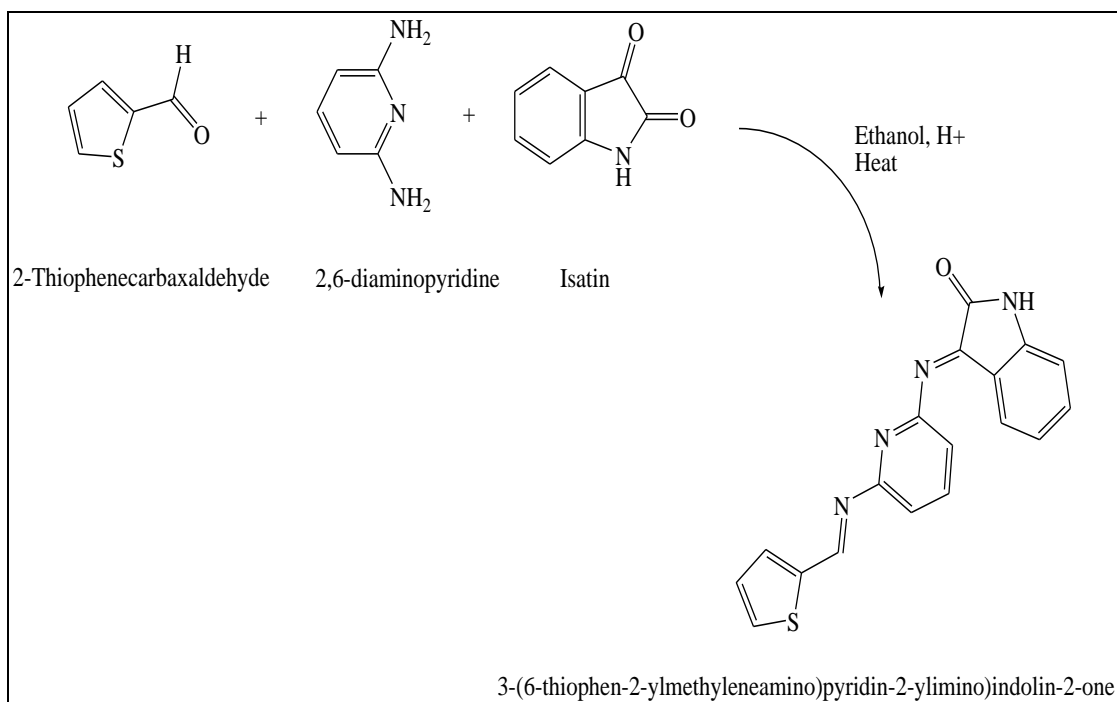
To a solution of 2-Aminothiazol (1.0003g, 0.0010 mol) in 20 mL Ethanol in a round bottom flask, a 20 mL solution of Isatin (1.4692g, 0.0010 mol) in Ethanol was added. Four drops of Acetic acid were added and the mixture was refluxed for about 5 hours. After, the solution was kept in fridge overnight for crystallization. The precipitate formed was then separated by suction filtration, washed with Ethanol and kept in the desiccator for drying.



Scheme 13: Reaction mechanism of Dye3

3.3.2.4 Synthesis of Dye4

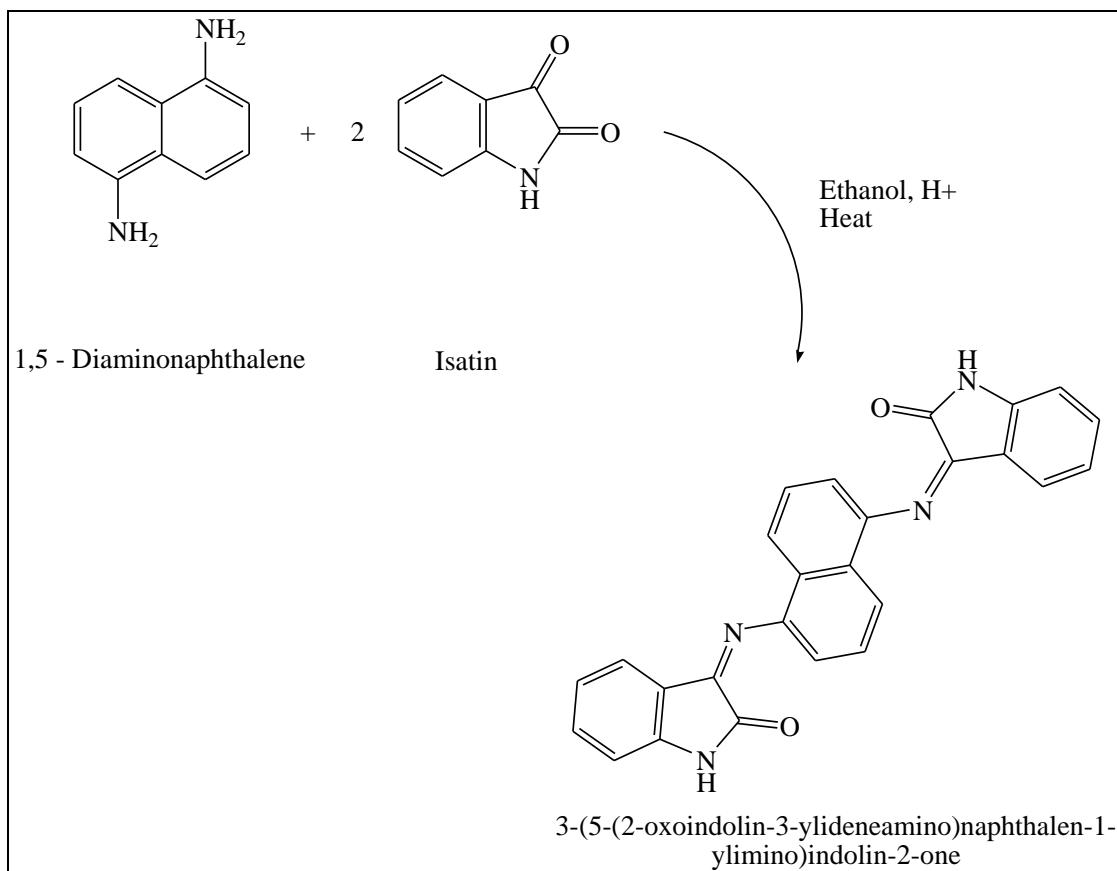
To a solution of 2-Thiophenecarboxaldehyde (1.0002g, 0.0089 mol) in 15 mL Ethanol in a round bottom flask, 15 mL solution of 2,6-diaminopyridine (0.9731g, 0.0089 mol) was added, followed by the same volume of Isatin (1.3120g, 0.0089 mol) in Ethanol. Four drops of Acetic acid were added and the mixture was refluxed for about 4 hours. A dark brown precipitate was formed, filtered and washed with hot Ethanol. The precipitate was kept in the desiccator. Scheme 11 presents the schematic of the synthesis of 3-(6-(Thiophen-2-ylmethyleneamino)pyridin-2-ylimino)indolin-2-one .



Scheme 14: Reaction mechanism of Dye4

3.3.2.5 Synthesis of Dye5

Two solutions of 1,5-Diaminonaphthalene (1.0002g, 0.0063 mol) and Isatin (1.8600g, 0.013 mol) in 20 mL Ethanol each were prepared. A solution of Isatin was added to a solution of 1,5-Diaminonaphthalene in a round bottom flask, followed by four drops of Acetic acid. The reaction mixture was refluxed for 3 hours and the red-brownish precipitate was filtered, washed with Ethanol and kept in the desiccator for drying.



Scheme 15: Reaction mechanism of Dye5

3.3.4 Preparation of solvatochromism dye samples

Solutions of each dye were prepared in different solvents, with same concentration (1×10^{-5} M) for absorption measurements. The solvents used are Methanol, Ethanol, Acetone, Acetonitrile, DMSO, Chloroform, THF, Ethyl acetate and DMF.

3.3.5 Characterization

3.3.5.1 ZnS nanoparticles characterization

A sample of ZnS nanoparticles in sodium hydroxide solution was prepared and the XRD ZnS spectrum was recorded using a Bruker D8 Advance X-ray diffractometer with Cu $\text{-K}\alpha$ radiation ($\lambda = 1.5406 \text{ \AA}$) in the 2θ range of $10 - 80^\circ \text{C}$. About 0.1 g of each solid dyes and ZnS nanoparticles were crushed into powder and their vibrational

frequencies were measured using a FTIR spectrometer. The spectrum was used to confirm the structures of ZnS. Characterization of ZnS nanoparticles by UV-vis spectroscopy was carried out by preparing solutions of three different concentrations (0.05g/L, 0.5g/L, 1g/L) of ZnS nanoparticles in Methanol solution to determine the optimum concentration. The transmittance spectra of each solution were recorded.

3.3.5.2 Metal-free dyes characterization

The ^1H NMR spectrophotometer was used to confirm the structure of the dye compounds. The FTIR spectra of powdered solid dyes were recorded to determine and confirm the vibrational frequencies of the dye compounds. For UV-vis characterization of dyes, three different concentrations (0.1mM, 0.3mM and 0.5mM) of each dye solutions were prepared and their absorbance spectra were measured by UV-vis spectrophotometer. The absorption spectra were recorded using 1 cm quartz cuvette at room temperature, over the wavelength range of 200 – 800 nm. Background correction was done for all the spectra by taking the absorbance of the solvent, for each measurement.

3.3.6 Fabrication and characterization of grafted ZnS-dye samples

Solutions of 0.1mM and 0.3mM concentrations of dyes were prepared each in its best solvent, determined from solvatochromism analysis. To 10 mL of each dye solution, 1g of ZnS powdered nanoparticles was added. The solution was stirred for 24 hours and centrifuged at 3000 rpm for 5 minutes. The residue (grafted ZnS-dye) was then washed with the solvent and left on air to dry. For characterization, 0.3mM solution of each grafted ZnS-dye was prepared and the absorbance spectrum of each solution was measured using a UV-vis spectrophotometer.

CHAPTER 4: RESULTS AND DISCUSSIONS

White crystals of ZnS nanoparticles and five different organic (metal-free) dyes were synthesized. The sample pictures of powdered ZnS nanoparticles and dyes are shown in the table in appendix A. All the synthesized materials were kept in the desiccator, at room temperature.

4.1 Grafted ZnS-dye Samples

The grafted ZnS-dyes samples were characterized by FTIR and UV-vis absorption spectroscopy. Each dye of two different concentrations (0.1mM and 0.3mM) was grafted on 1g of powdered ZnS nanoparticles. The picture below is some of the samples of grafted ZnS nanoparticles.

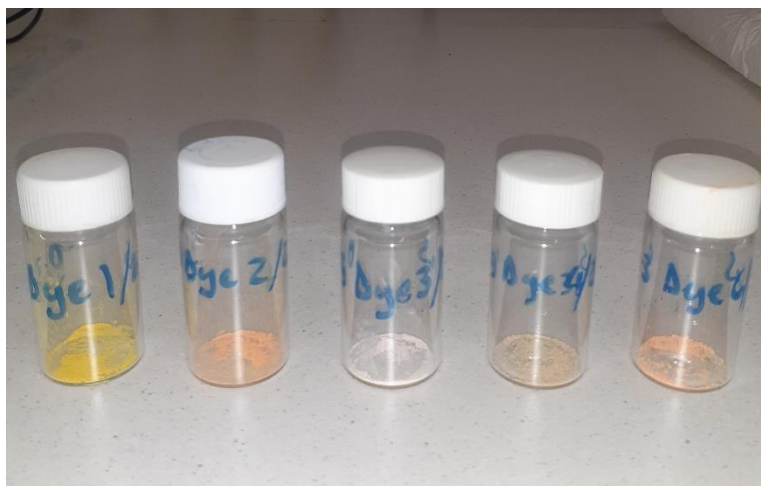


Figure 2: Grafted ZnS-dye1 to ZnS-dye5 samples (from left to right)

The change of color for ZnS nanoparticles from white to different colors may be an indication that dyes were successfully grafted on ZnS nanoparticles. The color of ZnS with the synthesized dyes were almost similar to the original color of the dyes. However, for the grafted ZnS-3-(thiazol-2-ylimino)indolin-2-one, the color did not change much and this is attributed due to very little or no dyes were successfully grafted on ZnS nanoparticles [98]. This may be due to weak molecular interactions

between ZnS nanoparticles and dyes or that the time for grafting was not enough for these two dyes. In addition, the grafted ZnS-dyes sample that were prepared with 0.1mM concentration were light in colors compared to the ones prepared with 0.3mM concentration. Hence, the grafted ZnS-dyes samples prepared with 0.3 mM dye concentrations was used for further investigation.

4.2 ¹H NMR spectral interpretation of dyes

The ¹H NMR spectra of the dyes are shown in the appendix B and the data extracted are given in the table below.

Table 4: H NMR Chemical shifts, (ppm) of Dyes

Dyes	¹ H Chemical Shifts, δ (ppm)				
	OH	NH	CH (Benzylidene)	CH (Protons of aromatic rings on oxindole / Benzene / pyridine/Naphthalene	Protons on thiazole rings
Dye1	15.2	10.0	8.2	6.7- 7.8	-
Dye2	15.2	10.0	8.4	7.5 – 8.0	-
Dye3	-	8.25	-	6.7 – 7.5	7.5 – 8.0
Dye4					
Dye5					

For dye 1, chemical shift δ in ppm, were observed at 15.2 (s, OH); 10.0 (s, 1H, NH); 8.2 (s, 1H, CH benzylidene); the range 6.7- 7.8 ppm are protons of the Aromatic rings

on Isatin, Pyridine and Naphthalene moiety. Chemical shift for Dye2 were observed at 5.2 (s, OH), 10.0 (s, 1H, NH), (s CH benzylidene), while protons of aromatic rings on Isatin, Pyridine and Naphthalene moiety occur in the range 7.5 -8.0 ppm. Signals of ^1H NMR spectra for all dyes were identified and recorded in the table above.

4.3 XRD analysis of ZnS

The analysis was executed to determine the crystalline structure and phase formation of Zinc Sulphide nanoparticles. The diffraction peaks at 2θ were detected at around 29° , 48° and 58° , which correspond to the reflection from (111), (220) and (311) lattice planes, respectively (Fig. 3). These XRD pattern revealed the cubic phase crystal structure of ZnS nanoparticles. Sharp peaks indicate a well crystalline form of ZnS, and broad peaks correspond to smaller particles. The results agree with the literature. Nosheen E. et al. [7], Bera K. et al.[41], Balavijayalakshmi and Manju S.[99], and Iqbal A., et al.[100], reported the XRD analysis of ZnS nanoparticles and similar diffraction pattern and peaks were observed. Sharp and broad peaks were also reported and revealed the Zinc blende cubic phase of ZnS nanoparticles.

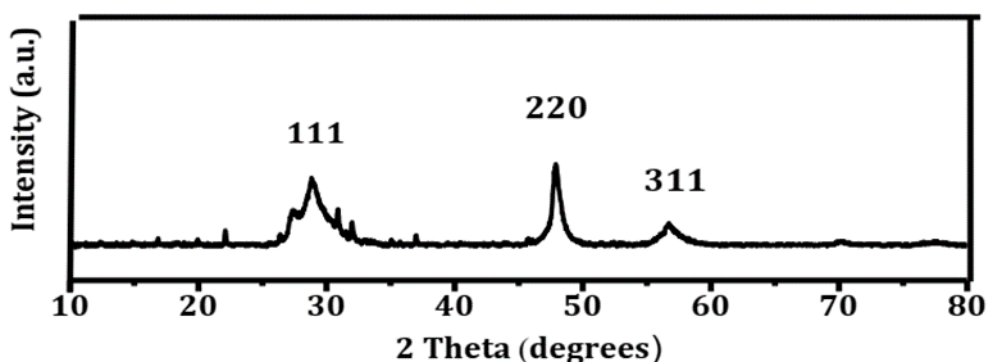


Figure 3: XRD pattern of ZnS

4.4 Analysis of vibrational Frequencies

4.4.1 FTIR transmittance spectrum: ZnS

The FTIR spectrum of ZnS is shown below. The peak that appears at 2980 and 2335 cm^{-1} correspond to C-H and O=C=O stretches respectively. Peak signals at 1651, 1564 and 1421 cm^{-1} can be related to C=O stretch, O-H bend and N-H bending. All these may be due to the presence of traces of solvents, moisture and CO_2 from the surrounding. The vibrational peaks at 953 and 671 cm^{-1} are characteristic absorption of ZnS bond. All the peaks observed are in close agreement with that is reported [7, 90]

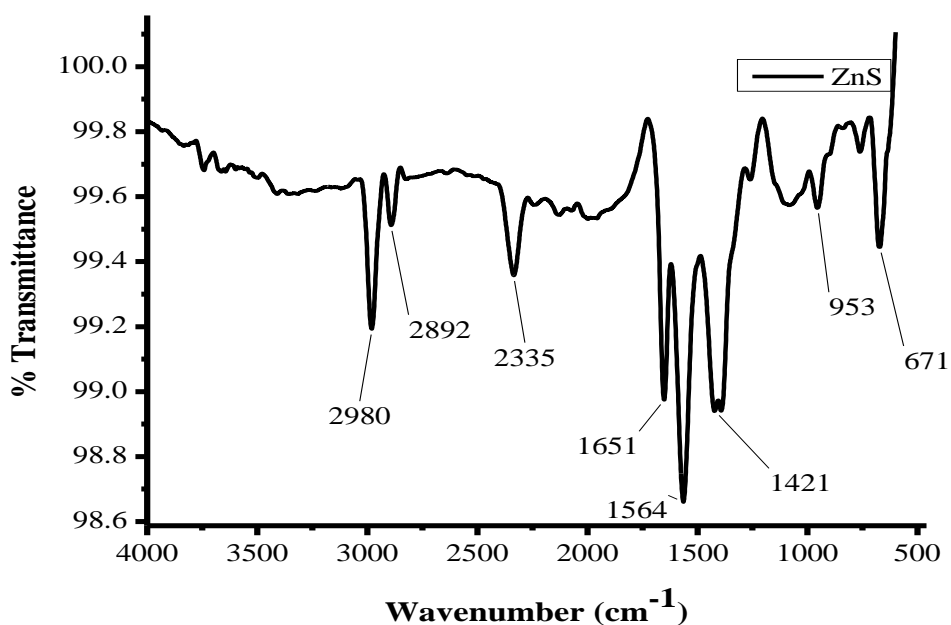


Figure 4: FTIR spectrum of ZnS

4.4.2 FTIR Transmittance spectrum of Dyes and grafted ZnS-dyes

In the FTIR spectra of dye compounds, the main IR peaks of the dyes were identified based on literature (see table 3). In addition, from the absorption frequency (ν) given by the equation:

$\nu = \frac{1}{2\pi} \sqrt{\frac{k}{\mu}}$, where k is the force constant for the bond, μ is the reduced mass of two atoms in the bond, it can be deduced that when the reduced mass of two atoms in the chemical bond is bigger, then the vibrational frequency will be lower. Thus, the peaks were also identified using the relationship between frequency and the reduced mass of atoms in a chemical bond from the equation.

The spectra of dyes are almost identical in the region between 2300 – 4000 cm^{-1} because they have similar chemical bonds. The signals of aromatic C-H were observed at 2800 – 3000 cm^{-1} and the stretching band of N-H unit appeared near 3700 cm^{-1} . Furthermore, for all synthesized dye compounds, the spectra displayed a strong peak at around 2330 cm^{-1} and a wide noisy band in range of 3500 – 4000 cm^{-1} overlapping with the N-H peak. These bands signify the presence of CO_2 and water vapor, respectively in the atmosphere [92]

On the other hand, the ZnS spectrum is maintained with little changes in the grafted ZnS-dyes spectra. This is because the ZnS spectra have some peaks of similar chemical bonds as the dyes. Thus, changes in the fingerprint region of grafted ZnS-dyes spectra may be an indication for successful grafting. In addition, a very weak or disappearance of N-H peak in the grafted ZnS-dyes spectra maybe due to anchoring of the dye onto ZnS nanoparticles, which also implies successful grafting. The frequencies values of all the synthesized compounds are summarized in section 4.4.2.1 to section 4.4.2.5.

4.4.2.1 FTIR spectra of Dye1 and ZnS-Dye1

In Figure 5 displays the FTIR spectrum for (3-(6-(2-hydroxynaphthalen-1-yl)methyleneamino)pyridin-2-ylimino)indolin-2-one (Dye1). The intense bands occurred at 3744, 3365, 2981, 2887, 2333, 1623, 1538, 1454, 1296, 1151, 836 and 742

cm⁻¹ frequencies. A peak at 3744 cm⁻¹ corresponds to the vibrational frequencies of N-H unit. The vibrational frequencies at 2984 and 2887 cm⁻¹ is attributed to the aromatic C-H (Sp² hybridized carbon) stretching bands. Strong peaks at 1623 cm⁻¹ and 1538 cm⁻¹ shows the presence of carbonyl group (C=O) and imine linkage (C=N), respectively. The frequency vibration band at 1454 cm⁻¹ confirm the presence of C=C connections in dye compound, while the vibrational frequency at 1296 cm⁻¹ is assigned to C-O stretch.

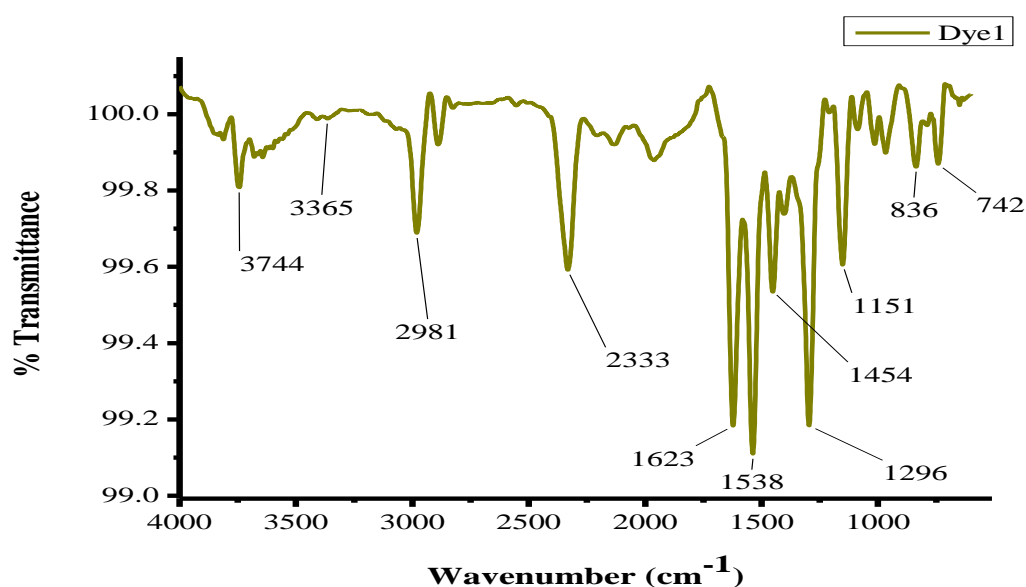


Figure 5: FTIR spectrum of Dye1

The FTIR spectra of ZnS nanoparticles, (3-(6-(2-hydroxynaphthalen-1-yl)methyleneamino)pyridin-2-ylimino)indolin-2-one and the grafted ZnS-(3-(6-(2-hydroxynaphthalen-1-yl)methyleneamino)pyridin-2-ylimino)indolin-2-one (ZnS-Dye1) are shown in figure 6 below. The peaks found in ZnS spectrum are maintained before and after grafting. However, the fingerprint region of ZnS-(3-(6-(2-hydroxynaphthalen-1-yl)methyleneamino)pyridin-2-ylimino)indolin-2-one spectrum have slightly changed due to the peaks observed at 1251 and 1153 cm⁻¹. In addition, there is a broad peaks observed at 667 and 3653 cm⁻¹ in the grafted ZnS-(3-(6-(2-

hydroxynaphthalen-1-yl)methyleneamino)pyridin-2-ylimino)indolin-2-one spectrum. These may be attributed to (3-(6-(2-hydroxynaphthalen-1-yl)methyleneamino)pyridin-2-ylimino)indolin-2-one particles being adsorbed on the ZnS nanoparticles.

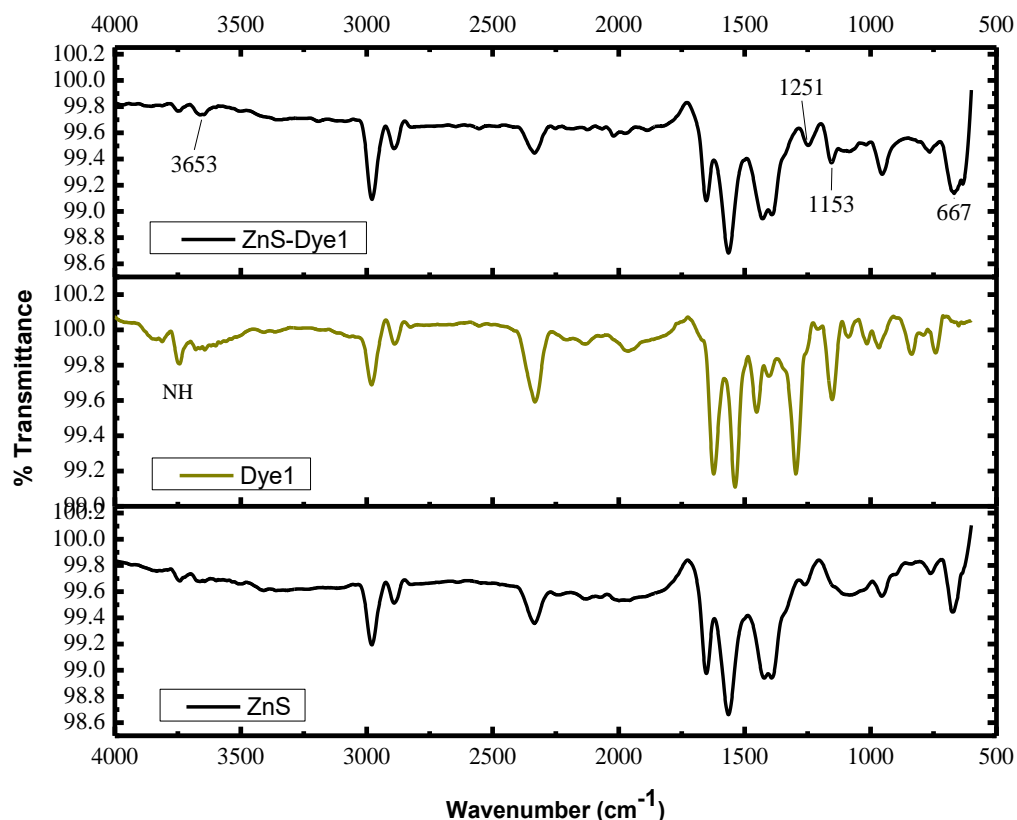


Figure 6: FTIR spectrum of ZnS, Dye1 and ZnS-Dye1

4.4.2.2 FTIR spectra of Dye2 and ZnS-Dye2

Figure 7 displays the FTIR spectrum of (3-(4-(2-hydroxynaphthalen-1-yl)methyleneamino)phenylimino)indolin-2-one (Dye2), with intense peaks observed at 3743, 3204, 2979, 2891, 2330, 2132, 1967, 1623, 1545, 1462, 1384, 1150, 953 and 756 cm^{-1} frequencies. A vibrational peak at 3743 cm^{-1} correspond to NH unit stretch, while a peak at 3204 cm^{-1} relate to OH group. Strong bands at 2979 and the shoulder peak at 2891 cm^{-1} display the aromatic C-H stretching of the aromatic rings. The

presence of the peak at 1623 cm^{-1} relate to C=O, and the peak at 1545 cm^{-1} display the presence of C=N linkage of the compound. The peak at 1462 cm^{-1} confirm the presence of C=C of the aromatic ring in the compound, while the peak at 1384 and 1150 cm^{-1} signify the C-O and C-N bond, respectively.

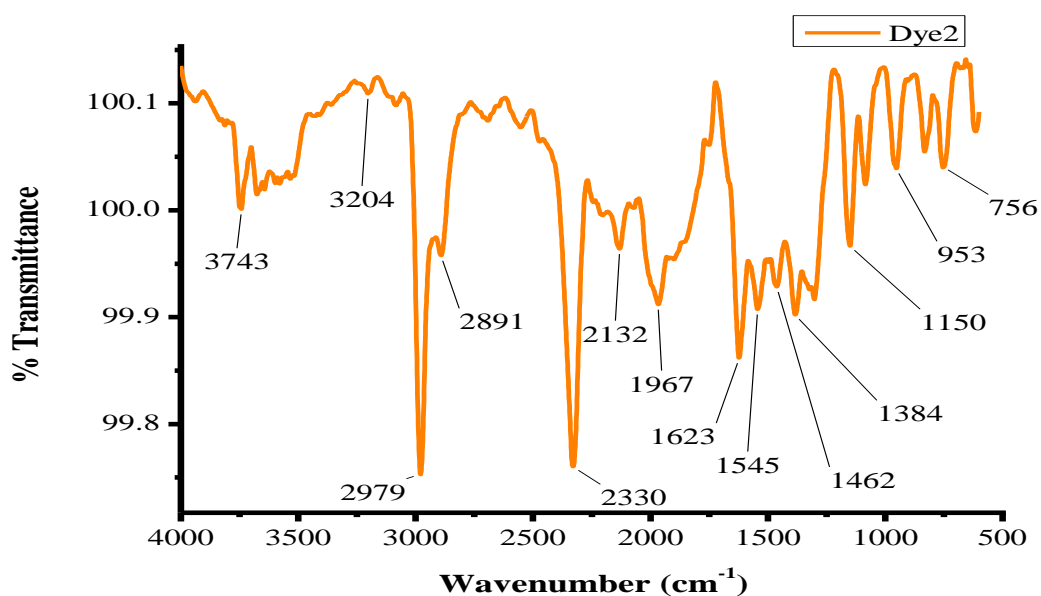


Figure 7: FTIR spectrum of Dye2

After ZnS nanoparticles was grafted with (3-(4-(2-hydroxynaphthalen-1-yl)methyleneamino)phenylimino)indolin-2-one, the fingerprint region changed slightly. Figure 8 below is the FTIR spectrum of ZnS-(3-(4-(2-hydroxynaphthalen-1-yl)methyleneamino)phenylimino)indolin-2-one (ZnS-Dye2). Two extra peaks are observed at 1146 and 1082 cm^{-1} in the ZnS-(3-(4-(2-hydroxynaphthalen-1-yl)methyleneamino)phenylimino)indolin-2-one spectrum. The shape of the peak at 1397 cm^{-1} in ZnS spectrum became sharp with a shoulder peak and the NH peak also became broad after grafting. These may indicate successful grafting of (3-(4-(2-hydroxynaphthalen-1-yl)methyleneamino)phenylimino)indolin-2-one on ZnS nanoparticles.

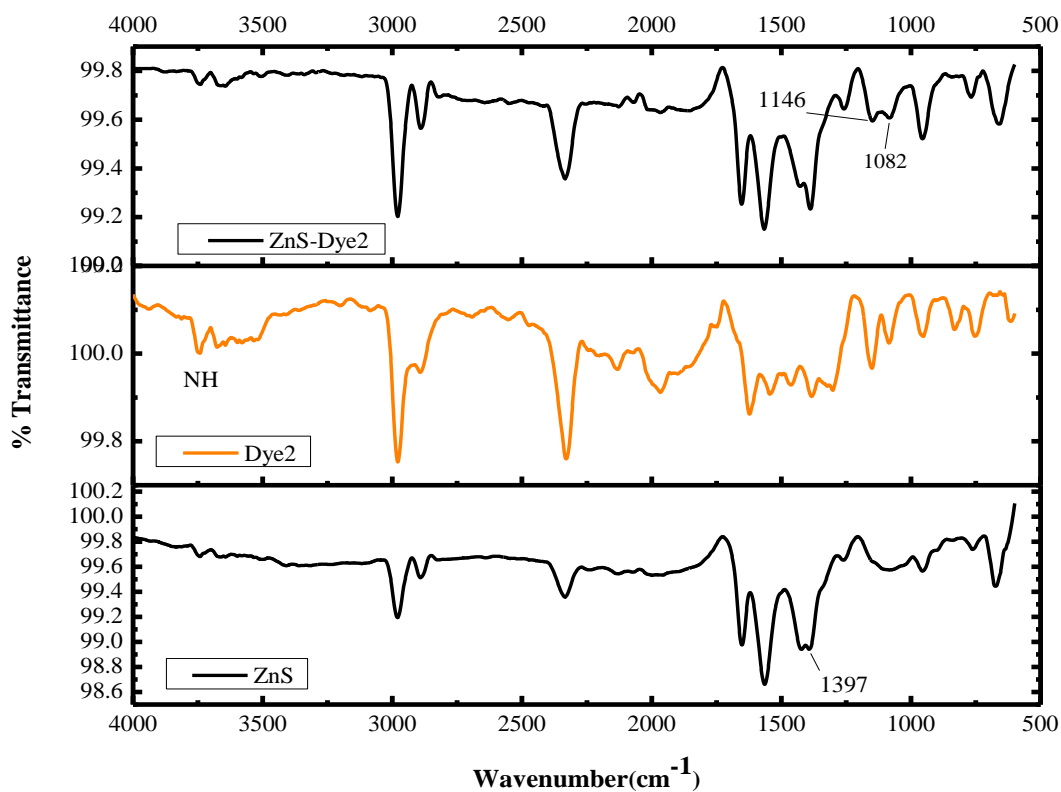


Figure 8: FTIR spectra of ZnS, Dye2 and ZnS-Dye2

4.4.2.3 FTIR spectra of Dye3 and ZnS-Dye3

The intense peak occurred in FTIR spectrum of 3-(thiazol-2-ylimino)indolin-2-one (Dye3) are, 2978, 2892, 2336, 1971, 1462, 1385, 1150, 1081, 951 and 766 cm^{-1} frequencies. The presence of N-H bond, and aromatic C-H group are signified by the peaks at 2978 and 892 cm^{-1} , respectively. The peak at 766 cm^{-1} confirm the presence of C-S bond, while the peaks at 1971, 1462 and 1385 cm^{-1} may be due to the presence of C=O, C=N and C=C bonds in the dye compound, respectively.

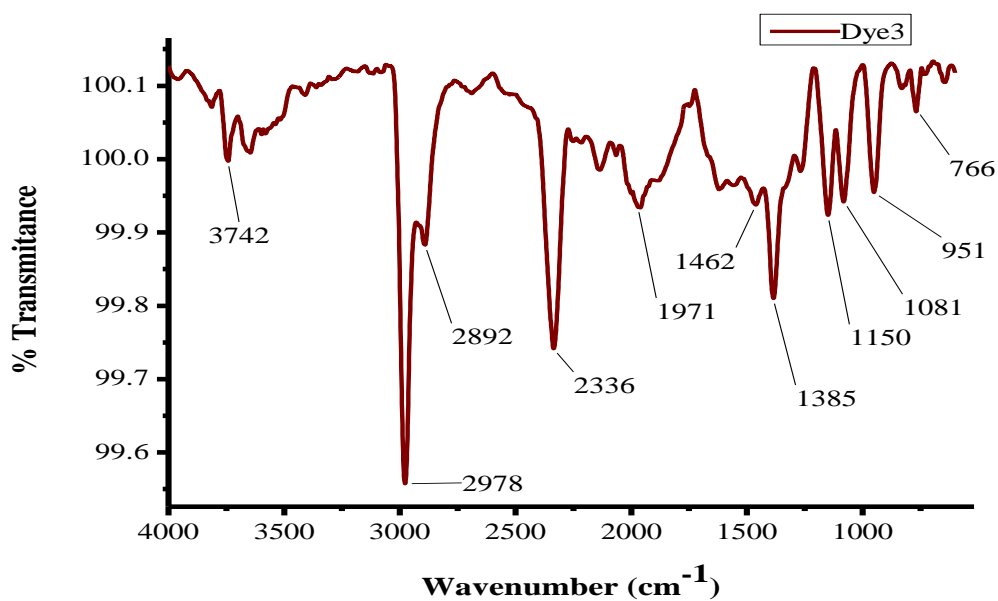


Figure 9: FTIR spectrum of Dye3

From the spectrum of ZnS-3-(thiazol-2-ylimino)indolin-2-one (ZnS-Dye3), the ZnS nanoparticles maintain the peaks before and after grafting. However, the intensities of these peaks have reduced. This result is in agreement with the faint color of the grafted ZnS-3-(thiazol-2-ylimino)indolin-2-one obtained. It implies that very little amount of 3-(thiazol-2-ylimino)indolin-2-one were adsorbed on ZnS nanoparticles.

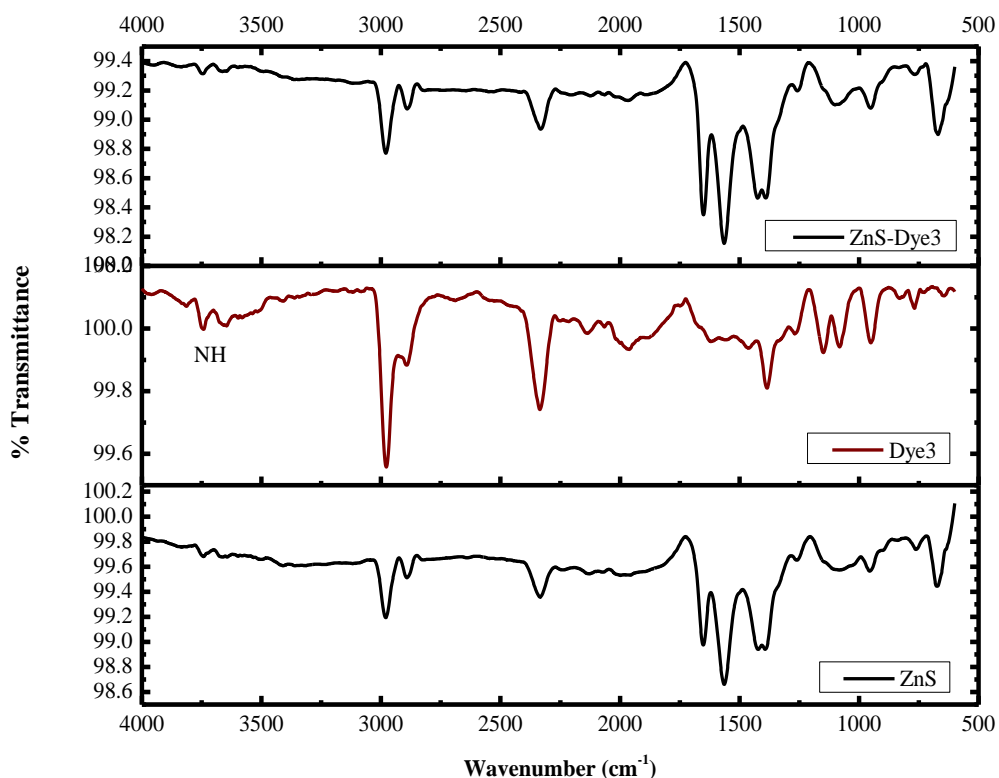


Figure 10: FTIR spectra of ZnS, Dye3 and ZnS-Dye3

4.4.2.4 FTIR spectra of Dye4 and ZnS-Dye4

Figure 11 and 12 below show the FTIR spectra of (3-(6-thiophen-2-ylmethyleneamino)pyridin-2-ylimino)indolin-2-one (Dye4) and ZnS-(3-(6-thiophen-2-ylmethyleneamino)pyridin-2-ylimino)indolin-2-one (ZnS-Dye4). The FTIR intense absorption bands occurred at 3744, 2979, 2890, 2336, 1607, 1452, 1386, 1149, 1080 and 948 cm^{-1} frequencies in (3-(6-thiophen-2-ylmethyleneamino)pyridin-2-ylimino)indolin-2-one spectrum. The spectrum showed peaks that signify the presence of N-H (3744 cm^{-1}), aromatic C-H ($2979, 2890 \text{ cm}^{-1}$), C-S bond (765 cm^{-1}), C=O (1607 cm^{-1}), C=N (1452 cm^{-1}) and C=C (1386 cm^{-1}). Peaks in the range of $1080 - 1149 \text{ cm}^{-1}$ confirm the presence of C-N stretch in the dye compound.

The spectrum of ZnS is maintained before and after grafting. However, the C-H peak on the ZnS-(3-(6-thiophen-2-ylmethyleneamino)pyridin-2-ylimino)indolin-2-one spectrum have a shoulder peak, while the peak at 1397 cm^{-1} became sharp after grafting. In addition, the peaks at 1155 and 1077 cm^{-1} in the fingerprint region of (3-(6-thiophen-2-ylmethyleneamino)pyridin-2-ylimino)indolin-2-one are noticeable in ZnS-(3-(6-thiophen-2-ylmethyleneamino)pyridin-2-ylimino)indolin-2-one after grafting. Thus, the adsorption of (3-(6-thiophen-2-ylmethyleneamino)pyridin-2-ylimino)indolin-2-one on ZnS nanoparticles was successful.

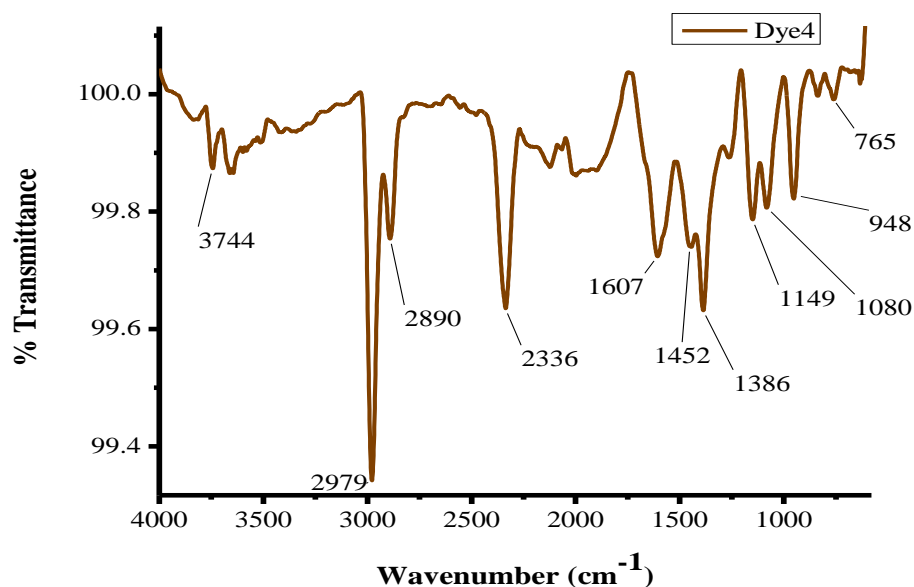


Figure 11: FTIR spectrum of Dye4

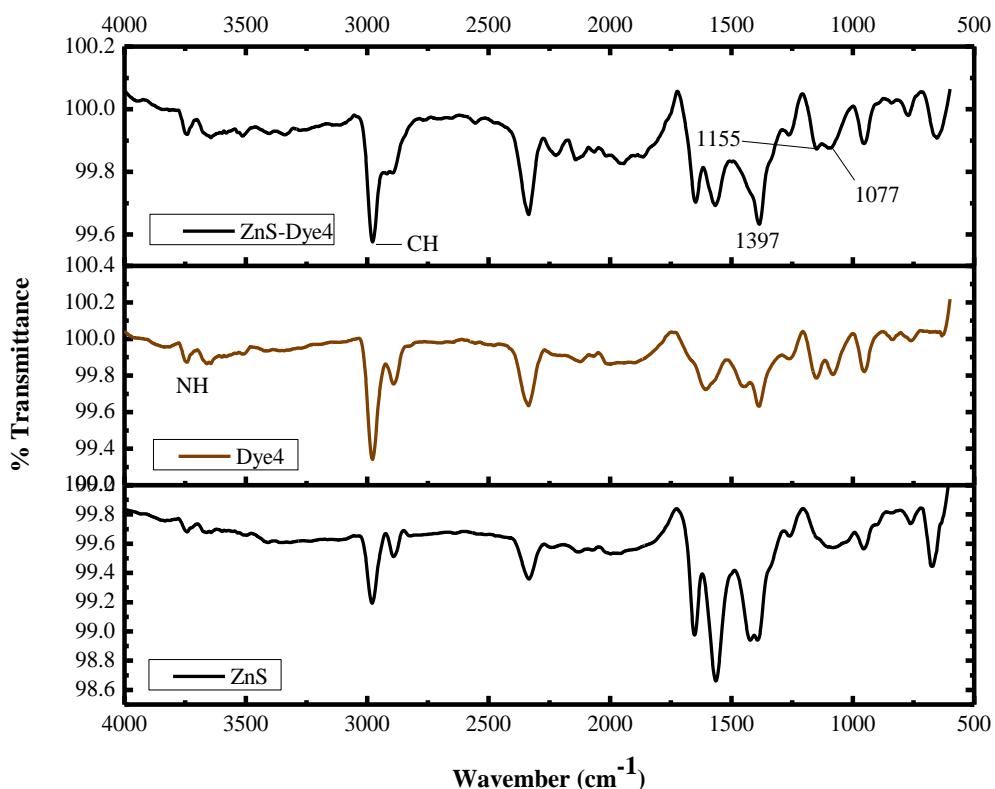


Figure 12: FTIR spectra of ZnS, Dye4 and ZnS-dye4

4.4.2.5 FTIR spectra of Dye5 and ZnS-Dye5

The observed intense peaks in the FTIR spectrum of (3-(5-(2-oxoindolin-3-ylideneamino)naphthalen-1-ylimino)indolin-2-one (Dye5) in Figure 13 are; 3749, 2969, 2924, 2856, 2338, 1979, 1743, 1455, 1381, 1153, 1084 and 951 cm^{-1} frequencies. The IR peak at 3749 cm^{-1} relates to N-H unit of the indolin-2-one moiety. A strong peak at 2924 cm^{-1} and two shoulder peaks (2924, 2856) cm^{-1} relates to aromatic C- H stretching vibrations. The spectrum also displays peaks at 1743, 1455 and 1381 cm^{-1} which signify the presence of C=O, C=N and C=C, respectively. The peaks in the region of 1153 cm^{-1} confirm the presence of C-N connection in the compound.

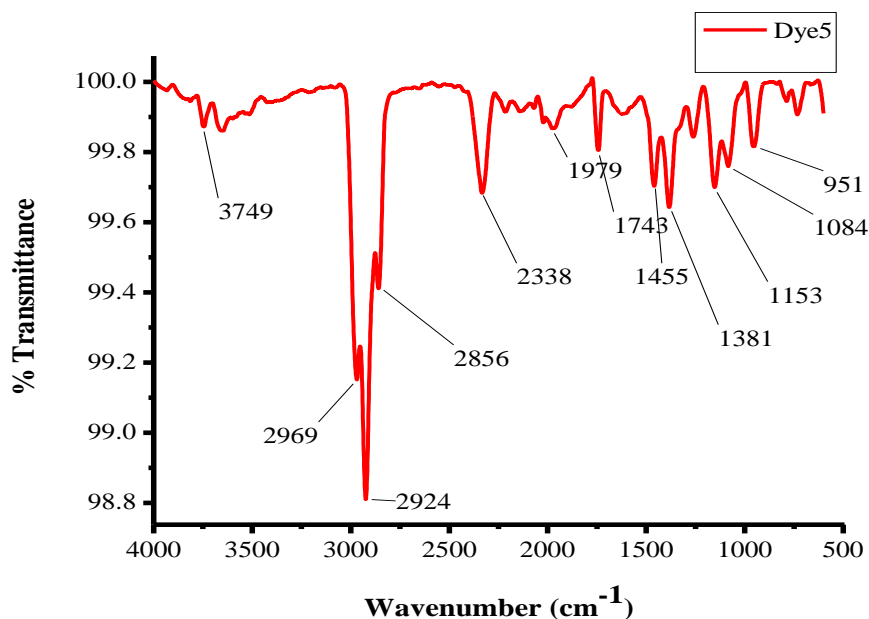


Figure 13: FTIR spectrum of Dye5

The ZnS spectrum is maintained with little changes in the ZnS-3-(5-(2-oxoindolin-3-ylideneamino)naphthalen-1-ylimino)indolin-2-one (ZnS-Dye5) spectrum (Figure 14). However, the C-H stretching vibration peak with a shoulder peak in ZnS-3-(5-(2-oxoindolin-3-ylideneamino)naphthalen-1-ylimino)indolin-2-one spectrum may be due to adsorption of 3-(5-(2-oxoindolin-3-ylideneamino)naphthalen-1-ylimino)indolin-2-one on the ZnS nanoparticles. Furthermore, a broad peak at 1085 cm^{-1} in fingerprint region of ZnS spectrum is observed with a shoulder peak after grafting.

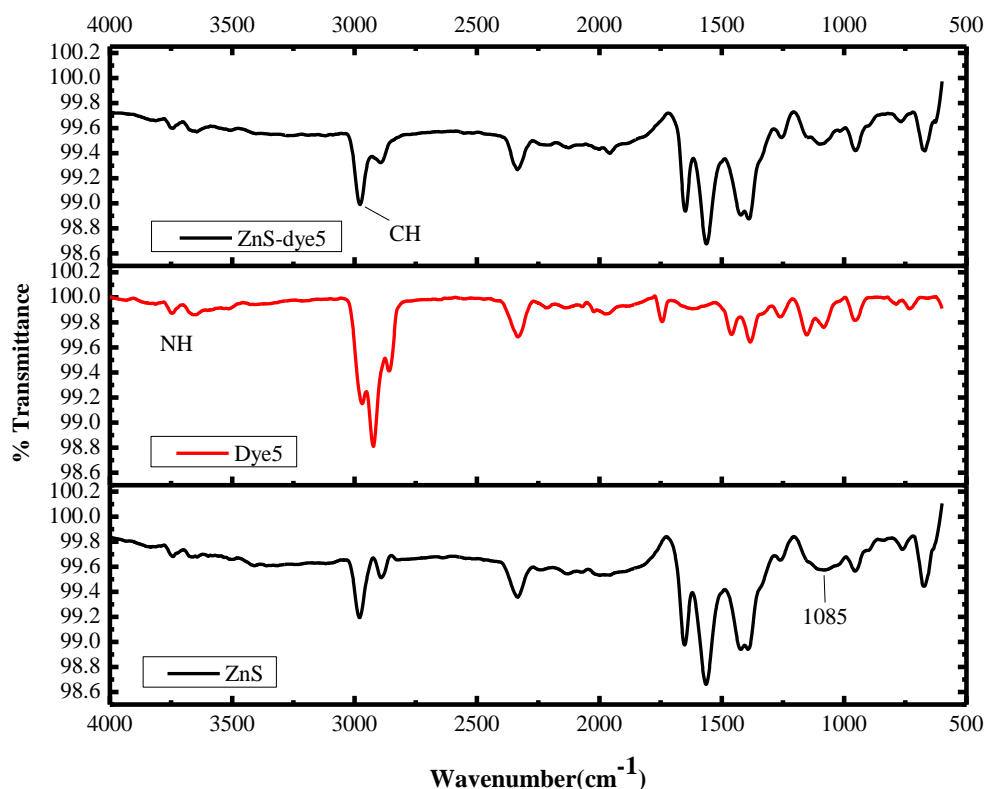


Figure 14: FTIR spectra of ZnS, Dye5 and ZnS-dye5

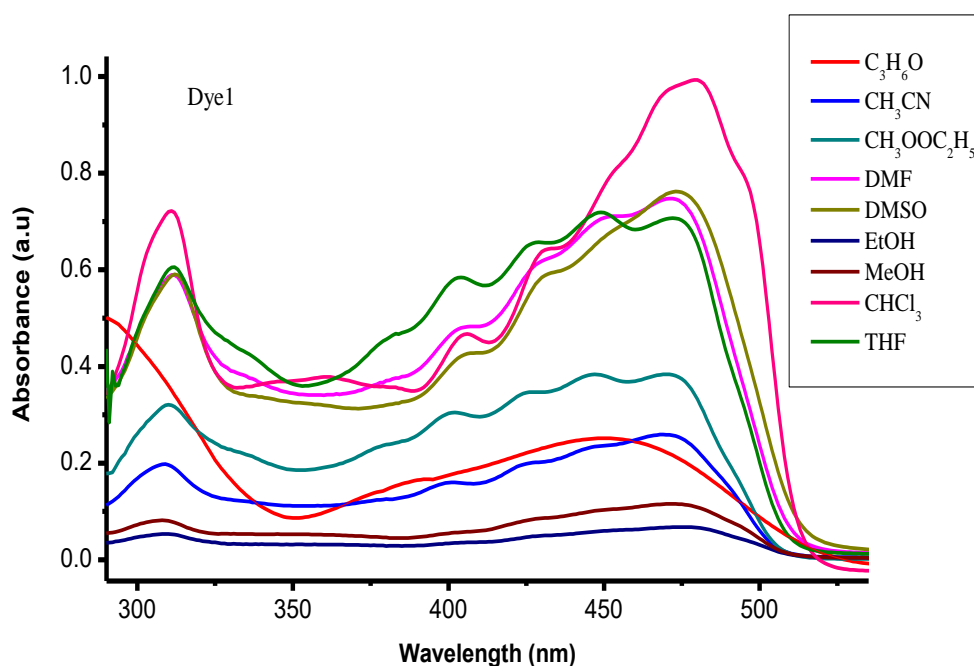
4.5 Solvatochromic effect and UV-vis analysis of metal-free dyes

4.5.1 Solvent effect on UV-vis absorption spectra of dyes

The solvatochromic effect of the five dyes were investigated in nine solvents of different polarities, by UV-vis spectroscopy and the absorption spectra were recorded. The order of the used solvent polarities from less to more polar is; $\text{CHCl}_3 < \text{CH}_3\text{COOC}_2\text{H}_5 < \text{THF} < \text{C}_3\text{H}_6\text{O} < \text{C}_2\text{H}_5\text{OH} < \text{CH}_3\text{OH} < \text{CH}_3\text{CN} < \text{DMF} < \text{DMSO}$. This was determined from their dielectric constants. Clearly, solvents with high dielectric constants such as DMSO, DMF and CH_3CN are more polar, while CHCl_3 , $\text{CH}_3\text{COOC}_2\text{H}_5$ and THF solvents are less polar. All dyes spectra displayed bands in the UV and visible regions of the spectrum, hence demonstrating one of the characteristics of dyes. However, the main focus for this study are the bands that

appear in the spectra from about 350 – 700 nm, where most of the radiation from the sun reach the earth.

From Figure 15, the graphs of (3-(6-(2-hydroxynaphthalen-1-yl)methyleneamino)pyridin-2-ylimino)indolin-2-one and (3-(4-(2-hydroxynaphthalen-1-yl)methyleneamino)phenylimino)indolin-2-one, the solvent effect on their absorption spectra showed bathochromic as well as great hyperchromic shift in CHCl_3 solution, compared to spectra of these dyes in all other solvents. However, the two dyes displayed hypochromic shift in $\text{C}_2\text{H}_5\text{OH}$ and CH_3OH solvents. Therefore, it is evident that there are good solute-solvent molecular interactions between these dyes and CHCl_3 solvent.



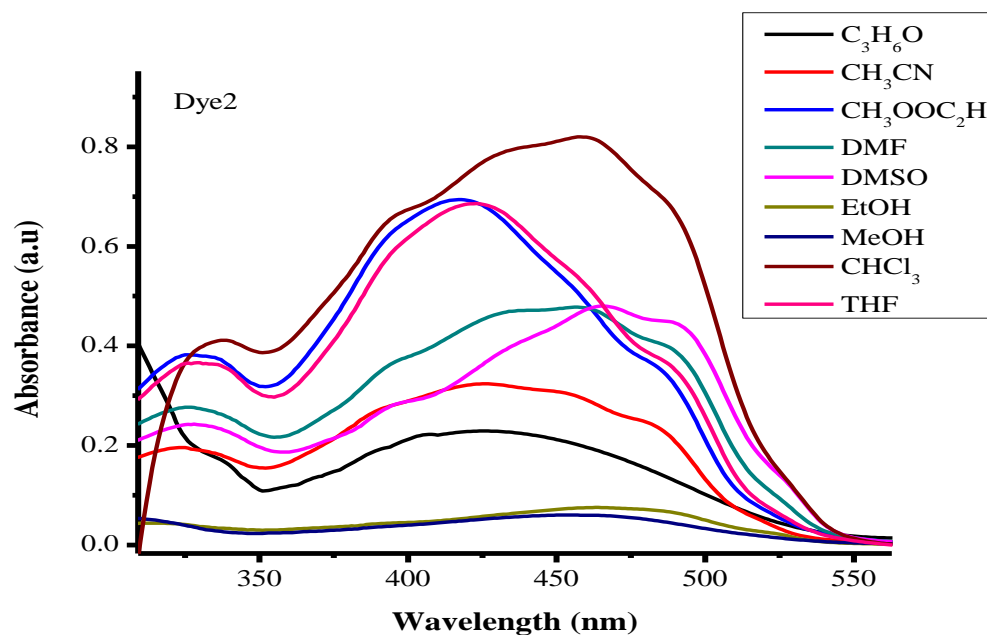
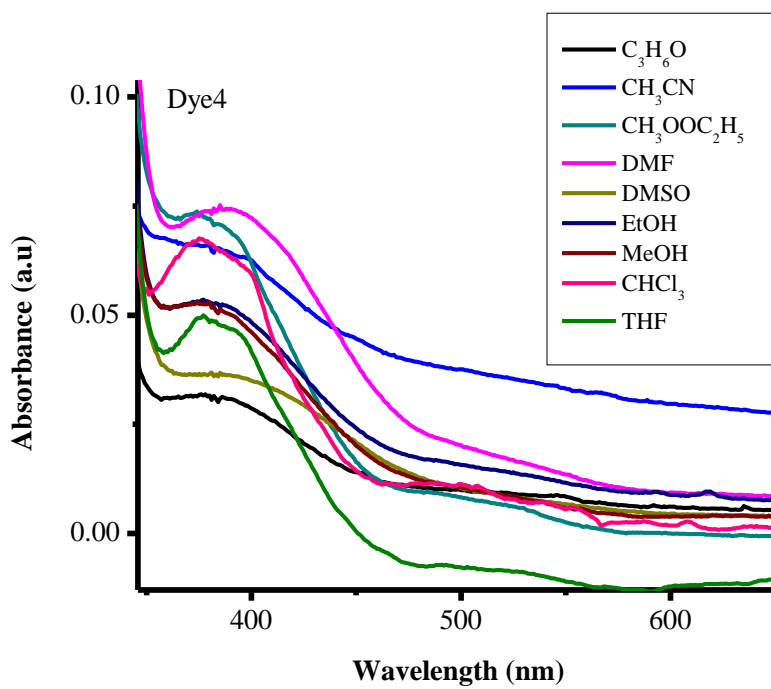
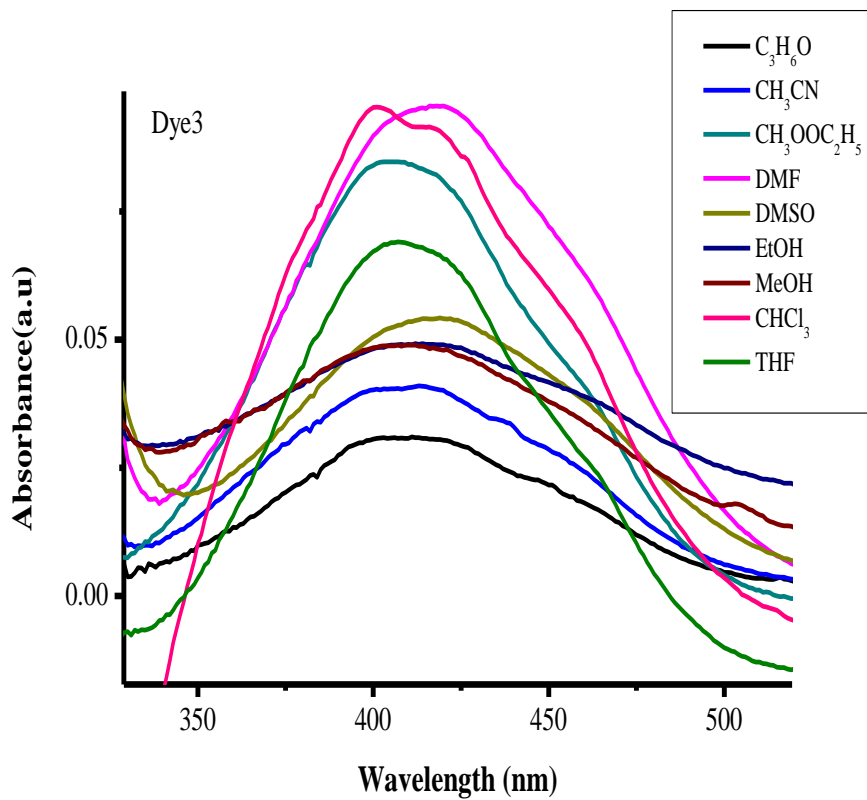


Figure 15: Solvatochromic effect of solvents on Dye1 and Dye2

In contrast, 3-(thiazol-2-ylimino)indolin-2-one, 3-(6-thiophen-2-ylmethyleneamino)pyridin-2-ylimino)indolin-2-one and 3-(5-(2-oxoindolin-3-ylideneamino)naphthalen-1-ylimino)indolin-2-one displayed a bathochromic as well as hyperchromic shift in DMF solution (Figure 16). A broad and high peak is observed in the absorption spectrum of 3-(thiazol-2-ylimino)indolin-2-one in DMF solution. However, a narrow band is observed in the spectrum of 3-(6-thiophen-2-ylmethyleneamino)pyridin-2-ylimino)indolin-2-one in all nine solvent solutions with hypochromic shift in DMF solutions. For 3-(5-(2-oxoindolin-3-ylideneamino)naphthalen-1-ylimino)indolin-2-one, a broad band and increase in absorption is observed in the spectrum of DMF solution, causing a hypochromic and bathochromic shift. Clearly, the absorption spectra of these three dyes in DMF indicates strong interactions between dyes and solvent molecules, compared to other solvents.



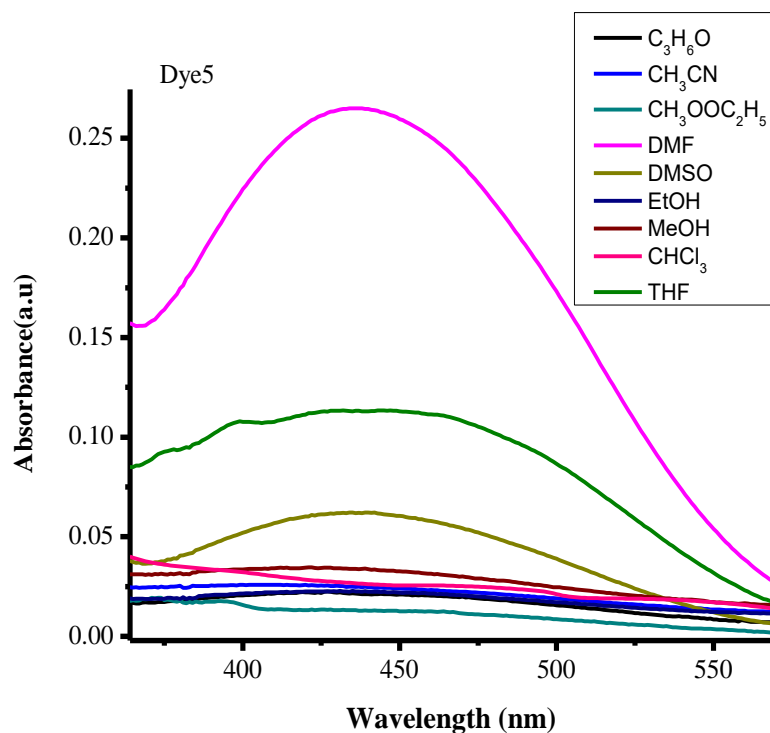


Figure 16: Solvatochromic effect on Dye3, Dye4 and Dye5

Table 5 display the data of λ_{\max} and absorption intensities extracted from the UV-vis absorption spectra of the five dyes. The solvents were arranged from less to more polar (top to bottom), with λ_{\max} and the intensity of each dye. These data plainly showed that solvents influence the spectra of these dyes. This is because the λ_{\max} and the intensity of the dyes are different in all the solvent used. In addition, it is also observed that the shape of the band in some solvents are differ from each other and these are all in agreement with Homocianu M. et al [25]. However, no correlation was found between λ_{\max} and the absorption intensity of the dyes, and the solvent polarities. That is, solvatochromism of the dyes in the present study does not depend on the polarity of the solvent, but merely on the interactions between the dyes and solvent molecules.

Table 5: The λ_{\max} and absorption intensities (a.u) of the dyes in different solvents

Solvent	Dye1		Dye2		Dye3		Dye4		Dye5	
	λ_{\max}	a.u	λ_{\max}	a.u	λ_{\max}	a.u	λ_{\max}	a.u	λ_{\max}	a.u
CHCl₃	480	0.993	460	0.819	401	0.055	376	0.088	462	0.026
CH₃OO C₂H₅	470	0.384	417	0.694	407	0.085	374	0.074	356	0.017
THF	450	0.718	423	0.686	407	0.089	378	0.046	447	0.113
C₃H₆O	452	0.251	428	0.229	408	0.031	378	0.032	439	0.021
EtOH	479	0.067	484	0.075	419	0.049	378	0.053	430	0.023
MeOH	475	0.115	465	0.059	412	0.049	377	0.054	428	0.034
CH₃CN	471	0.258	426	0.324	413	0.041	379	0.066	422	0.026
DMF	471	0.748	456	0.478	420	0.096	390	0.074	436	0.265
DMSO	474	0.762	468	0.479	421	0.054	385	0.039	434	0.062

From the solvatochromism analysis, a solvent with strong interactions with each dye molecules were determined. For (3-(6-(2-hydroxynaphthalen-1-yl)methyleneamino)pyridin-2-ylimino)indolin-2-one and (3-(4-(2-hydroxynaphthalen-1-yl)methyleneamino)phenylimino)indolin-2-one in Figure 15, the solvent observed with strong interactions is chloroform (CHCl₃) while for 3-(thiazol-2-ylimino)indolin-2-one, (3-(6-thiophen-2-ylmethyleneamino)pyridin-2-ylimino)indolin-2-one and 3-(5-(2-oxoindolin-3-ylideneamino)naphthalen-1-ylimino)indolin-2-one (Figure 16), DMF displayed strong interactions from the absorption spectra. Therefore, these two solvents were used for further investigations.

4.5.2 Optimized dye concentration for UV-vis analysis of dyes

The absorption spectra of three different concentrations (0.1mM, 0.3mM and 0.5mM) of each dye were recorded and analyzed. From the spectra, the absorptivity of 0.3mM

and 0.5mM is very high, indicating that the concentration is too much (see Appendix C). In addition, the curves of the spectra of these dye concentrations are not smooth, compared to the absorption spectra of 0.1mM dyes. Hence, the concentration of 0.1mM was chosen as an optimized concentration of the five dyes, for further study. Figure 17 is the UV-vis absorption spectra of the dyes in 0.1mM of CHCl₃ and DMF solutions.

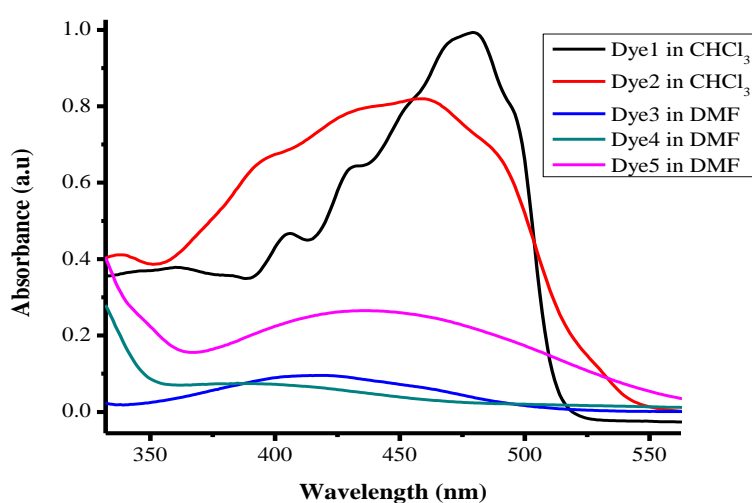


Figure 17: UV-Vis absorption spectra of dyes in 0.1 mM of Solutions

From Figure 17, it is evident that (3-(6-(2-hydroxynaphthalen-1-yl)methyleneamino)pyridin-2-ylimino)indolin-2-one and (3-(4-(2-hydroxynaphthalen-1-yl)methyleneamino)phenylimino)indolin-2-one have good optical properties. An increase in absorptivity of (3-(6-(2-hydroxynaphthalen-1-yl)methyleneamino)pyridin-2-ylimino)indolin-2-one at the wavelength of 480nm and a band in the range of 389 – 525nm is observed. The λ_{max} of (3-(6-(2-hydroxynaphthalen-1-yl)methyleneamino)pyridin-2-ylimino)indolin-2-one is in the visible region (longer wavelength) with higher intensity compared to other dyes. (3-(4-(2-hydroxynaphthalen-1-yl)methyleneamino)phenylimino)indolin-2-one has

wider band than other dyes, covering wide range of wavelength with high intensity. It is also observed that 3-(5-(2-oxoindolin-3-ylideneamino)naphthalen-1-ylimino)indolin-2-one displayed better optical properties, compared to 3-(thiazol-2-ylimino)indolin-2-one and (3-(6-thiophen-2-ylmethyleneamino)pyridin-2-ylimino)indolin-2-one. The absorption spectrum of 3-(5-(2-oxoindolin-3-ylideneamino)naphthalen-1-ylimino)indolin-2-one show a broad absorption band in the range of 367 – 559 nm and a hyperchromic effect relative to 3-(thiazol-2-ylimino)indolin-2-one and (3-(6-thiophen-2-ylmethyleneamino)pyridin-2-ylimino)indolin-2-one.

The 3-(thiazol-2-ylimino)indolin-2-one and (3-(6-thiophen-2-ylmethyleneamino)pyridin-2-ylimino)indolin-2-one have the absorption bands which are more on shorter wavelength of the spectra and they are all observed with very low absorption intensity. Despite all these, the observed absorption bands of all dyes are in the UV-vis region of the electromagnetic spectrum. This shows that these dyes can be used as light absorber in the DSSCs.

4.6 UV-vis analysis of ZnS and grafted ZnS-Dyes nanoparticles

Powdered ZnS nanoparticles were characterized in Methanol solution at the concentration of 1g/mL. The spectrum below shows the UV-vis spectrum of ZnS. The absorption intensity increases in the area of Ultraviolet region of the spectrum, with a shoulder peak at 304 nm. The literature reports the UV-vis absorption maxima of ZnS nanoparticles in the UV region of a spectrum [7, 101, 102]. This correspond to the spectrum obtained from the present study.

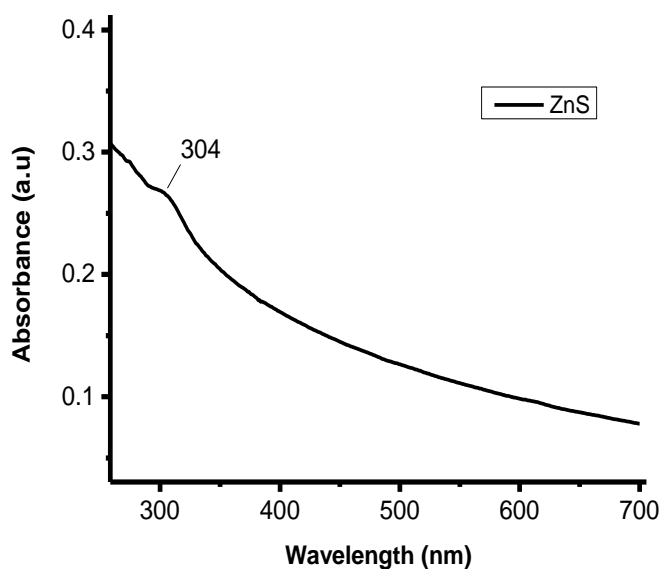
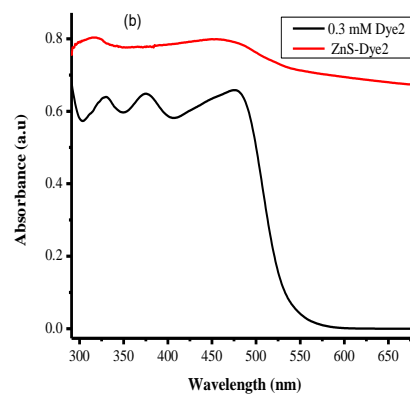
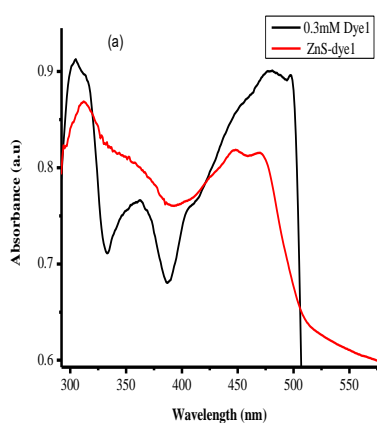


Figure 18: UV-vis spectrum of ZnS nanoparticles

The prepared grafted ZnS-dyes samples were characterized by both FTIR and UV-vis absorption spectroscopy. The optical absorption spectra of pure dyes and grafted samples are shown in Figure 19. It can be observed that pure organic (3-(6-(2-hydroxynaphthalen-1-yl)methyleneamino)pyridin-2-ylimino)indolin-2-one in Figure 19(a), (3-(4-(2-hydroxynaphthalen-1-yl)methyleneamino)phenylimino)indolin-2-one in Figure 19(b) and 3-(5-(2-oxoindolin-3-ylideneamino)naphthalen-1-ylimino)indolin-2-one in Figure 19(e) showed successful grafting on ZnS nanoparticles, while 3-(thiazol-2-ylimino)indolin-2-one in Figure 19(c) and (3-(6-thiophen-2-ylmethyleneamino)pyridin-2-ylimino)indolin-2-one in Figure 19(d) showed no or little adsorption on the ZnS nanoparticles.

For (3-(6-(2-hydroxynaphthalen-1-yl)methyleneamino)pyridin-2-ylimino)indolin-2-one, the absorption peak edge is observed at 510 nm. Upon grafting (3-(6-(2-hydroxynaphthalen-1-yl)methyleneamino)pyridin-2-ylimino)indolin-2-one onto ZnS nanoparticles to produce ZnS-(3-(6-(2-hydroxynaphthalen-1-

yl)methyleneamino)pyridin-2-ylimino)indolin-2-one, a broadening absorption band edge shifted to about 550 nm. This indicate a red-shifted broad absorption peak. Furthermore, the absorption intensity has risen in the range of 350 – 425 nm, making it to be wider, but there is also hypochromic shift observed in the range of longer wavelength. The spectrum of ZnS-(3-(4-(2-hydroxynaphthalen-1-yl)methyleneamino)phenylimino)indolin-2-one displayed a broad band and an increase in the absorption intensity. An increase in intensity is also observed in ZnS-3-(5-(2-oxoindolin-3-ylideneamino)naphthalen-1-ylimino)indolin-2-one, with a broader maxi peak. However, for ZnS-3-(thiazol-2-ylimino)indolin-2-one and ZnS-(3-(6-thiophen-2-ylmethyleneamino)pyridin-2-ylimino)indolin-2-one samples, no peaks displayed in their spectra. This maybe an indication that very little or these two dyes does not adsorb on ZnS nanoparticles.



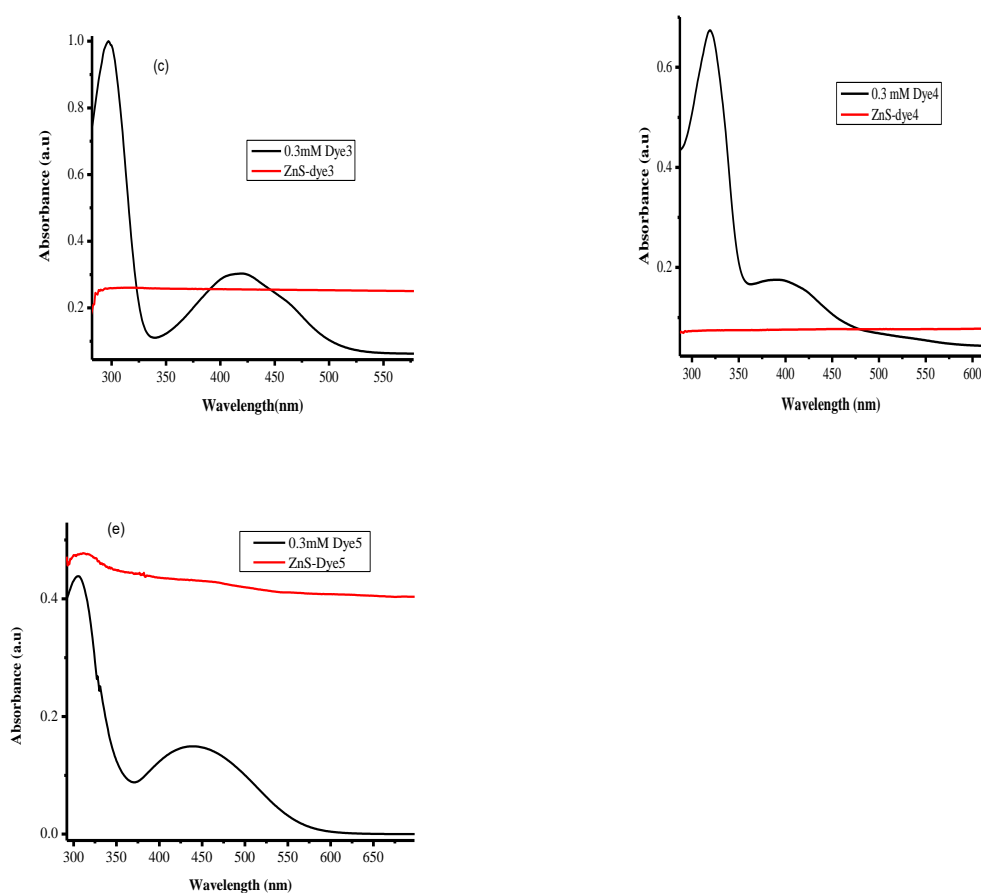


Figure 19: UV-vis absorption spectra of (a) ZnS-Dye1, (b) ZnS-Dye2, (c) ZnS-Dye3, (d) ZnS-Dye4 and (e) ZnS-Dye5

Overall, the UV-vis analysis shows that among the 5 dyes that was synthesized, only (3-(6-(2-hydroxynaphthalen-1-yl)methyleneamino)pyridin-2-ylimino)indolin-2-one, (3-(4-(2-hydroxynaphthalen-1-yl)methyleneamino)phenylimino)indolin-2-one and 3-(5-(2-oxoindolin-3-ylideneamino)naphthalen-1-ylimino)indolin-2-one showed good optical absorption properties on the grafted samples, as shown in figure 20. The 3-(thiazol-2-ylimino)indolin-2-one and (3-(6-thiophen-2-ylmethyleneamino)pyridin-2-ylimino)indolin-2-one showed the lowest absorption intensity and little or no band appeared in the longer wavelength of their spectra. Thus, only (3-(6-(2-hydroxynaphthalen-1-yl)methyleneamino)pyridin-2-ylimino)indolin-2-one, (3-(6-(2-

hydroxynaphthalen-1-yl)methyleneamino)phenylimino)indolin-2-one and 3-(5-(2-oxoindolin-3-ylideneamino)naphthalen-1-ylimino)indolin-2-one indicated good sensitization properties on ZnS nanoparticles.

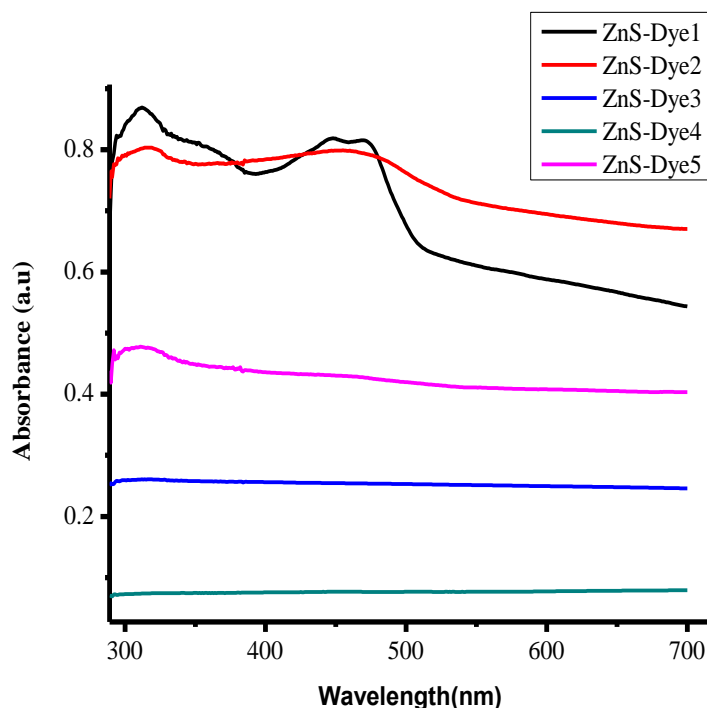


Figure 20: Absorption spectra of grafted samples

Table 6 illustrate the band wavelength range (width), λ_{\max} and intensities of the dyes spectra for both dyes and grafted samples. These data were extracted from UV-vis spectra of pure dyes and grafted ZnS-dyes samples. The spectrum band of ZnS-(3-(6-(2-hydroxynaphthalen-1-yl)methyleneamino)pyridin-2-ylimino)indolin-2-one became broader, showed hypochromic and bathochromic shift compared to (3-(6-(2-hydroxynaphthalen-1-yl)methyleneamino)pyridin-2-ylimino)indolin-2-one spectrum. The λ_{\max} shifted from 480 nm to 447 nm. The λ_{\max} of ZnS-(3-(4-(2-hydroxynaphthalen-1-yl)methyleneamino)phenylimino)indolin-2-one shifted slightly from 460 nm to 463 nm, causing bathochromic shift with great hyperchromic shift.

No band observed in spectra of ZnS-3-(thiazol-2-ylimino)indolin-2-one ZnS-(3-(6-thiophen-2-ylmethyleneamino)pyridin-2-ylimino)indolin-2-one, but they display small absorption intensity throughout UV-vis wavelength range. This might be that very little dye molecules were adsorbed on ZnS nanoparticles. For ZnS-3-(5-(2-oxoindolin-3-ylideneamino)naphthalen-1-ylimino)indolin-2-one, λ_{\max} shifted from 436 to 460, displaying red shift as well as hyperchromic shift. The changes in the spectra in the spectra of the dyes after being grafted on ZnS nanoparticles indicates that there were interactions between the nanoparticles and dye molecules, leading to successful adsorption.

Table 6: Band width, λ_{\max} and absorption intensity (a.u) of pure dyes and grafted ZnS-dyes

Dyes	Band width (Wavelength range)	λ_{\max} , a.u	Grafted nanoparticles	Band width (Wavelength range)	λ_{\max} , a.u
Dye1	389 - 525	480, 0.993	ZnS-Dye1	390 – 570	447, 0.818
Dye2	353 – 548	460, 0.819	ZnS-Dye2	361 – 545	463, 0.797
Dye3	340 – 504	420, 0.097	ZnS-Dye3	-	-
Dye4	355 – 478	390, 0.074	ZnS-Dye4	-	-
Dye5	367 - 559	436, 0.265	ZnS-Dye5	394 – 540	460, 0.429

4.7 Naked eye analysis and comparisons of the synthesized dye structures in relation to UV-vis spectra data

The table 7 below shows the electron-donating, conjugation linker and electron-accepting moieties identified in each dye structures (see Appendix D also). All dyes are observed to have the same configuration structure D- π -A and all dyes synthesized have the same electron withdrawing (Anchoring) group, the indolin-2-one moiety. The indolin-2-one group is reported as an electron acceptor, and can also help with electron injection and facilitate electron transfer into the semiconductor, due to its amide group [81]. Comparing to all dyes, 3-(thiazol-2-ylimino)indolin-2-one, has the shortest conjugation length. The longer conjugation facilitate the intramolecular charge transfer [4] and thus, low absorption intensity on 3-(thiazol-2-ylimino)indolin-2-one may be attributed due to the shorter conjugation length. Furthermore, (3-(6-(2-hydroxynaphthalen-1-yl)methyleneamino)pyridin-2-ylimino)indolin-2-one and (3-(4-(2-hydroxynaphthalen-1-yl)methyleneamino)phenylimino)indolin-2-one have the same electron donating moiety, the 2-hydroxynaphthalen-1-yl group which is known to be the strong electron donating group [103]. These two dyes displayed high absorption intensity and wider band than other dyes, and so this may be attributed to 2-hydroxynaphthalen-1-yl group present on their structures. (3-(6-thiophen-2-ylmethyleneamino)pyridin-2-ylimino)indolin-2-one is a Thiophene based dye and has displayed low absorption intensity with a band near shorter wavelength region, while 3-(5-(2-oxoindolin-3-ylideneamino)naphthalen-1-ylimino)indolin-2-one showed a broad and high absorption intensity, following (3-(6-(2-hydroxynaphthalen-1-yl)methyleneamino)pyridin-2-ylimino)indolin-2-one and (3-(4-(2-hydroxynaphthalen-1-yl)methyleneamino)phenylimino)indolin-2-one.

Table 7: Dyes moieties and their deduced structural configuration

Dyes	Electron-donating moiety	π - linker moiety	Electron-accepting moiety	Deduced Dye configuration
Dye1	2-hydroxynaphthalen-1-yl	Methyleneaminopyridin-2-ylimino	Indolin-2-one	D- π -A
Dye2	2-hydroxynaphthalen-1-yl	Methyleneaminophenylimino	Indolin-2-one	D- π -A
Dye3	3-thiazol-2-yl	Imino	Indolin-2-one	D- π -A
Dye4	Thiophen-2-ylmethyleneamino	Pyridine-2-ylimino	Indolin-2-one	D- π -A
Dye5	2-oxoindoline-3-ylideneamino	Naphthalene-1-ylimino	Indolin-2-one	D- π -A

4.8 Evaluation of dyes based on UV-vis analysis and naked eyes analysis of dye structures

The solvatochromic and UV-vis analysis determine the ability of the dyes to sensitize ZnS nanoparticles and the moieties of the dyes affect light absorbing properties of dyes. Among the five synthesized metal-free dyes, (3-(6-(2-hydroxynaphthalen-1-yl)methyleneamino)pyridin-2-ylimino)indolin-2-one and (3-(4-(2-hydroxynaphthalen-1-yl)methyleneamino)phenylimino)indolin-2-one displayed the highest absorption intensities and broader peaks, ranging from ultraviolet to visible region of the electromagnetic radiation spectrum, followed by 3-(5-(2-oxoindolin-3-ylideneamino)naphthalen-1-ylimino)indolin-2-one. This was observed in the UV-vis spectra of the two dyes in their best solvents. These dyes were also successfully adsorbed on ZnS nanoparticles and the absorption range of ZnS nanoparticles were extended to visible region of the spectrum, with increased intensities and broader

peaks, which indicate good sensitization properties. Furthermore, the 2-hydroxynaphthalen-1-yl moieties is observed to be best electron donating moiety, hence attributed to good absorption properties of (3-(6-(2-hydroxynaphthalen-1-yl)methyleneamino)pyridin-2-ylimino)indolin-2-one and (3-(4-(2-hydroxynaphthalen-1-yl)methyleneamino)phenylimino)indolin-2-one . Thus, the study found out that these dyes are the best sensitizers of ZnS nanoparticles and can be utilized as photo anode materials in DSSCs.

CHAPTER 5: CONCLUSION AND RECOMMENDATIONS

5.1 Conclusion

ZnS nanoparticles and the new designed (Isatin and Thiazole derived based) dyes were successfully synthesized by precipitation and Schiff based condensation respectively, for DSSCs application. The formation of ZnS nanoparticles were evidenced by XRD, FTIR and UV-vis spectroscopy results. XRD results confirm the cubic phase crystal structure of ZnS nanoparticles, while the FTIR and UV-vis confirmed the vibrational peaks and the UV band of ZnS nanoparticles based on the literature. The structures of the new synthesized dyes were confirmed by FTIR and ¹H NMR spectroscopy data. Vibrational frequencies and the proton chemical shifts were also in agreement with similar chemical bond vibrational frequencies and proton chemical shifts from the literature. However, some observed peaks appeared in the FTIR spectra of both ZnS and dyes maybe due to change in atmospheric condition of the surrounding while taking the measurements, despite the background correction that was done before taking measurements.

The study of solvatochromic effect of the synthesized dyes was done by spectrophotometric analysis. The λ_{max} and large absorption intensities of the dyes and grafted ZnS-dye samples were observed in the UV and visible region of the spectrum (350nm – 600nm). The position, intensity and shapes of the spectra in different solvents were not the same and this indicate the impacts of solvent on the absorption spectra of the samples. From the spectral analysis of dyes in all nine different solvents, (3-(6-(2-hydroxynaphthalen-1-yl)methyleneamino)pyridin-2-ylimino)indolin-2-one and (3-(4-(2-hydroxynaphthalen-1-yl)methyleneamino)phenylimino)indolin-2-one displayed bathochromic shift as well

as hyperchromic shift in CHCl_3 , while 3-(thiazol-2-ylimino)indolin-2-one, 3-(6-thiophen-2-ylmethyleneamino)pyridin-2-ylimino)indolin-2-one and 3-(5-(2-oxoindolin-3-ylideneamino)naphthalen-1-ylimino)indolin-2-one showed bathochromic and hyperchromic shift in DMF relative to other eight solvents. These results imply strong molecular interactions between these dyes and the two (CHCl_3 and DMF) solvents. Hence, CHCl_3 solvent was used as the suitable solvent to dissolve 3-(6-(2-hydroxynaphthalen-1-yl)methyleneamino)pyridin-2-ylimino)indolin-2-one and 3-(4-(2-hydroxynaphthalen-1-yl)methyleneamino)phenylimino)indolin-2-one for analysis, while DMF was the best solvent to dissolve 3-(thiazol-2-ylimino)indolin-2-one, 3-(6-thiophen-2-ylmethyleneamino)pyridin-2-ylimino)indolin-2-one and 3-(5-(2-oxoindolin-3-ylideneamino)naphthalen-1-ylimino)indolin-2-one for analysis.

The grafting of the synthesized dyes on ZnS nanoparticles was noticed by color changing of white ZnS nanoparticles to similar color of the dye adsorbed on the nanoparticles. A detailed study of UV-vis and FTIR spectroscopy confirmed the successful grafting of the dyes on ZnS nanoparticles. However, among the five dye synthesized, only 3-(6-(2-hydroxynaphthalen-1-yl)methyleneamino)pyridin-2-ylimino)indolin-2-one, 3-(4-(2-hydroxynaphthalen-1-yl)methyleneamino)phenylimino)indolin-2-one and 3-(5-(2-oxoindolin-3-ylideneamino)naphthalen-1-ylimino)indolin-2-one displayed good sensitization properties. The data of λ_{max} , intensities and band width were extracted from the spectra of both pure dyes and grafted ZnS-dyes samples, for comparison. A broad absorption band edge of ZnS-3-(6-(2-hydroxynaphthalen-1-yl)methyleneamino)pyridin-2-ylimino)indolin-2-one shifted to longer wavelength. The λ_{max} of 3-(5-(2-hydroxynaphthalen-1-yl)methyleneamino)phenylimino)indolin-2-one and 3-(5-(2-oxoindolin-3-

ylideneamino)naphthalen-1-ylimino)indolin-2-one increases after grafted onto the nanoparticles, causing bathochromic shift. All these was compared to the spectra of pure dyes. However, no band was observed in the UV-vis spectra of ZnS-3-(thiazol-2-ylimino)indolin-2-one and ZnS-(3-(6-thiophen-2-ylmethyleneamino)pyridin-2-ylimino)indolin-2-one, and this may indicate poor adsorption of these dyes on ZnS nanoparticles.

5.2 Recommendations

Challenge encountered in this study was lack of the UV-vis spectrophotometer with an accessory for measuring solid samples. ZnS was found insoluble in most of the solvents available, however, it was found partially soluble in Methanol. So, only some of the sample prepared for taking the measurements of ZnS and grafted ZnS-dyes samples dissolved and this may affect the data. Furthermore, co-sensitization of these dyes should be analyzed and the DSSCs based on the synthesized dyes in this study should be carried out to determine their effectiveness.

REFERENCES

- [1] Nosheen E. *Band gap Tuning, Photosensitization and Applications of ZnS and CdS Nanoparticles in Solid State Dye Sensitized Solar Cells Doctor of Philosophy In Physical Chemistry*. Quaid-i-Azam University, 2018.
- [2] Amin N, Ahmad Shahahmadi S, Chelvanathan P, et al. *Solar Photovoltaic Technologies: From Inception Toward the Most Reliable Energy Resource*. Elsevier. Epub ahead of print 2017. DOI: 10.1016/B978-0-12-409548-9.10092-2.
- [3] Benesperi I, Michaels H, Freitag M. The researcher's guide to solid-state dye-sensitized solar cells. *J Mater Chem C* 2018; 6: 11903–11942.
- [4] Carella A, Borbone F, Centore R. Research Progress on Photosensitizers for DSSC. *Front Chem* 2018; 6: 1–24.
- [5] Sharma K, Sharma V, Sharma SS. Dye-Sensitized Solar Cells: Fundamentals and Current Status. *Nanoscale Res Lett*; 13. Epub ahead of print 2018. DOI: 10.1186/s11671-018-2760-6.
- [6] Kaur Navneet, Kaur Sukhmeen, Singh Jagpreet RM. A Review on Zinc Sulphide Nanoparticles: From Synthesis, Properties to Applications. *J Bioelectron Nanotechnol* 2016; 1: 1–5.
- [7] Nosheen E, Shah SM, Hussain H, et al. Photo-sensitization of ZnS nanoparticles with renowned ruthenium dyes N3, N719 and Z907 for application in solid state dye sensitized solar cells: A comparative study. *J Photochem Photobiol B Biol* 2016; 162: 583–591.

- [8] Karunakaran C, Karuthapandian S. Enhancement of TiO₂-photocatalyzed organic transformation by ZnO and ZnS. Oxidation of diphenylamine. *Egypt J Basic Appl Sci* 2015; 2: 32–38.
- [9] Reda SM, El-Sherbieny SA. Dye-sensitized nanocrystalline CdS and ZnS solar cells with different organic dyes. *J Mater Res* 2010; 25: 522–528.
- [10] He LJ, Wang J, Chen J, et al. The effect of relative position of the π -spacer center between donor and acceptor on the overall performance of D- π -A dye: a theoretical study with organic dye. *Electrochim Acta* 2017; 241: 440–448.
- [11] Liu Z, Duan K, Guo H, et al. The enhancement of photovoltaic properties of the DSSCs based on D-A- π -A organic dyes via tuning auxiliary acceptor. *Dye Pigment* 2017; 140: 312–319.
- [12] Tomas D-M, Soto-Rojo R, Jesus B-L, et al. Theoretical Study of the Effect of Different π Bridges Including an Azomethine Group in. *Molecules* 2019; 24: 1–16.
- [13] Yemene AE, Venkatraman V, Almenningen DM, et al. Synthesis of Novel 3,6-Dithienyl Diketopyrrolopyrrole Dyes by Direct C-H Arylation. *Molecules* 2020; 25: 1–17.
- [14] Subbaiah M, Sekar R, Palani E, et al. One-pot synthesis of metal free organic dyes containing different acceptor moieties for fabrication of dye-sensitized solar cells. *Tetrahedron Lett* 2013; 54: 3132–3136.
- [15] Khanasa T, Prachumrak N, Kochapradist P, et al. The design, synthesis, and characterization of D- π -A- π -A type organic dyes as sensitizers for dye-sensitized solar cells (DSSCs). *Tetrahedron Lett* 2014; 55: 3244–3248.

- [16] IARC monographs on the evaluation of carcinogenic risks to humans. *IARC Monogr Eval Carcinog Risks to Humans* 2010; 93: 63–67.
- [17] G2V optic Inc. The Solar spectrum & Molecular Absorption, <https://g2voptics.com/solar-simulation/solar-spectrum/>.
- [18] Stalindurai K, Karuppasamy A, Peng J De, et al. Azafluorene Ornamented Thiazine Based Novel Fused Heterocyclic Organic Dyes for Competent Molecular Photovoltaics. *Electrochim Acta* 2017; 246: 1052–1064.
- [19] Nam S-H, Lee KH, Yu J-H, et al. Review of the Development of Dyes for Dye-Sensitized Solar Cells. *Appl Sci Converg Technol* 2019; 28: 194–206.
- [20] Kim BG, Chung K, Kim J. Molecular design principle of all-organic dyes for dye-sensitized solar cells. *Chem - A Eur J* 2013; 19: 5220–5230.
- [21] Wu H, Huang Z, Hua T, et al. Metal-free organic dyes with di(1-benzothieno)[3,2-b:2',3'-d]pyrrole as a donor for efficient dye-sensitized solar cells: Effect of mono- and bi-anchors on photovoltaic performance. *Dye Pigment* 2019; 165: 103–111.
- [22] Qin Y, Li M, Yan C, et al. Simple synthesis regarding novel bianchored metal free organic dyes based on indole for dye sensitized solar cells. *J Mater Sci Mater Electron* 2016; 27: 3974–3981.
- [23] Khattab TA, Allam AA, Othman SI, et al. Synthesis, solvatochromic performance, ph sensing, dyeing ability, and antimicrobial activity of novel hydrazone dyestuffs. *J Chem*; 2019. Epub ahead of print 2019. DOI: 10.1155/2019/7814179.

- [24] Franzese S, Neto S, Wong WWH. Extended Reichardt ' s Dye – Synthesis and Solvatochromic Properties. 2024; 202400314: 1–9.
- [25] Homocianu M, Airinei A, Dorohoi DO. Solvent Effects on the Electronic Absorption and Fluorescence Spectra. *J Adv Res Phys* 2011; 2: 1–9.
- [26] Sinha T, Roymahapatra G, Khatua PK, et al. An overview on interaction of solvents with different dyes through photo physical studies. *Int J Res Sci &Engineering* 2018; 47–57.
- [27] Kenji Kakiage, Aoyama Y, Yano T, et al. Highly-efficient dye-sensitized solar cells with collaborative sensitization by silyl-anchor and carboxy-anchor dyes†. *Chem Commun* 2015; 51: 15894–15897.
- [28] Mariotti N, Bonomo M, Fagiolari L, et al. Recent advances in eco-friendly and cost-effective materials towards sustainable dye-sensitized solar cells. *Green Chem* 2020; 22: 7168–7218.
- [29] Mozaffari S, Nateghi MR, Zarandi MB. An overview of the Challenges in the commercialization of dye sensitized solar cells. *Renew Sustain Energy Rev* 2017; 71: 675–686.
- [30] Pallikkara A, Ramakrishnan K. Efficient charge collection of photoanodes and light absorption of photosensitizers: A review. *Int J Energy Res* 2021; 45: 1425–1448.
- [31] Yu Z. *Liquid Redox Electrolytes for Dye-Sensitized Solar Cells* Ze Yu Doctoral Thesis, <http://urn.kb.se/resolve?urn=urn:nbn:se:kth:diva-64139> (2012).
- [32] Karthick SN, Hemalatha K V., Balasingam SK, et al. Dye-sensitized solar cells:

- History, components, configuration, and working principle. *Interfacial Eng Funct Mater Dye Sol Cells* 2019; 1–16.
- [33] Fakharuddin A, Jose R, Brown TM, et al. A perspective on the production of dye-sensitized solar modules. *Energy Environ Sci* 2014; 7: 3952–3981.
- [34] Mehmood U, Rahman SU, Harrabi K, et al. Recent advances in dye sensitized solar cells. *Adv Mater Sci Eng*; 2014. Epub ahead of print 2014. DOI: 10.1155/2014/974782.
- [35] Yum JH, Chen P, Grätzel M, et al. Recent developments in solid-state dye-sensitized solar cells. *ChemSusChem* 2008; 1: 699–707.
- [36] Aslam A, Mehmood U, Arshad MH, et al. Dye-sensitized solar cells (DSSCs) as a potential photovoltaic technology for the self-powered internet of things (IoTs) applications. *Sol Energy* 2020; 207: 874–892.
- [37] Xu X, Li S, Chen J, et al. Design Principles and Material Engineering of ZnS for Optoelectronic Devices and Catalysis. 2018; 1802029: 1–24.
- [38] Sookhakian M, Amin YM, Baradaran S, et al. A layer-by-layer assembled graphene/zinc sulfide/polypyrrole thin-film electrode via electrophoretic deposition for solar cells. *Thin Solid Films* 2014; 552: 204–211.
- [39] Bhoi DK. Study of Zinc Blende and Wurtzite Zns. *Int J Res all Subj Multi Lang* 2017; 5: 80–82.
- [40] Quynh Hoa TT, Vu L Van, Canh TD, et al. Preparation of ZnS nanoparticles by hydrothermal method. *J Phys Conf Ser*; 187. Epub ahead of print 2009. DOI: 10.1088/1742-6596/187/1/012081.

- [41] Bera K, Saha S, Jana PC. Fabrication and Characterization of Dye-Sensitized Solar Cell using Chemically grown ZnS Nanoparticles. *J Nanosci Technol* 2018; 4: 237–239.
- [42] Zaman MB, Chandel T, Dehury K, et al. Synthesis and characterization of spin-coated ZnS thin films. *AIP Conf Proc*; 1953. Epub ahead of print 2018. DOI: 10.1063/1.5033002.
- [43] Mana PM, Bhujbal PK, Pathan HM. Fabrication and Characterization of ZnS based Photoelectrochemical Solar Cell. 2021; 77–85.
- [44] Rao SS, Punnoose D, Tulasivarma CV, et al. A strategy to enhance the efficiency of dye-sensitized solar cells by the highly efficient TiO₂/ZnS photoanode. Epub ahead of print 2014. DOI: 10.1039/C4DT03102D.
- [45] Rouhi J, Mamat MH, Ooi CHR, et al. High-performance dye-sensitized solar cells based on morphology-controllable synthesis of ZnO-ZnS heterostructure nanocone photoanodes. *PLoS One*; 10. Epub ahead of print 2015. DOI: 10.1371/journal.pone.0123433.
- [46] Balis N, Dracopoulos V, Bourikas K, et al. Quantum dot sensitized solar cells based on an optimized combination of ZnS, CdS and CdSe with CoS and CuS counter electrodes. *Electrochim Acta* 2013; 91: 246–252.
- [47] Abdul Kareem T, Anu Kaliani A. Fabrication and characterization of ZnSCubic: P3HT, ZnSHexa: P3HT and ZnSHexa: P3HT: PVA-Ag bulk heterojunction solar cells. *J Nano- Electron Phys* 2015; 7: 1–6.
- [48] Tomar N, Agrawal A, Dhaka VS, et al. Ruthenium complexes based dye sensitized solar cells: Fundamentals and research trends. *Sol Energy* 2020; 207:

59–76.

- [49] Yella A, Lee HW, Tsao HN, et al. Porphyrin-sensitized solar cells with cobalt (II/III)-based redox electrolyte exceed 12 percent efficiency. *Science* (80-) 2011; 334: 629–634.
- [50] Giribabu L, Kanaparthi RK, Velkannan V. Molecular engineering of sensitizers for dye-sensitized solar cell applications. *Chem Rec* 2012; 12: 306–328.
- [51] Adedokun O, Titilope K, Awodugba AO. Review on Natural Dye-Sensitized Solar Cells (DSSCs). *Int J Eng Technol IJET* 2016; 2: 34.
- [52] Shelke RS, Thombre SB, Patrikar SR. Status and perspectives of dyes used in dye sensitized solar cells. *Int J Renew Energy Resour* 2013; 3: 12–19.
- [53] Kabir F, Bhuiyan MMH, Manir MS, et al. Development of dye-sensitized solar cell based on combination of natural dyes extracted from Malabar spinach and red spinach. *Results Phys* 2019; 14: 102474.
- [54] Pratiwi DD, Nurosyid F, Kusumandari, et al. Performance improvement of dye-sensitized solar cells (DSSC) by using dyes mixture from chlorophyll and anthocyanin. *J Phys Conf Ser*; 909. Epub ahead of print 2017. DOI: 10.1088/1742-6596/909/1/012025.
- [55] Taya SA. Dye-Sensitized Solar Cells Using Fresh and Dried Natural Dyes. *Int J Mater Sci Appl* 2013; 2: 37.
- [56] Raftani M. New Organic Dyes with Low Bandgap Based on Heterocyclic Compounds for Dye-sensitized Solar Cells Applications. 2023; 13: 1–16.
- [57] Yang YS, Kim H Do, Ryu JH, et al. Effects of anchoring groups in multi-

- anchoring organic dyes with thiophene bridge for dye-sensitized solar cells. *Synth Met* 2011; 161: 850–855.
- [58] Chaurasia S, Chen YC, Chou HH, et al. Coplanar indenofluorene-based organic dyes for dye-sensitized solar cells. *Tetrahedron* 2012; 68: 7755–7762.
- [59] Kim MJ, Yu YJ, Kim JH, et al. Tuning of spacer groups in organic dyes for efficient inhibition of charge recombination in dye-sensitized solar cells. *Dye Pigment* 2012; 95: 134–141.
- [60] Singh SP, Roy MS, Thomas A, et al. Effect of linker used in D-A- π -A metal free dyes with different π -spacers for dye sensitized solar cells. *Org Electron* 2012; 13: 3108–3117.
- [61] Saritha G, Mangalaraja RV, Anandan S. High-efficiency dye-sensitized solar cells fabricated using D-D- Π -A (donor-donor/ Π -spacer-acceptor) architecture. *Sol Energy* 2017; 146: 150–160.
- [62] Murali MG, Wang X, Wang Q, et al. New banana shaped A–D– π –D–A type organic dyes containing two anchoring groups for high performance dye-sensitized solar cells. *Dye Pigment* 2016; 134: 375–381.
- [63] Ahn HJ, Thogiti S, Cho JM, et al. Comparison of triphenylamine based single and double branched organic dyes in dye-sensitized solar cells. *Electron Mater Lett* 2015; 11: 822–827.
- [64] Zang XF, Zhang TL, Huang ZS, et al. Impact of the position isomer of the linkage in the double D-A branch-based organic dyes on the photovoltaic performance. *Dye Pigment* 2014; 104: 89–96.

- [65] He LJ, Chen J, Bai FQ, et al. Fine-tuning π -spacer for high efficiency performance DSSC: A theoretical exploration with D- π -A based organic dye. *Dye Pigment* 2017; 141: 251–261.
- [66] Shalini S, Balasundaraprabhu R, Satish Kumar T, et al. Status and outlook of sensitizers/dyes used in dye sensitized solar cells (DSSC): a review. *Int J Energy Res* 2016; 40: 1303–1320.
- [67] Devadiga D, Selvakumar M, Shetty P, et al. Recent progress in dye sensitized solar cell materials and photo-supercapacitors : A review. *J Power Sources* 2021; 493: 229698.
- [68] Zhao Y, Jiang K, Xu W, et al. Macrocyclic triphenylamine based organic dyes for efficient dye-sensitized solar cells. *Tetrahedron* 2012; 68: 9113–9118.
- [69] Haid S, Marszalek M, Mishra A, et al. Significant improvement of dye-sensitized solar cell performance by small structural modification in π -conjugated donor-acceptor dyes. *Adv Funct Mater* 2012; 22: 1291–1302.
- [70] Xu F, Testo TT, Wang L, et al. Cause , Regulation and Utilization of Dye Aggregation in Dye-Sensitized Solar Cells. *Molecules* 2020; 25: 1–32.
- [71] Chen X, Jia C, Wan Z, et al. Effects of different solvent baths on the performances of dye-sensitized solar cells: Experimental and theoretical investigation. *Org Electron* 2014; 15: 2240–2249.
- [72] Wielgus M, Zaleśny R, Murugan NA, et al. Two-photon solvatochromism II: Experimental and theoretical study of solvent effects on the two-photon absorption spectrum of reichardt's dye. *ChemPhysChem* 2013; 14: 3731–3739.

- [73] Reza M, Javad M. Solvatochromism Effect of Different Solvents on UV-Vis Spectra of Fluoresceine and its Derivatives. 2008; 27: 9–14.
- [74] Masoud MS, Ali AE, Shaker MA, et al. Solvatochromic behavior of the electronic absorption spectra of some azo derivatives of amino pyridines. *Spectrochim Acta - Part A Mol Biomol Spectrosc* 2004; 60: 3155–3159.
- [75] Abdel-latif E, Mansour A, Abdel-Galil E. Solvent Effects on the UV-visible Absorption Spectra of some New Thienylazo-thiazole and Thienylazo-thiophene Dyes. *J Text Color Polym Sci* 2018; 15: 1–13.
- [76] Abdulsayid FA, Hasan HMA. Study of Solvent Effect on UV-Visible Spectra of a Newly Synthesized Zn (II), Co (II) and Cd (II) Complexes with L-Tryptophan. 2020; 7: 78–85.
- [77] Nigam S, Rutan S. Principles and Applications of Solvatochromism. *Appl Spectrosc* 2001; 55: 362A.
- [78] Reichardt C. Solvatochromic dyes as solvent polarity indicators. *Chem Rev* 1994; 94: 2319–2358.
- [79] Brandão P, Marques CS, Carreiro EP, et al. Engaging Isatins in Multicomponent Reactions (MCRs) – Easy Access to Structural Diversity. 2021; 1–115.
- [80] Moradi R, Ziarani GM, Lashgari N. Recent applications of isatin in the synthesis of organic compounds. *Arkivoc* 2017; 2017: 148–201.
- [81] Tingare YS, Su C, Shen MT, et al. New oxindole-bridged acceptors for organic sensitizers: Substitution and performance studies in dye-sensitized solar cells.

Molecules 2020; 25: 40–42.

- [82] Ji JM, Zhou H, Eom YK, et al. 14.2% Efficiency Dye-Sensitized Solar Cells by Co-sensitizing Novel Thieno[3,2-b]indole-Based Organic Dyes with a Promising Porphyrin Sensitizer. *Adv Energy Mater* 2020; 10: 1–12.
- [83] Lin Y, Fan H, Li Y, et al. Thiazole-Based Organic Semiconductors for Organic Electronics. 2012; 3087–3106.
- [84] Soto-Rajo R, Baldenebro-López J, Glossman-Mitnik D. Theoretical Study of the π -Bridge Influence with Different Units of Thiophene and Thiazole in Coumarin Dye-Sensitized Solar Cells. *Int J Photoenergy*; 2016. Epub ahead of print 2016. DOI: 10.1155/2016/6479649.
- [85] James W. Robinson., Eileen M. Skelly France. GMFI. *Undergraduate instrumental analysis*. 7th ed. USA, 2014. Epub ahead of print 2014. DOI: 10.1016/S0166-526X(05)80100-X.
- [86] Harwood LM, Claridge TDW. *Introduction to Organic Spectroscopy*. New York: Oxford university Press, 1997.
- [87] Nesbitt GJ. Principles of NMR microscopy. *TrAC Trends Anal Chem* 1992; 11: XVIII.
- [88] Dienhl B. Principles in NMR spectroscopy. *NMR Spectrosc Pharm Anal* 2008; 1–41.
- [89] Bage D. *Synthesis and Characterisation of Zinc*. Central University of Jharkhand, 2015. Epub ahead of print 2015. DOI: 10.13140/RG.2.1.1087.8887.
- [90] Sharmili P, Revathy MS, Rajesh S, et al. Optical Examination on Zinc Sulphide

- Nanoparticles for Photovoltaic Applications. *Int J Innov Technol Explor Eng* 2019; 9: 260–263.
- [91] Nicolet T, All C. Introduction to Fourier Transform Infrared Spectrometry.
- [92] Stuart BH. *Infrared Spectroscopy: Fundamentals and Applications*. 2005. Epub ahead of print 2005. DOI: 10.1002/0470011149.
- [93] Volland W, Volland W. Organic Compound Identification Using Infrared Spectroscopy. 1999; 1–7.
- [94] L.C. Passos M, M.F.S. Saraiva ML. Detection in UV-visible spectrophotometry: Detectors, detection systems, and detection strategies. *Meas J Int Meas Confed* 2019; 135: 896–904.
- [95] Chen Z, Jaramillo TF. The Use of UV-visible Spectroscopy to Measure the Band Gap of a Semiconductor. *Dep Chem Eng Stanford Univ* 2017; 1–18.
- [96] Weckhuysen BM. Ultraviolet-Visible Spectroscopy. *In-situ Spectrosc Catal* 2004; 255–270.
- [97] Schmid F. Biological Macromolecules: UV-visible Spectrophotometry. *eLS* 2001; 1–4.
- [98] Krawczak E, Zdyb A. The influence of the dye adsorption time on the DSSC performance. *E3S Web Conf*; 100. Epub ahead of print 2019. DOI: 10.1051/e3sconf/201910000040.
- [99] Balavijayalakshmi J, Manju S. Investigation of structural, optical and morphological properties of copper doped zinc sulphide nanoparticles. *Mater Sci Semicond Process* 2016; 48: 101–105.

- [100] Dilpazir S, Siddiq M, Iqbal A. Synthesis of Zinc Sulphide Nanostructures by Co-precipitation: Effects of Doping on Electro-optical Properties. *Kenkyu J Nanotechnol Nanosci* 2015; 1: 34.
- [101] John R, Florence SS. Optical, structural and morphological studies of bean-like ZnS by aqueous chemical method. *Chalcogenide Lett* 2010; 7: 269–273.
- [102] Reda SM, El-Sherbieny SA. Dye-sensitized nanocrystalline CdS and ZnS solar cells with different organic dyes. *J Mater Res* 2010; 25: 522–528.
- [103] Das AK, Goswami S. 2-Hydroxy-1-naphthaldehyde: A versatile building block for the development of sensors in supramolecular chemistry and molecular recognition. *Sensors Actuators, B Chem* 2017; 245: 1062–1125.

APPEDICES

APPENDIX A: Research permission letter and Ethical clearance

CENTRE FOR RESEARCH SERVICES

Office of the Pro-Vice Chancellor: Research, Innovation & Development

University of Namibia, Private Bag 13301, Windhoek, Namibia

340 Mandume Ndemufayo Avenue, Pioneers Park, Office F223 - Pblock, Second Floor

☎ +264 61 206 4673; E-mail:kmbulu@unam.na; URL: <http://www.unam.edu.na>



RESEARCH PERMISSION LETTER

Date: 11/08/2022

Student Name: NDAPEWA ENKALI

Student Number: 200610333

Programme: Master of Science in Chemistry

Approved Research Title: PHOTSENSITIZATION OF ZNS NANOPARTICLES WITH METALBASED DSSCS BASED ON ISATIN DERIVATIVES FOR APPLICATION IN SOLID STATE DYE SENSITIZED SOLAR CELL

TO WHOM IT MAY CONCERN

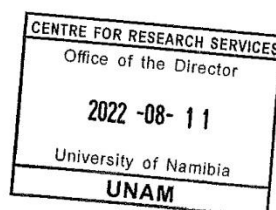
I hereby confirm that the above-mentioned student is registered at the University of Namibia for the programme indicated. The proposed study met all the requirements as stipulated in the University guidelines and has been approved by the relevant committees.

The proposal adheres to ethical principles as per attached Ethical Clearance Certificate. Permission is hereby granted to carry out the research as described in the approved proposal.

Best Regards

A handwritten signature in black ink, appearing to read 'AEE Shikongo'.

Dr. AEE Shikongo
Head: Postgraduate Support Services
Tel: +264 61 206 3129
E-mail: aeshikongo@unam.na





ETHICAL CLEARANCE CERTIFICATE

Ethical Clearance Reference Number: SOS-0096 Date: 18 July 2022

This Ethical Clearance Certificate is issued by the University of Namibia Ethics Committee (REC) in accordance with the University of Namibia's Research Ethics Policy and Guidelines. Ethical approval is given in respect of undertakings contained in the Research Project outlined below. This Certificate is issued on the recommendations of the ethical evaluation done by the ethics committee.

Title of Project: PHOTSENSITIZATION OF ZNS NANOPARTICLES WITH METAL-BASED DSSCS BASED ON ISATIN DERIVATIVES FOR APPLICATION IN SOLID STATE DYE SENSITIZED SOLAR CELL

Student: NDAPEWA ENKALI

Student Number: 200610333


Supervisor(s): PROF. VEIKKO UAHENGO
 PROF. LIKIUS DANIEL

Centre for Research Services

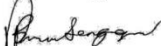
Take note of the following:

1. Any significant changes in the conditions or undertakings outlined in the approved Proposal must be communicated to the ethics committee. An application to make amendments may be necessary.
2. Any breaches of ethical undertakings or practices that have an impact on ethical conduct of the research must be reported to the ethics committee
3. The Principal Researcher must report issues of ethical compliance to the ethics committee (through the Chairperson) at the end of the Project or as may be requested by the ethics committee
4. The ethics committee retains the right to:
 - i) Withdraw or amend this Ethical Clearance if any unethical practices (as outlined in the Research Ethics Policy) have been detected or suspected,
 - ii) Request for an ethical compliance report at any point during the course of the research.

The ethics committee wishes you the best in your research.

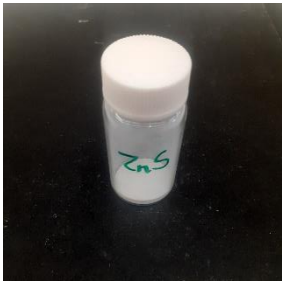
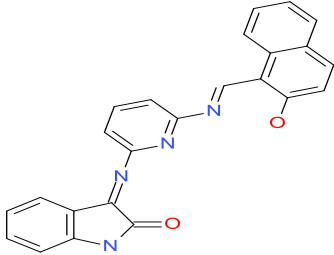



Dr. Zivayi Chiguvare (Chairperson Ethics Committee)

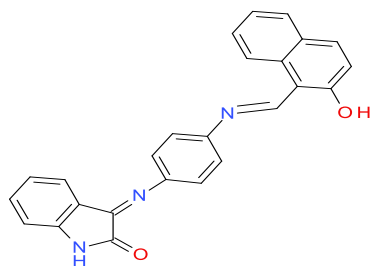


Prof. Davis Mumbengegwi (Head, Multidisciplinary Research)

APPENDIX B: Pictures of the synthesized ZnS nanoparticles and metal free dyes

<p>ZnS</p> <p>MW= 97.474 g/mol</p>	
<p>Dye1</p>  <p>(Z)-3-(6-((E)-(2-hydroxynaphthalen-1-yl)methyleneamino)pyridin-2-ylimino)indolin-2-one</p>	

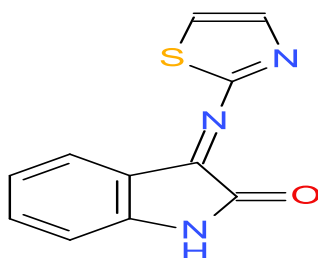
Dye 2



(E)-3-(4-((E)-(2-hydroxynaphthalen-1-yl)methyleneamino)phenylimino)indolin-2-one



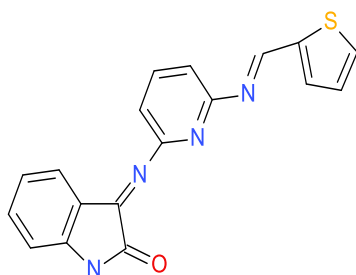
Dye 3

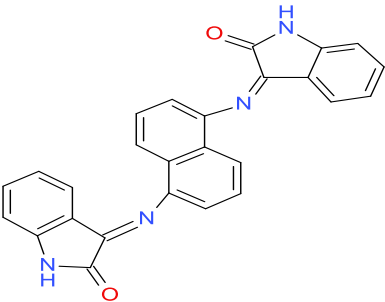
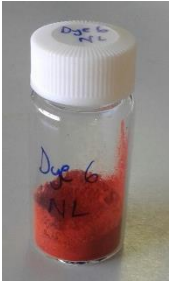


3-(thiazol-2-ylimino)indolin-2-one



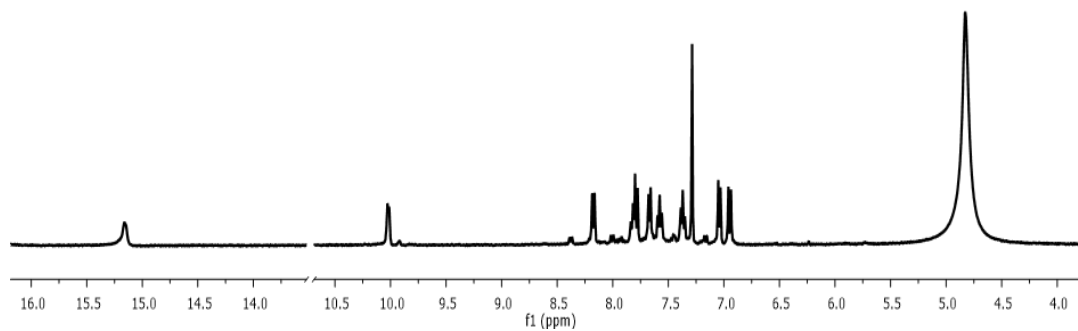
Dye 4



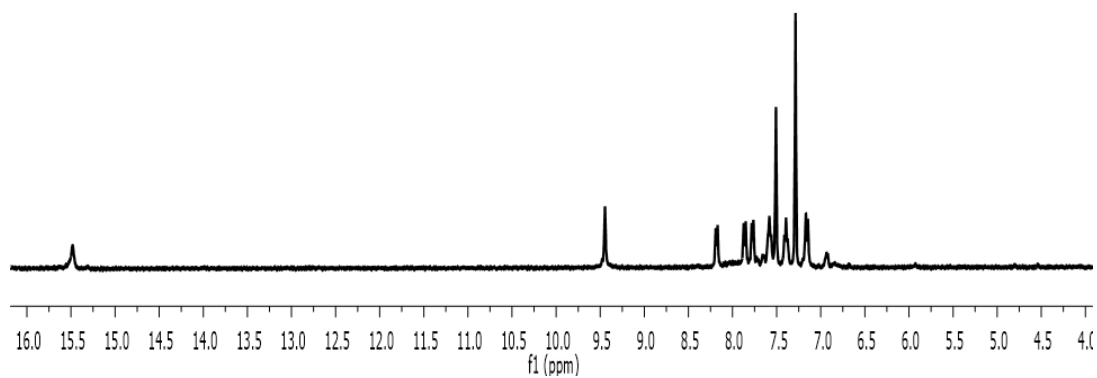
<p>(E)-3-(6-((E)-thiophen-2-ylmethyleneamino)pyridin-2-ylimino)indolin-2-one</p>	
<p>Dye5</p> <div style="text-align: center;">  </div> <p>(Z)-3-(5-((Z)-2-oxoindolin-3-ylideneamino)naphthalen-1-ylimino)indolin-2-one</p>	<div style="text-align: center;">  </div>

APPENDIX C: ^1H NMR Spectra of Dyes

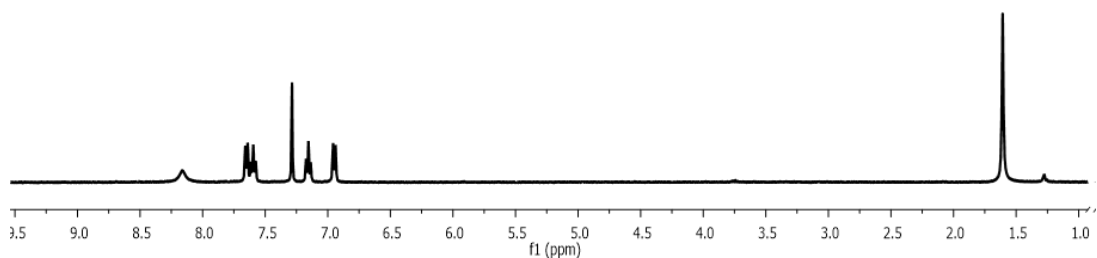
Dye1



Dye2

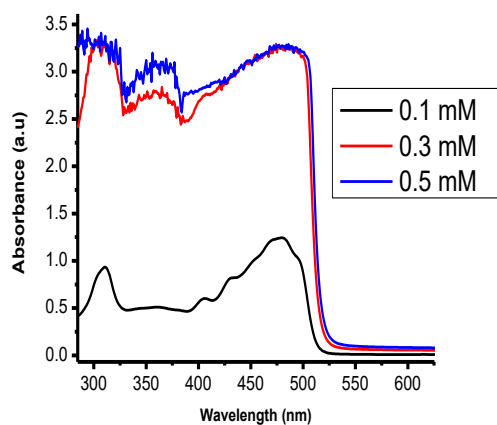


Dye3

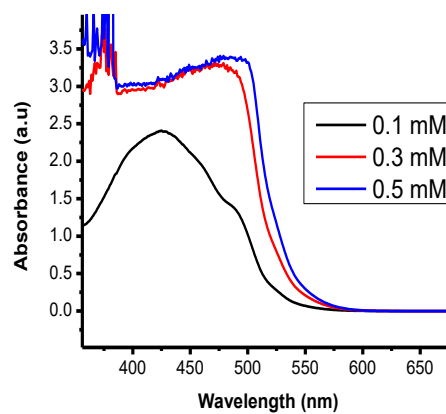


APPENDIX D: Dye graphs at different concentrations

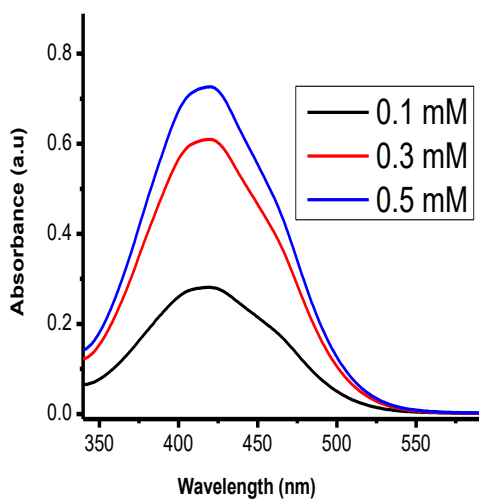
Dye1



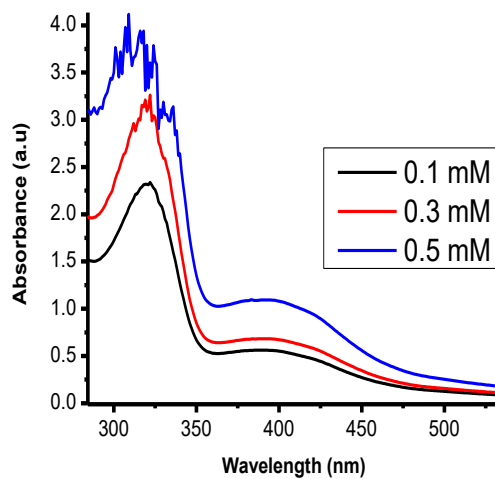
Dye2



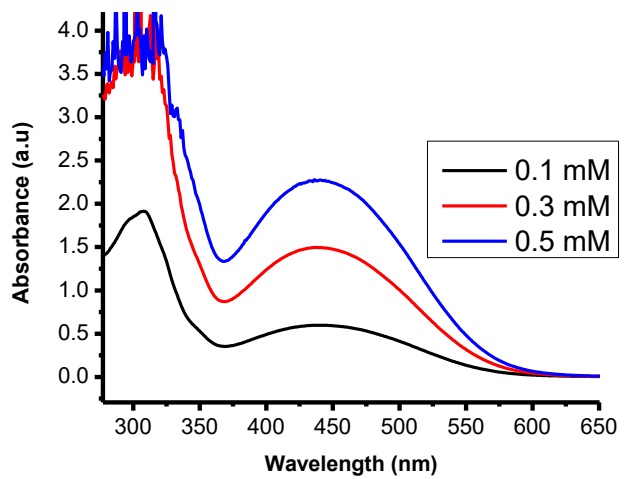
Dye3



Dye4

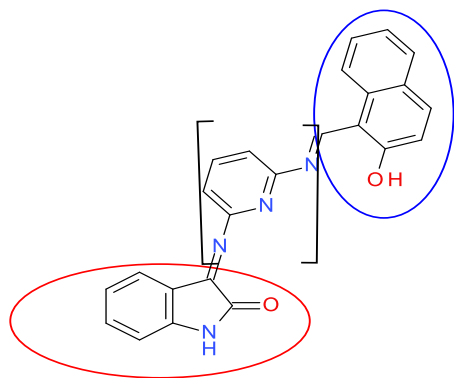


Dye 5

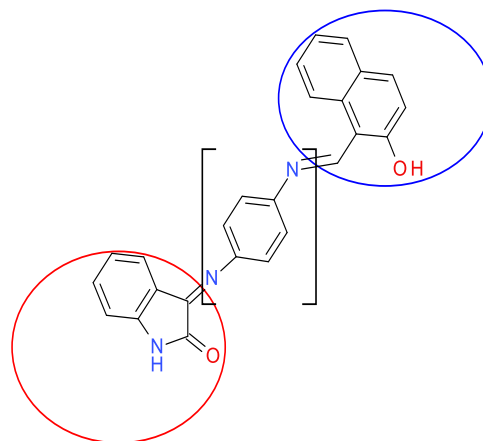


APPENDIX E: Identified moieties on dye structures

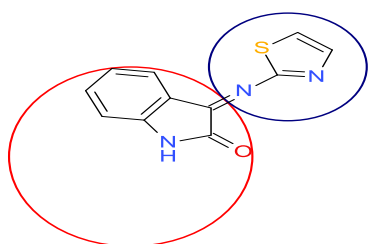
Dye1



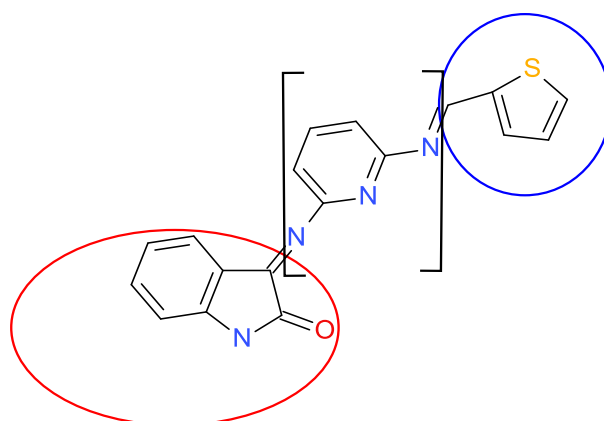
Dye2



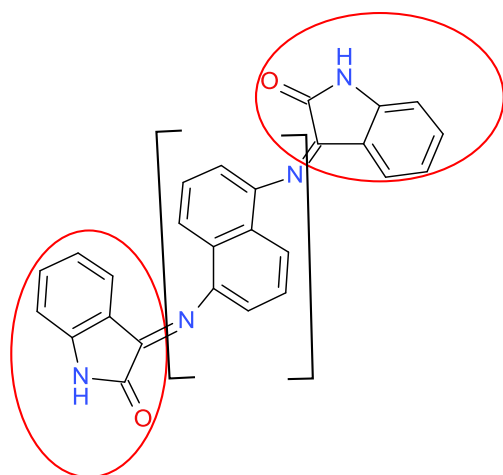
Dye3



Dye4



Dye5



NOTE:

- Acceptor
- Donor
- [] π -conjugation linker